

Selection, processing, properties and applications of ultra-high temperature ceramic matrix composites, UHTCMCs – a review

Binner, Jon; Porter, Matthew; Baker, Benjamin; Zou, Ji; Venkatachalam, Vinu; Rubio Diaz, Virtudes; D'Angio', Andrea; Ramanujam, Prabhu; Zhang, Tailin; Tammana, S R C Murthy

DOI:

[10.1080/09506608.2019.1652006](https://doi.org/10.1080/09506608.2019.1652006)

License:

None: All rights reserved

Document Version

Peer reviewed version

Citation for published version (Harvard):

Binner, J, Porter, M, Baker, B, Zou, J, Venkatachalam, V, Rubio Diaz, V, D'Angio', A, Ramanujam, P, Zhang, T & Tammana, SRCM 2019, 'Selection, processing, properties and applications of ultra-high temperature ceramic matrix composites, UHTCMCs – a review', *International Materials Reviews*.
<https://doi.org/10.1080/09506608.2019.1652006>

[Link to publication on Research at Birmingham portal](#)

Publisher Rights Statement:

Checked for eligibility: 19/09/2019

This is an Accepted Manuscript of an article published by Taylor & Francis in *International Materials Reviews* on 16/09/2019, available online: <http://www.tandfonline.com/10.1080/09506608.2019.1652006>

General rights

Unless a licence is specified above, all rights (including copyright and moral rights) in this document are retained by the authors and/or the copyright holders. The express permission of the copyright holder must be obtained for any use of this material other than for purposes permitted by law.

- Users may freely distribute the URL that is used to identify this publication.
- Users may download and/or print one copy of the publication from the University of Birmingham research portal for the purpose of private study or non-commercial research.
- User may use extracts from the document in line with the concept of 'fair dealing' under the Copyright, Designs and Patents Act 1988 (?)
- Users may not further distribute the material nor use it for the purposes of commercial gain.

Where a licence is displayed above, please note the terms and conditions of the licence govern your use of this document.

When citing, please reference the published version.

Take down policy

While the University of Birmingham exercises care and attention in making items available there are rare occasions when an item has been uploaded in error or has been deemed to be commercially or otherwise sensitive.

If you believe that this is the case for this document, please contact UBIRA@lists.bham.ac.uk providing details and we will remove access to the work immediately and investigate.

Selection, Processing, Properties and Applications of Ultra-High Temperature Ceramic Matrix Composites, UHTCMCs – A Review

Jon Binner^{a,*}, Matt Porter^a, Ben Baker^a, Ji Zou^{a,*}, Vinothini Venkatachalam^a, Virtudes Rubio Diaz^b, Andrea D'Angio^b, Prabhu Ramanujam^c, Tailin Zhang^a and Tammana S R C Murthy^{a,d,*}

^a School of Metallurgy and Materials, University of Birmingham, B15 2SE, UK;

^b National Composites Centre, NCC, Bristol & Bath Science Park, Emersons Green, Bristol, BS16 7FS;

^c Wendt India Ltd, Hosur, India;

^d Materials Group, Bhabha Atomic Research Centre, Mumbai 400085, India

* Corresponding authors: J.Binner@bham.ac.uk (Jon Binner), murthi@iitkalumni.org (Tammana S.R.C. Murthy), J.Zou@bham.ac.uk (Ji Zou)

Short biographical notes of all contributors:

Jon Binner

Jon is Professor of Ceramic Science & Engineering at the University of Birmingham, UK; until April 1st 2019 he was also the Deputy Head of the College of Engineering & Physical Sciences. He has been active in ceramics processing research since 1981 and has published ~220 refereed papers, as well as editing or contributing to 19 books and holding 7 patents with an 8th recently submitted. He has attracted 129 research grants to date, totalling ~£16.5M, this includes a current portfolio of about £1.9M. The focus of his research is the generation of both the necessary scientific understanding and the required engineering solutions for the design and development of materials and process routes that display technical and/or economic advantages over existing approaches. The range of products worked on ranges from nanostructured to traditional ceramics, interpenetrating composites to ultra-high temperature ceramic matrix composites. He has worked closely with industry to translate key developments, e.g. through the creation of a spin-out company to develop a ceramic sensor for measuring soil matric potential (1991), or via licensing, e.g. manufacturing routes for producing engineering ceramic foams (1995) and nanostructured ceramics (2012). He has supervised 35 Ph.D. students and 2 M.Phil. students to successful completion and 38 postdoctoral researchers. A further 7 Ph.D. students and 6 postdoctoral researchers are currently being supervised with more positions currently advertised. His research has received both national and international recognition; he has given ~65 keynotes, plenary and invited talks at international conferences, whilst the Institute of Materials, Minerals and Mining has awarded him the Holliday Prize (1995), Ivor Jenkins Medal (2007), Verulam Medal & Prize (2011) and Pfiel Award (2017). In March 2016 a research

programme that he was involved with funded by MBDA, a major European defence manufacturer, was presented an Innovation Award. He is a Fellow of the Institute of Materials, Minerals & Mining in the UK, the European Ceramic Society and the American Ceramic Society and in September 2017 he was voted to be one of only 5 Fellows worldwide of the Association for Microwave Power in Europe for Research and Education (AMPERE). In April 2018 the EU Academy of Sciences invited him to become a Member. He is a Past-President of the Institute of Materials, Minerals & Mining and the current President of the European Ceramic Society, taking over as President in June 2019 for two years.

Matthew Porter

Matthew is currently a Ph.D. student in the School of Metallurgy & Materials at the University of Birmingham, UK, looking at the effectiveness of microwave energy for the densification of SiC/SiC CMCs using chemical vapour infiltration for aerospace applications, under the supervision of Prof Jon Binner. Matt obtained his B.Sc. from the University of Birmingham in Materials science in 2015, he then spent a short period at a textiles engineering firm who specialised in timing belt materials for the automotive industry before returning to Birmingham to undertake his Ph.D. in the Advanced Ceramics & Composites group. During this time Matt has been a visiting researcher at the Wright-Patterson Air Force Base, Ohio and Worcester Polytechnic Institute, Massachusetts. Matt has given two invited talks, presented at three international conferences and given a number of posters, of which he won the best poster at the 3rd Global Congress on Microwave Energy Applications (2016). Matt is an active member of the American Ceramic Society where he is a chair on the President's Council of Student Advisors and on the committee for the UK Chapter of ACerS.

Benjamin Baker

Ben is currently a Ph.D. student in the School of Metallurgy & Materials at the University of Birmingham, UK, looking at the production and testing of ultra-high temperature ceramic matrix composites, UHTCMCs, with controlled heterogeneity, under the supervision of Prof Jon Binner. He graduated from the University of Durham with an M.Chem. in Chemistry in 2017. During this time, he completed industrial work with Infineum, a petrochemical additive company, in which he completed a research project into the electrostatic behaviours of additives in apolar media, a highly significant field in the understanding and processing of colloids and suspensions.

Ji Zou

Ji is currently a Research Fellow in the School of Metallurgy & Materials at the University of Birmingham, UK, looking at advanced materials for energy generation and transmission, under the supervision of Prof Jon Binner. Ji received his Ph.D. from the Shanghai Institute of Ceramics, Chinese Academic of Sciences. Before joining UoB, he worked as a postdoctoral researcher in KU Leuven (Belgium) and University of Stockholm (Sweden) for three years each. Ji has been active in the Processing-Structure-Property correlation of ceramics, especially for boride ceramics since 2007 and the additive manufacturing of ceramics and alloys since 2016. Ji has published 53 articles in peer-reviewed journals (including 4 in *Acta Materialia*, 9 in *Scripta Materialia*, 10 in the *Journal of the European Ceramic Society* and 8 in the *Journal of the American Ceramic Society*) with >800 citations. He serves as a member in the organizing committee of the International Conference on High-Performance Ceramics (CICC) series and an Editorial Board Member of the international journal, *Recent Patents in Materials Science*.

Vinothini Venkatachalam

Vinothini is currently a Research Fellow in the School of Metallurgy & Materials at the University of Birmingham, UK, looking at the development of ultra-high temperature ceramic matrix composites (UHTCMCs) using radio frequency-enhanced chemical vapour infiltration for aerospace applications, under the supervision of Prof Jon Binner. Vinu worked as a Scientist at the National Aerospace Laboratory, India, on ternary carbides and joining of advanced materials for aerospace applications prior to obtaining her Ph.D. from the Department of Materials at Loughborough University, also under the supervision of Jon Binner. Then she moved to industrial R&D, working at Syfer Technology on developing a new range of capacitor devices, which received an outstanding innovative product of the year at the 10th Elektra European Electronics Industry Awards, 2012. She resumed her academic research, as a Research Fellow, at the Technical University of Denmark, working on high-temperature corrosion & protective coatings. Vinu has wide international experience of ceramic processing, from powders to the product, in both academia and industry. She has published 4 international journal papers, 4 peer-reviewed conference papers, presented in 13 international conferences and 8 national conferences.

Virtudes Rubio Diaz

Virtudes is currently an Advanced Research Engineer at the National Composites Centre in Bristol, UK, leading multiple CMC focused research initiatives with the overall aim of developing the UK's CMC capabilities by working both with academia and industry partners.

1 She obtained her Ph.D. from the Universidad Miguel Hernandex de Elche in 2012 and then
2 worked on ultra-high temperature composites, first at Loughborough University and then as a
3 senior research fellow at the University of Birmingham. During the latter, she researched the
4 development of UHTCMCs on a programme involving the European defence company MBDA
5 and DSTL in the UK and DGA in France. This work contributed significantly to the
6 fundamental understanding of UHTCMC processing and thermo-ablative characterisation that
7 underpins much of the current work at UoB. Her subsequent project, funded by the Horizon
8 2020 programme of the European Commission, C3Harme, focused on the use of radio
9 frequency as an alternative energy source for chemical vapour infiltration to densify UHTCMCs
10 more rapidly. Virtu has delivered many research papers at international conferences, published
11 3 papers and was involved in the research with funded by MBDA that was awarded an
12 Innovation Award.

21 *Andrea D'Angio*

23 Andrea is Engineering Capability Lead of the Advanced Materials Team at the National
24 Composites Centre in Bristol, UK, working on the manufacture and performance assessment of
25 ceramic matrix composites. Andrea started his research in the field of UHTCs in 2013 as a
26 Research Associate at The Institute of Science & Technology for Ceramics (CNR-ISTEC)
27 where he worked on the development of dual architecture UHTCs. He graduated in 2017 from
28 the University of Birmingham with a Doctorate of Philosophy in Material Science; his area of
29 research, supervised by Prof Jon Binner, was the manufacture of SiC/SiC composites using
30 microwave field-assisted chemical vapour infiltration. During this research, Andrea spent four
31 months at the University of Missouri Science & Technology, Missouri, USA, working on the
32 microstructure-property relationship of UHTCs. Andrea has delivered many presentations at
33 international conferences and has 4 research papers.

43 *Prabhu Ramanujam*

45 Prabhu is a Materials Specialist, R&D at Wendt India Ltd, Murugappa Group. Prior to that he
46 worked as a Research Fellow at the University Of Birmingham and in Loughborough University
47 on UHTCs and electroceramics. He received his PhD from Loughborough University, UK, from
48 the Department of Materials under the supervision of Prof. Jon Binner and Prof. Bala
49 Vaidhyanathan. His research interests are the synthesis & characterisation of nanoparticles,
50 colloidal processing of ceramics and flash sintering of UHTC composites for hypersonic and
51 super abrasives applications.

Tailin Zhang

Tailin Zhang is a Ph.D. student in the School of Metallurgy and Materials at the University of Birmingham, UK, working in the area of high entropy & ultra-high temperature ceramics. He obtained his B.Sc. from the Taiyuan University of Technology in Materials science and engineering in 2015, with an experience of additive manufacture of alloys, and he graduated from the University of Manchester with M.Sc. in materials in 2016.

Tammana S.R.C. Murthy

Murthy is currently a Senior Research Fellow in the School of Metallurgy & Materials, University Of Birmingham, UK and also a Scientific Officer (F) in the Materials Group in Bhabha Atomic Research Centre, Mumbai, India, 400085. Murthy has been active in the processing-structure-property correlation of non-oxide ceramics since 2002 and has published 70 articles for peer-reviewed journals and book chapters. His H-index in Scopus is 20 and in Google Scholar is 21. He has developed a process flow-sheet and infrastructure from the lab scale to pilot scale production of various borides and carbides for nuclear applications. He is recipient of Awards and Fellowships including Marie Curie Post-Doctoral Research Fellowship, 2018-2020; Distinguished Young Alumni Professional Achievement Award, 2017 (NIT-Warangal, India); Young Metallurgist of the Year Award - 2011 (Ministry of Steel, Govt. of India); Young Engineer Award, 2008; Group Achievement Awards in 2013 & 2014 (Department of Atomic Energy, India); All India Innovative Student Project Award in 2005 (Indian National Academy of Engineers) and Best /Merit Poster Awards at various conferences.

Selection, Processing, Properties and Applications of Ultra-High Temperature Ceramic Matrix Composites, UHTCMCs - A Review

Abstract

Composites are, in general, a rapidly evolving and growing technical field with a very wide range of applications across the aerospace, defence, energy, medical and transport sectors as a result of their superior mechanical and physical properties. Ultra-high temperature ceramic matrix composites, UHTCMCs, are a new subfield within the wider grouping of CMCs that offer applications in rocket and hypersonic vehicle components, particularly nozzles, leading edges and engine components. The design and development of structural materials for use in oxidizing and rapid heating environments at temperatures above 1600°C is therefore of both great scientific and engineering importance. UHTC materials are typically considered to be the carbides, nitrides, and borides of the transition metals, but the Group IV compounds (Zr, Hf & Ti) plus TaC are generally considered to be the main focus of research due to the superior melting temperatures and stable high-melting temperature oxide that forms in situ. The combination of properties makes these materials potential candidates for a variety of high-temperature structural applications, including engines, hypersonic vehicles, plasma arc electrodes, advanced nuclear fuels, fusion first walls and diverters, cutting tools, furnace elements and high-temperature shielding. This review presents on the selection, processing, properties, applications, outlook and future directions of UHTCMCs.

Keywords: Ultra high temperature ceramics; composites; review; matrix; fibre; chemical vapour infiltration; impregnation; oxidation; ablation; microstructure

Introduction

As with everything in the 20th century, time was at a premium and no more so than in the aerospace industry during the 1960s [1]. During this period, the interest in ultra-high temperature ceramics (UHTCs) began; this group of materials were thought to have potential to withstand the severe aero-thermo-chemical environments of hypersonic flight, paving the foundations for flight speeds exceeding Mach 5. However, although research into UHTCs for this application still continues today these materials do not have sufficient thermal shock resistance and, hence interest began to focus on ultra-high temperature ceramic matrix composites, UHTCMCs, over the last decade.

The hypersonic regime, usually defined as speeds greater than Mach 5 (6173 km/h), continues to receive a great deal of attention from the scientific community. The potential benefits are numerous, military systems would become more effective [2], [3], whilst for potential future commercial travel it would translate into flight times between Europe and the US East Coast of around 1 – 1½ hours or to the Far East in under 3 hours.

Hypersonic speeds are generally associated with flight in the upper stratosphere where gas pressures can be very low but the presence of oxygen radicals is high [4]. There are numerous inhibiting physical factors to consider when travelling at these speeds inside the stratosphere, but the primary issue is the behaviour of air, which becomes very unstable as it no longer behaves as a perfect gas. Hypersonic flow behaviour is not governed by any one equation nor has a definitive definition been established as of yet [5], especially at high altitude. Coupled with the fact that at lower altitudes air is considered to be a continuum, but at near orbital travel the sparsity of molecules means special considerations must be made for the flow dynamics only adds to its unpredictability [6]. The non-linear nature of flow means that shock waves are curved and produce vorticity, which alters the flow field of over the aircraft body.

This is also a dependency on the shape of the leading edge; the shock wave of sharp leading edges propagate on the surface of the structure whereas for blunt edges the flow field propagates ahead, as shown in schematic Fig.1. Both induce frictional heating at the vehicle surface, though less so on the blunt edge, this becoming sufficiently intense they generate high enough thermal loads that alter the properties of

1 the surrounding gases, causing it to vibrate, dissociate, react, excite and eventually
2 become fully ionizing, all whilst being surrounded by a corrosive plasma layer [7]–[9].
3 Efforts have been made to combat this using a multitude of approaches including
4 internal active cooling systems, heat shielding designs and aerodynamic engineering to
5 increase or decrease drag of components to increase the conversion kinetic energy to
6 thermal or vice versa. However, these methods work against the primary principle of
7 aviation to keep mass to a minimum.
8
9
10
11
12

13 With the primary issue being able to endure extreme heating profiles in corrosive
14 environments under substantial and varying mechanical loads, the principle candidate
15 materials were identified as being the highly refractory transitional metal carbides and
16 borides. Collectively referred to as Ultra-High Temperature Ceramics, these non-oxides
17 are able to operate at beyond 1800°C in air with the resulting oxide melting points being
18 around 3000°C [10]. So far UHTCs have been investigated for potential use as sharp
19 leading edges on sub-orbital and earth-to-orbital vehicles amongst other applications
20 [1]. They have shown some potential in being able to facilitate manoeuvring during
21 atmosphere exit and re-entry, whilst surviving shock wave loading and severe oxidation
22 without significantly compromising their geometrical integrity[11], [12].
23
24
25
26
27
28
29
30
31
32

33 The relatively recent utilisation of these UHTCs means their definition is somewhat
34 incomplete to distinguish them from advanced ceramics. They fit the widely regarded
35 standard apophatic criteria of ceramics, in that they are inorganic, non-metallic solids
36 and are defined by three other classifications as described by Fahrenholtz [13]. The
37 most frequently used definition of UHTCs is that materials have a melting point greater
38 than 3000°C. However, this definition has a large degree of uncertainty due to the
39 difficulty associated with measuring temperatures experimentally in this region, with
40 multiple studies regularly reporting melting points of UHTC's with approximately
41 500°C difference [14], [15]. The second less commonly used criteria is the engineering
42 definition determined by the application, where the ceramics highest operating
43 temperature in air defines its classification as a UHTC. This has been set at ~2000°C [1]
44 due to the temperatures experienced at hypersonic speed. The final method is a
45 qualitative definition of UHTCs by their chemistry, which carbides, nitrides and borides
46 of early transition metals are considered to possess the potential to be a UHTC. A
47 combination of all three definitions currently best defines a UHTC.
48
49
50
51
52
53
54
55
56
57
58
59
60
61
62
63
64
65

UHTCs are severely limited as single phase monolithic components for structural applications since they have low fracture toughness. This makes them highly susceptible to thermal shock, hindering their short-term and long-term use as external thermal protection systems on leading edges and propulsion systems. This necessitates the addition of a secondary phase that enhances toughness but without degrading other properties. Attempts have been made to use addition of other ceramic phases to negate these effects, such as SiC and LaB₆, but they have had limited success to date [16]. In spite of this, research effort continues to be focused on improving oxidation resistance and the thermomechanical properties, whilst, in parallel, effort is also being extended with respect to replicating the extreme conditions that components would experience in service [17] and during land-based tests [18]. This has led to the utilisation of reinforcing fibrous phases. The later are designed to symbiotically operate with the UHTC matrix to increase the toughness, whilst also permitting the tailoring of the mechanical and thermal properties towards specific applications. Fibre architecture, fibre type and the volume fractions of the different composite phases will all be described in more detail later in this review.

The rapid expansion of carbon fibres into the commercial aerospace market [19] is a testament to this ability to be readily formed into a wide range of large complex shapes whilst not compromising on their excellent strength to weight ratio [17]. They exhibit many excellent advantages compared to other reinforcing fibres; high specific modulus, specific strength and stiffness, outstanding fatigue properties, a negative coefficient of longitudinal thermal expansion and low coefficient of thermal expansion. Carbon fibre also has relatively good temperature resistance under vacuum or inert gases, but is readily oxidised at ~500°C in air [10]. The literature has shown that this can be offset by the addition of borides or silicides as filler phases, coatings or dopants. At high or ultra-high temperatures, these additions help to protect the fibres from oxidation, enhancing the high-temperature performance of the composites [20].

Of the UHTCs, hafnium and zirconium diborides, with a continuous carbon fibre reinforcing phase, have emerged as candidate for use in hypersonic flight applications due to their desirable combination of high mechanical and good physical properties coupled with the ability to form refractory oxides that resist melting to temperatures >2500°C [21]. These materials also possess high thermal conductivity and a low

coefficient of thermal expansion, advantageous for dissipating heat and withstanding the high thermal gradients that are experienced in service. Their future success is hinged on understanding in detail the protection mechanisms offered by the formation of the oxides of the UTHCs during service.

As indicated previously, the UHTC materials are typically considered to be the carbides, nitrides, and borides of the transition metals, but the Group IV compounds (Ti, Zr, Hf) plus TaC are generally considered to be the main focus of research due to their superior melting temperatures and stable high-melting temperature oxides that forms in situ. Though UHTCMCs are primarily considered for aerospace applications, their ability to offer a combination of properties useful for extreme environments make them potential candidates for a variety of other high-temperature, structural applications. This includes the nuclear energy industry as fuel rod cladding, neutron absorbers (due to the presence of B or Hf or Ta), fusion first walls and tokamak diverters due to their anticipated excellent neutronic properties [22]–[25]. Other applications include, but are not limited to, plasma facing materials, plasma arc electrodes, cutting tools, refractories in metal processing, for example thermowell tubes in the steel refinement process, and electrical devices such as heaters and igniters [13], [26], [27]. Concentrating solar power (CSP) is one of the most promising renewable energy technologies; sun radiation is collected and concentrated on a receiver, which makes the latter a key component. Recent studies have shown that some UHTCs offer good spectral selectivity and low emittance at high temperatures, enabling them to be considered for this application [28].

A major focus of recent work is to combine the properties of the UHTC compounds with the concepts behind the design and manufacture of ceramic matrix composites, to form a new class of materials known as UHTCMCs. Whilst the type of reinforcement influences the mechanical properties, especially fracture toughness, it also affects processing. UHTCMCs are not easy to process; if sintered they require very high sintering temperatures ($>2000^{\circ}\text{C}$). Whilst fine diameter continuous ceramic fibres offer superior mechanical properties, particularly fracture toughness, processing these materials without damaging the fibres or generating grain growth in the matrix is a major challenge for conventional sintering techniques such as hot pressing, which is commonly used for consolidation of particulate or chopped fibre reinforced composites. Techniques such as spark plasma sintering as well as non-sintering techniques including

chemical vapour infiltration (CVI), reactive melt infiltration (RMI), and precursor infiltration and pyrolysis (PIP) are all being investigated.

Interest in UHTCMCs has increased significantly in recent years as it has increasingly become apparent that monolithic UHTCs do not have sufficient thermal shock resistance to provide thermal protection in a number of applications, including hypersonic vehicles [13]. A number of research groups around the world, including from Europe, the US, China, Japan, South Korea and India have now begun to research these materials.

This review will cover the selection, processing, properties, applications, outlook and future directions of UHTCMCs, with the greatest emphasis being given to the continuous fibre reinforced composites since these are likely to be the first materials to be commercialised, and the properties required of them.

Materials selection

For any composite, selection of a matrix and second phase are very important in order to achieve the desired properties. This section covers the selection, properties and compatibility of matrix and second phase for UHTCMCs.

Matrix selection

Materials chosen for UHTCMC matrices can be many and varied, dependent upon the intended applications. The latter may suit one specific set of material properties over another and comparisons, Fig. , [13], [29]–[35] between factors such as melting point, oxidation resistance, density, CTE and thermal conductivity can all affect the most appropriate choices [1], [12], [36], [37]. Given the extreme environments that these materials are used in, oxidation is inevitable during the lifecycles of the components. Therefore, if reusability is a criterion then materials that oxidise in a controlled manner to produce passivating oxidation products are beneficial. For other, less reusable UHT applications, such requirements are less applicable provided they survive the application environment.

Passivating oxidation products may be defined by their ability to retain particular thermomechanical properties and a level of resistance to further oxidation, all the while resisting ablation and denudation. Hence, the melting points and

1 microstructural properties of the oxide products of the materials used are critical. The
2 high conductivities and melting points of TaC and TiB₂ are attractive qualities for
3 potential components, but their oxidation products have an inappropriately low melting
4 point. The borides, nitrides and carbides of Zr and Hf possess high melting temperature,
5 hardness [38] oxidation resistance [39] and electrical and thermal conductivity [40],
6 additionally boasting high oxide melting points. However, the specific oxidation
7 resistances of each have ramifications on the stable oxidation products that form with
8 regards to microstructure and protection capability. In a UHTCMC, protection of the
9 reinforcement phase by the matrix from the aggressive external conditions is critical.
10

11 The boride and carbide systems are generally the most frequently studied for
12 aerospace and other applications as indicated in the previous section. Boride ceramics
13 oxidise with the production of B₂O₃, which at relatively low temperatures becomes a
14 liquid [29]. Nevertheless, even at ≤1000°C formation of an amorphous glassy or molten
15 B₂O₃ phase provides oxidation protection for the bulk boride beneath [41]. In higher
16 temperature regimes, this liquid vaporises and this protection mechanism is lost. The
17 group IV carbides benefit from incredibly high eutectic temperatures with a carbon /
18 carbon (C / C) substrate [13] (3180 and 2910°C respectively for HfC and ZrC).
19 However, studies have found that their oxidation resistance is lower than that of the
20 borides [42] and that the formation of gases during oxidation produces non-protective
21 scales up to 1500°C, which results in substantial denudation. Nitrides are the least well
22 studied of the group IV UHTCs. Whilst they have comparably high melting points, they
23 are reported to have equally poor oxidation protection and non-passivating oxidation
24 products as the carbides [13], [43], [44]. Rather, they find many applications as coatings
25 for cutting tools or in electronics applications due to their electrical properties [44].
26

27 Additives can be included in the matrix to modify the oxidation / ablation
28 behaviour [45]–[48]. SiC inclusions are known to increase the performance of UHTC
29 materials at moderate temperatures by the formation of a silicate glass / molten silica
30 layer from the oxidation of SiC to SiO₂. This is supported by the UHTC-oxide solid
31 scale to provide an effective barrier against oxygen ingress [45]. At higher
32 temperatures, however, the oxidation mechanism of SiC shifts from ‘passive oxidation’,
33 via a solid or liquid SiO₂ product, to ‘active oxidation’, where gaseous SiO is formed
34 [46]. This is lost from the component, reducing or removing the efficacy of the
35

1 protection. Equally, the oxidation of SiC produces a SiC-depleted region in the upper
2 layers of UHTCs with an associated pore network. The latter, without a protective SiO₂
3 surface layer, provides a significant avenue for oxygen ingress and could lead to
4 component failure [49]. The regime in which SiC provides enhanced oxidation
5 protection is up to around 1650°C.
6
7
8
9

10 Other modifications to the matrix material can be made on the basis of
11 manipulating the wetting and rheological characteristics of the surface oxides formed. A
12 study using Zr / Ta boride ceramics [47] found that the glassy layer formed during
13 plasma torch testing at 2900-3000°C provided a healing surface layer that filled matrix
14 cracks and lowered the surface catalycity. Effects of other matrix dopants on the
15 oxidation resistance of components will be discussed in detail in a later section, where it
16 will be shown that the compatibility of dopants with the predominant matrix material is
17 an influential selection criterion.
18
19
20
21
22
23
24

25 In summary, the selection of the matrix phases used is highly dependent upon
26 both the properties desired for a component with respect to its intended operability
27 window and also the fabrication technique used. The latter directly affects the material
28 quality, particularly maximum density achievable; these aspects are discussed in the
29 subsequent sections.
30
31
32
33
34
35

36 **Second phase selection**

37 **Particulate, chopped fibre / whisker / CNT / graphene reinforcement**

38
39 As mentioned earlier, despite their excellent high-temperature properties,
40 UHTCs suffer, like other ceramics, from intrinsic brittleness, which restricts their
41 engineering applications [50]. Hence, the toughening of UHTCs has been the focus of
42 considerable research with particle dispersion toughening, chopped fibres, carbon
43 nanotubes, graphite, graphene and whisker toughening all being examined [50].
44
45
46
47
48
49
50
51

52 A range of different types of particle reinforcement of UHTCs have been
53 reported by various authors [51]–[71]. Use of sinter-additives has traditionally been one
54 of the methods to improve the densification at lower temperatures, especially for
55 difficult to sinter materials like UHTCs. Sinter-additives typically lead to liquid phase
56 sintering by creating a liquid phase, whilst other additives can lead to solid state
57
58
59
60
61
62
63
64
65

1 reactions during sintering that can also be beneficial for the densification process [53],
2 [69], [71]. Metallic additives such as Fe, Ni and Co melt at lower temperatures and wet
3 the refractory boride / carbide / nitride particles, which lead to faster mass transport and
4 particle rearrangement and concomitantly result in attaining better densification at lower
5 temperatures and shorter times due to liquid phase sintering [53], [69], [71], [72].
6
7 However, the problem with using metallic additives is that at the ultra-high
8 temperatures, the metallic and intermetallics phases soften and melt, which degrades the
9 mechanical properties and creep resistance significantly. Hence, the use of metallic
10 sinter-additives are generally considered unsuitable for densification of UHTCs [53],
11 [69], [71].
12
13
14
15
16
17
18

19 Liquid phase assisted sintering has also been observed with non-oxide sintering
20 additives, especially Si-based such as SiC, MoSi₂, ZrSi₂, TiSi₂, WSi₂ and TaSi₂ [22],
21 [53], [69]–[80]. Such additions have led to improved densification and mechanical
22 properties for most of the refractory borides as well as carbides [81]. The Si-based
23 additives have also been reported to react with the surface oxide phases (such as B₂O₃)
24 to form SiO₂, which is a transient liquid above ~1850°C and enhances the densification.
25 In fact, improvements to the mechanical, tribological properties and oxidation resistance
26 on addition of the Si-based additives have been reported in the literature.
27
28
29
30
31
32
33

34 In addition, nitrides such as AlN and ZrN and rare earth oxides / borides
35 including La₂O₃, LaB₆, NdB₆ and EuB₆ have also been explored as sintering additives
36 for the borides to enhance both sinterability and the subsequent properties [22], [53],
37 [71], [82], [83]. Removal of the B₂O₃ surface oxide layer by the nitrides also prevents
38 grain growth, which in turn aids densification. For the reasons mentioned above, the last
39 two decades have witnessed extensive research activity related to exploring the use of
40 particulate sinter-additives for attaining improved densification via solid-state sintering
41 and concomitantly improved mechanical properties of the UHTCs. Even though
42 sintering additives help in attaining better sinter densities for the UHTCs, it has been
43 difficult to attain near theoretical densities by pressureless sintering routes. Hence, most
44 UHTCs and their composites are densified using external pressure assisted sintering
45 techniques such as hot pressing and spark plasma sintering. More details of the
46 processing routes are described in the later sections, though there is still much room for
47
48
49
50
51
52
53
54
55
56
57
58
59
60
61
62
63
64
65

improvement of the toughness, thermal properties, etc. for UHTCs by using a different type of reinforcements as discussed in the next section.

Hence, other researchers have explored the use of carbon nanotubes (CNTs), chopped fibres (carbon / SiC / ZrO₂), non-oxide whiskers and graphene as reinforcement phases for UHTCs in the past few years. Table 1 [57], [84]–[121] summarises the results of various UHTCs consolidated through sintering processing routes, e.g. hot pressing or SPS, and using different forms of reinforcements. Improved fracture toughness and strength values were observed. Chopped fibres are particularly attractive, benefiting from excellent mechanical properties coupled with resistance to neutron irradiation, improved thermal conductivity and stability. Graphene has a high two-dimensional aspect ratio, which has also been shown to enhance the thermomechanical properties of UHTCs [86], [122]. Multi-walled carbon nanotube (MWCNT) reinforced UHTCs exhibited superior mechanical and transport properties, making them attractive candidates (at a reasonable cost) for nanoscale reinforcement of UHTCs. A maximum fracture toughness of 7.8 MPam^{1/2}, with a strength of 894 MPa, was reported by incorporating multiwall CNTs in a HfB₂ matrix [87]. The major toughening mechanisms are reported to be one or more of the combination of reinforcement pull out, bridging, debonding, branching, stress-induced transformation and three dimensional crack deflection. Possible reactions between CNT or graphene with any oxide present in the UHTC during high temperature sintering might be a problem [87]. Homogenization of these additives in the UHTCs matrix is also challenging [87].

For fibre-toughened ceramics, the interfacial bonding plays an important role for load transfer and therefore affects the fracture toughness of the ceramics significantly. Thus, finding a method to optimize the fibre-matrix interfacial bonding strength is important when fabricating UHTCMCs with high fracture toughness [123]. The design parameters for the interface have been comprehensively reviewed by Faber [124] for conventional CMCs and include interface toughness and sliding resistance. These are related to the elastic properties of the fibre and matrix and are characteristic of the fibre / matrix interface. A brief discussion of these parameters has been included in the section covering the composites' microstructure.

Another challenge for these reinforcements (especially CNTs and graphene) is achieving uniform dispersion and minimising / avoiding agglomeration, which arises due to van der Waals interactions, in the matrix. A range of dispersion techniques have been used / reported to overcome the above issues, such as conventional ball-milling, colloidal processing, sol-gel processing and in-situ growth of CNTs within the UHTC particle by catalytic chemical vapour deposition and in situ thermal reduction of graphene oxide [88] and hetero-coagulation [84].

More recently, research has been focused on the use of continuous carbon / SiC fibres reinforced UHTC composites to improve the fracture toughness and strength. More details are discussed in the next section.

Continuous Fibre reinforcement

In fibre reinforced ceramic matrix composites (FRCMCs), fibres are required to overcome the brittleness, low elongation to rupture and poor thermal shock resistance of the monolithic ceramics. Embedding fibres into a UHTC matrix implies that the associated fibres must also be able to withstand the extreme temperature and harsh environment in which long-term thermal and oxidation stability are priorities, however, it must be noted, that the deployment of UHTCMCs is also planned for non-reusable applications where the fibres need to withstand harsh environments only for a limited amount of time.

Organic polymer-based fibres cannot be used because of their low degradation temperature and, analogously, glass fibres are also excluded because they soften far below the operating temperatures of UHTCMCs. Inorganic fibres include those based on metals, carbon, oxides (e.g. alumina, mullite and zirconia) and non-oxide ceramics (e.g. Si-C-O, SiC, Si-C-N, Si-B-C-N, UHTCs). Oxide fibres exhibit relatively low temperature capabilities (up to 1200°C for short periods of time) and the low maturity of the commercial manufacture of Si-C-N and Si-B-N-C limit the options to carbon fibres, silicon carbide fibres and UHTC fibres. These are reviewed below.

Carbon fibres

Carbon fibres technically contain at least 92 wt.% carbon in the form of graphite. The anisotropic thermo-mechanical properties of the carbon fibres are due to

1 the strong covalent C - C bond of the graphite oriented along the axis of the fibre, whilst
2 the properties are poor in the transverse direction since the interatomic forces between
3 the basal planes are weak [125], [126]. Carbon fibres have a typical tensile strength
4 ranging from 1.5 to 7 GPa and elastic modulus between 200-900 GPa [127]. The low
5 density of carbon offers the highest specific modulus and highest specific strength of all
6 reinforcing fibres. They are classified prevalently on the basis of their mechanical
7 properties into four groups as shown in Fig. 3 [128]; super high strength (SHT),
8 intermediate modulus / high strength (IM / HT), high modulus (HM) and ultra-high
9 modulus (UHM). As a general trend, very high strength fibres are produced by drawing
10 a high-carbon yield polymeric precursor such as polyacrylonitrile (PAN) [129], [130],
11 [131]; such fibres account for ~90% of the total production. In contrast, very high
12 modulus fibres are manufactured by the drawing of pitch, a tar-like mixture of branched
13 hydrocarbons [132], [133] that is capable of forming a crystal-liquid mesophase during
14 the manufacturing process [131]. The mechanical properties of carbon fibres obtained
15 from both PAN and pitch are reported in Table 2 [128], [134]–[141].

26 It should be noted, however, that the development of carbon fibres has not been
27 driven by the need to overcome their intrinsically low oxidation resistance (as low as
28 400-500°C [10]), but rather from the mechanical performance required by different
29 industry sectors and, of course, cost reduction. Some studies have shown that the choice
30 of different carbon fibres in UHTC matrices does not affect key mechanical properties
31 such as fracture toughness [113]. Similarly, the different thermal conductivities of PAN-
32 and pitch-derived carbon fibres (being higher for the latter) is also not usually the
33 determining factor in the choice of carbon fibres for UHTC applications. Rather, the
34 primary factors that typically affect the choice between PAN- and pitch-derived fibres
35 are the very high modulus of the latter, which makes weaving harder, in turn limiting
36 preform architecture, and also their more limited availability.

49 Silicon carbide fibres

52 The early development of SiC fibres occurred in the 1970s [142]. Since then,
53 they have been continuously developed and improved with the primary goal being to
54 offer a better oxidation resistance than carbon fibres [143]. Other goals underpinning
55 the development of the different generations of SiC fibres have been to improve the
56 maximum operational temperature and provide a better thermal endurance. The

schematic in Fig. 4 [144] shows the evolution of the microstructure and the properties of the commercially available SiC fibres over the three generations presented in Table 3 [144]–[147].

Two different approaches are available commercially to prepare SiC fibres [146]: chemical vapour deposition on a core filament and the spinning of preceramic polymers.

SiC fibres produced by CVD, such as the Tisics SigmaTM (Tisics Ltd., Farnborough, UK) [148] and the SCS (Speciality Materials Inc., MA) [149] have a diameter above 100 μm . As a consequence, they have a high bending stiffness and therefore are difficult to weave. These fibres are generally used for intermediate temperatures in metal matrix composites as creep retardants and stiffeners [150].

The second manufacturing process is similar to that used for carbon fibres and is based on the melt or dry spinning of organic polymers. A polymer with a high molecular weight, adequate viscoelasticity and thermal stability enables a stable melt spinning process to be used without breaking the filament. Typical polymers used include polycarbosilanes or polycarbosilazanes. Subsequently, the green fibres are cured and then converted into ceramic fibres by pyrolysis [142], [151] in a controlled atmosphere and temperature from 1200°C to above 1700°C. The microstructural, mechanical and thermal properties are dependent on the precise production conditions [147]; the finer the microstructure, the higher the tensile strength whilst the creep, Young's modulus and thermal resistance are determined by the oxygen content and sintering aids [145]. The first generation of fibres (Nicalon, Tyranno S and Lox-M) had a high oxygen content due to the curing in air that lead to an amorphous Si-C-O matrix with an oxygen content of up to 20 wt.% Above 1200°C the glassy phase evaporates with a consequent degradation of the fibres and dramatic loss of strength. The low production temperature (around 1200°C) implies the formation of small crystallites (2-5 nm) of β -SiC which, combined with an inter-granular amorphous phase, poorly resists creep at high temperature. Oxygen is also responsible for their low Young's modulus and thermal conductivity. This first generation of SiC fibres cannot be used for the fabrication of CMCs for long-term performance at 1100-1200°C [152], let alone in UHTCMCs.

Oxygen reduction was the guideline for the development of the second generation of SiC fibres (Hi-Nicalon and Tyranno ZMI) [145]. New organometallic precursor (zirconium grafted in the polymeric chain of the polycarbosilane) for Tyranno ZMI and electron beam curing for the Hi-Nicalon allowed the oxygen content to be reduced below 10 and 1 wt.% respectively. Higher production temperatures were possible, with the formation of larger grains and, hence, reduced creep rates [146].

Further improvement led to the third generation of SiC fibres (Hi-Nicalon Type S, Tyranno SA3, Sylramic, Sylramic i-BN) [146]. They are characterized by an even lower oxygen content and near-stoichiometric composition. The creep rate has been drastically reduced with the presence of 200 nm β -SiC crystals, achieved due to the higher temperature production occurring at above 1700°C. In this generation of fibres, sintering aids like aluminium for Tyranno SA3 and boron for Sylramic are incorporated in the fibre structure to form a dense fibre [145], [146], [152]–[154]. Hi-Nicalon Type S fibres are the product of choice for the CMC components in Leap Engine and GE9X, where the operational temperatures can reach 1400°C with a lifetime >25,000 hours [155].

iBN-Sylramic silicon carbide fibres are an exclusive product developed by NASA Glenn Research Center (Ohio, USA) [147] and commercialised by COI Ceramics Inc. (San Diego, California, USA). These fibres are coated with boron nitride by modifying the gaseous atmosphere used during the curing process [146]; the BN coating enhances fibre pull-out [156]. Subsequent study at the NASA Glenn Research Centre [157] has led to the development of the Super Sylramic-iBN and -iC fibres, BN and C coated respectively. The creep rate in particular has been shown to decrease if the fibres have a larger and more homogeneous grain size (up to 500 nm) and the microstructure is also free from pores and impurities. These fibres are not yet commercially available, being still in the process of laboratory development, and therefore have not yet been trialled for UHTCMC applications.

As discussed in the section dedicated to oxidation, above 1600°C the oxidation of SiC in general turns from passive to active. This implies that in the UHTC range, SiC fibres offer little long term oxidation resistance. However, as already noted the same is also true for C fibres, thus SiC fibres are extensively studied as reinforcement for

UHTCMCs with other mechanisms being used to protect them. These are discussed elsewhere in this review.

UHTC fibres

As already discussed C and SiC fibres can only partially fulfil all the requirements to withstand the extremely demanding environments that are required, for example, by re-entry vehicles in the hypersonic regime [1], [33], [38], [158]. At the laboratory scale, efforts have been made to prepare ZrC [159]–[163] and ZrB₂ [162] micro and nanofibers via electrospinning. Cui et al. [161] produced ZrC by electrospinning a solution of novolac phenolic resin and zirconium (IV) acetyl acetonate (following annealing). The fibres obtained had a diameter of ~300 nm. Electrospinning combined with a polymeric precursor was also used to produce ZrC nanofibres of similar diameters [164]. Li et al. [165] electrospun polyzirconoxane (PZO) as the zirconium source and polyacrylonitrile (PAN) as the spinning aid and primary carbon source. A larger, 20 µm, fibre of Zr-Si-C was obtained by the spinning of a sol-gel precursor made from zirconium tetra-kis(2,4-pentanedionate), novolac phenolic resin and tetraethoxysilane [163]. Chelich et al. [162] synthesised ZrB₂ nanofibres by electrospinning of a hybrid polymer solution of PVP / zirconium n-propoxide and boric acid. NbC and ZrC textiles were obtained by carbothermal reduction of electrospun niobia-complex and zirconia-complex fibre mats [166].

At the pilot scale, Matech GSM (Matech Global Strategic Materials Inc., California, USA) [167] has developed and patented [168] hafnium nitride and hafnium carbide fibres (e.g. HfC 2000-X) with potential applications for rocket nozzles and sharp leading edges; HfC is the highest known melting compound [168]–[170]. A hafnium-based preceramic polymer was produced through the reaction of hafnium chloride with amines or imines. Depending on the atmosphere of the heat treatment, HfN(C) or HfC fibres were obtained. The final density of the fibres was 7.0 g cm⁻³ due to an excess of carbon, which acted as both a grain growth inhibitor and as a sintering aid. The fibres had a diameter of 5.0 µm, a Young's modulus of 500 GPa and tensile strength of 1.7 GPa. In 2009 Matech GSM transferred the HfC-preceramic polymer to a pilot production line capable of spinning multi-hundred filaments [171]. Matech GSM has also produced TaC fibres (TaC 1600-X) for aluminised propellant solid rocket

nozzles [172] and some mini-composites TaC_f/ TaC_m have been developed [171], [173].

As shown above, the manufacturing of UHTC fibres is still at the pilot scale at best. Although there is no data available in the literature with regard to the cost of future commercial HfC and TaC fibres, it is known that the cost of Hf and Ta-based preceramic polymers is higher than those used to produce SiC fibres and therefore it seems highly probable that the cost of the product will also be much higher. It is also not yet known whether these fibres will offer any advantages over C and SiC fibres since the authors are unaware of any research yet undertaken to investigate the potential that UHTC fibres offer to UHTCMCs.

Preform selection

The fibre preform design is essential for achieving the composite performance required mechanical and thermal properties [174]–[176]. The ability to impregnate with a matrix is governed by the porosity (size and distribution) and hence the permeability of the preform to the matrix precursor, which can be in the form of solid, liquid or gas. This, in turn, is a function of the fibre orientation / architecture and fibre volume fraction [175]. Pre-existing technology from textile forming has been widely utilised for designing carbon / SiC fibre preforms using weaving, braiding, stitching, etc. The fibre orientation is very critical for both the in-plane and out-of-plane strength and life of the composites [177]–[180].

The fibre reinforcement architectures are classified (following the textile literature), first on the technologies used and then on the fibre topology, e.g., the number of fibre directions. When the fibres are oriented only in one direction they are referred to as unidirectional fibres and provide stiffness along the fibre direction but a lack of it in the orthogonal directions. Therefore, the fibres are commonly stacked in two directions (0° and 90°), yielding two dimensional (2D) preform structures. Various textile technologies has been utilised for manufacturing such preform structures, including weaving, braiding, knitting, stitching, etc. During weaving, two directional fibres (0° / 90°) are interlaced - warp and weft; in knitting, two directional fibres (0° / 90°) are drawn by loops of yarns over previous loops, whereas in braiding the fibres are typically limited to only one direction by intertwining. Most commonly used 2D

preform designs are classified as Plain [181], Twill, Satin [175] or Matt, the designations being based on the number of fibre tows used and the positions in which they are laid. Each preform design pattern, and the processing techniques used, offers different benefits and limitations, as outlined in Table 4.

Nevertheless, in the 2D preforms, the fibres are oriented only in the plane of the laminate and are therefore vulnerable to delamination. Therefore through thickness fibre reinforcement has been included to develop three-dimensional (3D) fibre reinforced structures. Consequently, efforts have been carried out to modify the 2D preform structures for additional in plane support using simple techniques such as stitching and needling [182] and the results are referred as 2.5D preform structures [179], [183]–[185]. Extensive research developments and products have been carried out using 2.5D carbon fibre preforms from Surface Transforms, UK, in the past decade [17], [179], [186]–[189]. Fig. 5 shows the structure of their preform; it is made of PANOX fibres and very easy to fill with a UHTC powder matrix. In addition the filled 2.5D fibre architectures have shown some promising resistance to mechanical stresses [179] and thermoablative properties as well [18], [187].

Further to the simple developments, complex 3D preform structures have also developed through advancements of computational analysis and robotic manufacturing technologies. Triaxial fibres of different orientation, referred to as 3D structures are made using various methods such as weaving, knitting and braiding. Based on the fibres' interlocking position, the 3D woven structures are further classified as layer to layer, angle and orthogonal interlock weave as shown in Table 4. The weaving design provides moderate properties and can be automated, but there are limits to the shape and drapability [190]. The 3D braided structure is suitable for complex shapes along with offering a good balance of in-plane and out-of-plane properties [191]. Some of the other techniques used for making 3D structure are like stitching, needling [192] and noobing.

Noobed structures are defined by a new process of producing 3D structured by non-interlacing, orienting orthogonally the three sets of yarns and integrating the structured through binding [193]. It is a new 3D technology and is being explored with carbon, SiC and oxide ceramic fibres. The noobed structures can be uniaxial or multiaxial, which include an additional set of yarns placed in the $\pm 0^\circ$ direction, as

shown in Table 4 [193]. The main advantage of the noobed preform is that the fibres are uncrimped and their paths are nearly orthogonal to each other.

Although the well-established 3D manufacturing methods have been demonstrated to produce near net-shape structures directly, control is essential to avoid damage occurring by the insertion of the through-thickness reinforcement, which will decrease the mechanical properties of the resulting 3D composites. Subsequently, in order to achieve the targeted outcome, the fibre preform design has to match with a suitable further matrix densification process to achieve the required performance, as detailed in the following sections.

Selection of a suitable preform is based on the required properties for the intended application and compatibility for the chosen fabrication process. In addition, cost and availability in the required shapes, sizes & quantities also are important. Structure-texture and properties are correlated with each other, hence obtaining tailored structures and textures is very important when targeting demanding mechanical & thermal properties. Processing method, type and conditions all play a role in achieving this and hence the next section covers the different methods used to obtain the UHTCMCs.

Materials processing

Various processing methods for UHTCMCs are reported in the literature and Fig. 6 summarises the different approaches considered. Details of each method are discussed in the following sections, whilst their advantages and disadvantages are summarised in Table 5.

PIP process

Precursor infiltration and pyrolysis (PIP) is a green-forming procedure, an overview of which is depicted in Fig. 7. A liquid chemical precursor is introduced to a reinforcement phase and subsequently pyrolysed at elevated temperatures. The pyrolysis reaction yields the required ceramic product, which is retained within the preform body. Due to the lower-than 100% efficiency of this process, the evolution of gaseous by-product and volume shrinkage from precursor to ceramic, this process must be performed iteratively many times, often a dozen or more, until a matrix of the desired

or otherwise limiting density is achieved.

Optimisation of the process requires achieving a high ceramic density whilst limiting the number of energy-intensive pyrolysis steps. Hence, a high ceramic yield from precursors is important and the precursor choice is critical. There are many instances in the literature of precursors for ZrB₂, ZrC, HfC and HfB₂ ceramics. Xie et al. [194] used a polymeric zirconium cyclopentadienyl / boron hydride species, Fig. [194], which led to a ceramic conversion yield of 65.5 wt% at 1200°C for 1 hour in inert conditions. The temperature of the pyrolysis was found to be critical with respect to ceramic product distribution. At 1200°C, a product ratio of 4 : 0 : 1 ZrB₂ : ZrC : ZrO₂ was obtained, which tended to 9 : 1 : 0 at 1800°C, though higher temperatures have, historically, been associated with graphitisation of carbon fibres [195]. The material possessed terminal vinyl groups to prevent excessive polymerisation of the precursor, thereby reducing precursor viscosity. In a previous study [196], an unmodified material lacking these groups showed a similar ceramic yield but poorer product ratio with respect to ZrB₂. This highlights the significance that physical properties such as viscosity or polymer conformation may have on precursor efficacy.

Zhang et al. [197], Zhao et al. [198] and He et al. [199] all used an ‘organic zirconium-containing polymer’ sourced from the Institute of Process Engineering from the Chinese Academy of Sciences, which produced both ZrC and ZrB₂. Zhang et al. [198] described a ceramic yield of around 30 wt%, whereas He et al. [199] reported a ceramic yield of 45 wt% at 1500°C and described the structure as a mixture of a polymeric zirconium complex of acetyl acetate and butoxide ligands, and an aminopolyborazine. The apparent range in ceramic yield is interesting and may reflect the pyrolysis temperature, given broadly as 1400 – 1600°C for 2 hours by Zhao et al. [198], but not given at all in the work of Zhang et al. [197].

Zhang et al. [200] produced 2D C / C-ZrB₂-ZrC-SiC composites from a similar combination of organic zirconium polymer and a polyborazine. The zirconium polymer alone could generate a ZrC phase at a ceramic yield of 44 wt%, which improved to 60 wt% for the ZrB₂ when combined with the polyborazine. The mixed precursor had a very low viscosity (5×10^{-3} Pa s) and the product ratio was seen to be controlled by both the pyrolysis temperature and the B : Zr molar ratio in the precursor mixture. Ratios of 1 : 1 generated both ZrB₂ and ZrN phases, whilst 2 : 1 was found to yield ZrB₂ in the

highest proportion. Ratios greater than this produced more complicated mixtures of ceramic phases, including boride, carbide, oxide and free carbon. 1650°C was the lowest pyrolysis temperature at which ZrB₂ was the thermodynamic product of the reaction, whereas at 1800°C it became the only major product. The mixed precursor required 16 PIP cycles to generate maximum density.

Mixed ceramic phases can be produced from some precursors, which in the case of ZrB₂-SiC-based ceramics may be ideal for moderate temperature applications. Lv et al. [201] fabricated ZrC / ZrB₂-SiC fibres from a mixed precursor of a zirconium cyclopentadienyl alkyl silane polymer with polyaminoborazine. The creation of both the UHTC phase with the self-healing SiC elements produced superior oxidation protection in temperature regimes up to 1650°C.

Whilst achieving mixed ceramic phases may be desirable in some applications, interpenetration of different ceramic phases of different crystal structures is difficult to control and may, in some cases, cause microstructural or application-based complications that detract from the overall usefulness of components. Producing pure phases of UHTC from PIP routes is, as has been described, complicated by the thermodynamic proclivity for the formation of other carbide, nitride and oxide phases due to the precursors frequently used. Li et al. [202] reported the production of ZrB₂ phase from polyzirconoxane ([ZrCl(OCH₂CH₂OH)(OH)₂(H₂O)]) [203], [204] boric acid and phenolic resin with pyrolysis at 1600°C; only small quantities of ZrC were present as an impurity.

Reports of the production of hafnium-based ceramics from PIP are fewer in number. Given the similarity of organozirconium and organohafnium chemistries, this is likely to be primarily due to material cost; hafnium-based chemicals tend to be much more expensive than zirconium-based chemicals though the resulting ceramic has much better oxidation and ablation resistance [33]. Nevertheless, the description of precursors for the HfC / HfB₂ systems are sparse [168]. Patra et al. [205] produced a hafnium/hydroxyquinone complex from hafnium tetrachloride for the production of HfC. Yan et al. [159] used an in-situ gelation method with an HfOCl₂.8H₂O salt, citric acid and ethylene glycol to produce a network where the glycol ester of citric acid complexes the Hf metal centres, this could then be pyrolysed to produce the HfC ceramic phase. This method has the potential of being industrially flexible in that the

precursor uses an aqueous solvent with environmentally benign gelling agents and the viscosity of the solution is tuneable based on the ethylene glycol: citric acid ratio. In contrast to the details provided by Yan et al. [159], however, many authors simply state the use of ‘an HfC precursor’ [206], [207]. The provision of greater detail in the composition and thermodynamics of developmental materials is beneficial to the growth of the area as a whole.

Issues with the PIP method centre around the microstructures produced, especially considering the numerous high temperature cycles required for densification and the frequent evolution of gaseous by-products. Many authors [182], [208] have reported that significant fibre degradation happens during the reaction of the carbon fibres with the precursor materials. This can result in either stronger bonding to fibres or loss of the structural integrity of the fibres, either causing a reduction in the degree of toughening achieved. The use of interphases coated onto the fibres to protect from this degradation [182], [209] has shown some improvements in mechanical properties. Having said that, the interphase coating, which is often PyC or SiC, can reduce the penetration of UHTC powders into the fibre tows. As a result, the in-situ UHTC content is low in close proximity to the fibres, which could result in poor oxidation protection. Pores are also generated during the volume shrinkage from precursor phase to ceramic [208], [210]–[212]. Pores and cracks generally form as the precursors shrink and any gaseous reaction products are evolved. Whilst these pathways allow pressure release from within the ceramic, they also allow oxygen ingress during testing or when in use.

Ziegler et al. [211] reported that the volume changes produce residual compressive stresses at the fibre / matrix interface, which resulted in the embrittlement of the CMC as density increased. It was observed that the direction of the shrinkage, towards or away from the fibres, was highly dependent upon local geometry. Reduction of the number of PIP cycles was clearly dependent upon the ceramic yield of the material [211]. King et al. [213] increased the ceramic yield of a SiC precursor by up to 7% by heat-treatments of the liquid before pyrolysis, this removed the more volatile oligomeric precursors that limited the ceramic yield. Heat treatments can also improve the rheological properties of the precursor liquid; Ziegler et al. [211] observed that by choosing precursors capable of chemical cross-linking at lower temperatures allowed the precursor to solidify within the reinforcement, minimising losses due to evaporation

or dripping as a result of gravity. Ziegler et al. [211] further suggested that precursors which underwent addition rather than condensation mechanisms were preferable in that mass loss and the creation of porous channels were both reduced. The wetting and rheological properties also need to be tuned whenever possible. The PIP process fills porosity by capillary pressure and Yan et al. [212] noted that high volumes of intertow porosity are apparent; superior interfacial energy balances between the substrate, precursor and atmosphere would result in superior coating and infiltration of the precursors.

Reactive melt infiltration

Reactive melt infiltration (RMI) is the introduction of a molten metal, typically zirconium in the case of UHTCMC fabrication, into a porous fibrous preform in-situ where it reacts with either pre-matrix carbon or boron phase to form the UHTC phase with a high matrix density. This is not an iterative process, hence there must be a high ceramic yield with the correct molar and spatial balance of pre-matrix, typically deposited by CVI (see next section), and the reactive melt to form a dense homogeneous matrix [207] as shown in Fig. 9. This is the technique, for example, that has been pioneered for the mass production of SiC_f/SiC CMCs by General Electric [214] for their advanced civilian aerospace engine. These CMCs were the first to be used commercially in the civil aviation industry on General Electric's CFM LEAP engines [214] that were launched in 2016.

The reactive metal infiltration processes has several advantages[215], [216]: (i) it produces a near fully dense matrix; (ii) the processing time is shorter than for most ceramic matrix composite fabrication processes and is subsequently relatively cheap; (iii) the closed porosity at the surface can often eliminate the need for a final oxidation resistant coating and (iv) a reaction bonded UHTC matrix is effectively produced.

The major disadvantages to this process are three-fold. For fibre composites the high temperatures required for reactive metal infiltration exposes the carbon fibres to very aggressive molten metals, often above 1400°C [217]. The exothermic nature of the reaction between constituents can also further increase the temperature locally, causing more damage [217]. The metal in this form is highly reactive and, if infiltration

1 conditions are not strictly controlled, serious degradation of the carbon fibre preform
2 [207], [218]–[220], Fig. 9a, will occur leading to deleterious consequences on the
3 properties [216]. Often interface materials are needed to protect the fibres, as the CVI
4 matrix is not sufficient to protect the fibres entirely [197], [218], such methods have met
5 with limited success so far. The other major issue is the 5-10 vol% residual metallic
6 phases [217], as shown in Fig. 9b [216], which have relatively low oxidation resistance
7 and a lower melting point than the ceramic phases present. This metallic phase can lead
8 to accelerated creep, crack propagation and further attack when the material is operating
9 at high temperature [221], [222]. The final issue is due to the molten metal needing to
10 react with the CVI matrix to form the UHTC in-situ; the reaction rate is limited by a
11 number of factors, including: available surface area per volume, the molar volume of
12 the UHTC produced, the thickness of the reaction barrier and the rate with which the
13 fibre preforms becomes saturated [223]. One of the pivotal characteristics of the RMI
14 process is the wettability of the transition metal alloy on the substrate. Table 6 [207],
15 [220], [224]–[232] describes a number of alloying elements that have been successfully
16 used to introduce zirconium into carbon fibre preforms to form ZrC and ZrB₂ in-situ.
17 The literature is very limited in terms of hafnium infiltration and non-existent in terms
18 of the production of hafnium diboride via this method to date. It is assumed that due to
19 the proximity of hafnium and zirconium in the periodic table, the alloying elements
20 needed to improve wetting characteristics will be somewhat similar as their effective
21 nuclear charge is similar [233].
22
23
24
25
26
27
28
29
30
31
32
33
34
35
36
37
38

39 The RMI process is attractive for fabricating high density, continuous fibre
40 reinforced UHTC composites. However, the process has limitations such as the
41 presence of residual metal phase, liquid metal corrosion of fibres, etc. as discussed more
42 generally above [223]. Nevertheless, as stated it has already been commercialised for
43 SiC_f – SiC_m composites [214].
44
45
46
47
48

49 **Chemical vapour infiltration processing**

50
51
52

53 The use of chemical vapour infiltration (CVI) to deposit UHTC matrices is still
54 very much a developing processing technique in the densification of UHTCMCs.
55 However, there has been a relatively large body of research conducted on the deposition
56 rather than infiltration of said matrices using chemical vapour deposition (CVD), a
57
58
59
60
61
62
63
64
65

1 somewhat similar process. CVD works on the same basic principal of the thermal
2 decomposition of a reactive gaseous mixture to form a solid product [234], in this case a
3 UHTC layer or coating. It is proven that UHTC coatings deposited by CVD on C/C
4 substrates can provide enhanced oxidation resistance and reduce ablation rate up to one
5 order of magnitude [10], [235]. This is accompanied by the production of a number of
6 chemical by-products, typically HCl and HF, which are exhausted out of the reaction
7 chamber along with any unreacted precursor gases. It is a relatively low temperature
8 and low-pressure densification route compared to other advanced manufacturing
9 methods and can be very versatile since a wide range of material compositions can be
10 produced, as shown in Table 7 [236], [237]. Fig. 10 presents a schematic of the growth
11 of the ceramic deposit on the cross section of the fibres to the point of full densification
12 by CVI.
13
14
15
16
17
18
19
20
21

22 The resultant solid deposit is dense, fine grained (from a few to hundreds of
23 nanometres) and potentially free from impurities if processing is controlled correctly
24 [236], [237]. It is particularly suitable for the deposition of carbides and borides, which
25 otherwise require high-temperature processing based on sintering techniques. Multiple
26 compositions can also be infiltrated by alternating the gaseous precursors introduced
27 into the reaction chamber [235], [238]–[241]; giving the ability to tailor microstructures,
28 which can also be controlled by tuning the process parameters including temperature,
29 chamber pressure and feed rate of the precursor. The main advantages and
30 disadvantages of CVI are summarised in Table 5.
31
32
33
34
35
36
37
38
39

40 Isothermal CVI, ICVI, is the most well-known and commonly used process by
41 industry and although the benefits are evident, ICVI (Fig. 11a) suffers from a main
42 drawback. The deposition occurs preferentially near the outer surface where the
43 concentration of reactants, and often the temperature, is highest [237]. As a result,
44 “crusting” occurs and seals the porosity at the surface of the preform prematurely, this
45 requires the infiltration to be stopped and the porosity to be reopened by machining. In
46 order to reduce the extent of crusting, the possibilities are to: i) decrease the process
47 temperature, though this decreases the deposition rate and hence increases the process
48 time, or ii) work at reduced pressure improving the gas diffusion in the preform.
49 Nevertheless, as result of crusting, the processing time can be up to 2000 hours and
50 hence the process is not cheap [242]–[244].
51
52
53
54
55
56
57
58
59
60
61
62
63
64
65

Overall, the process is complex because it requires detailed awareness of the reaction chemistry, kinetics, temperature distribution, heat source, pressure and preform geometry [245], [246]. The final microstructure depends on all these variables and hence so do the thermo-mechanical properties. On this basis, a variety of CVI processes have been developed which can be classified by: i) temperature, ii) pressure and iii) heating method [247] as shown in the Table 8 [242]. For example, the deposition can be conducted in both hot-wall and cold-wall reactors, at chamber pressures as low as $100 - 10^{-1}$ Pa or at above-atmospheric pressure, with and without carrier gases, and at temperatures typically ranging from 200-1600°C. There are also a variety of enhanced CVI processes that involve the use of plasmas, lasers, hot filaments, or combustion reactions to increase deposition rates and/or lower deposition temperatures. A thermal gradient can be applied as shown in Fig. 11b, radiantly or inductively, to the fibre preform [242], [248]. This gradient causes the deposition to occur preferentially in the hot zone at a faster rate and the densification front then proceeds from the hotter zone toward the cooler region as the hot zone moves as a result of the changing thermal conductivity of the product. The gas phase flows into the cooler side of the preform so that the gas does not encounter a sealed region and can proceed unimpeded to the reaction zone. The advantage is a shorter infiltration time compared to isothermal CVI, typically only about 120 h. One preform can be densified per run, however, and controlling the deposition is difficult without very sophisticated and hence expensive temperature control systems [242].

In terms of kinetics of the ceramic deposition from the gas phase, this is highly dependent on the processing variables and is gaseous species specific, though reaction rates have been described in a number of models [249]–[253]. In terms of the physical deposition rate, this is again reported for UHTC matrices in the CVD literature and can be somewhat translational in terms of the ceramic material deposited, though due to the diffusion times being slower in CVI rates are always lower [249].

In summary, the CVI process is very useful in that it enables the formation of reasonably dense, complex-shaped components at low processing temperatures that do not damage the fibres used for reinforcement. There is also the ability to create different matrix compositions and to achieve high purity whilst tailoring the microstructure. However, it is an intrinsically slow process and therefore the product can be expensive.

Amongst the different variations developed to overcome the limitations, one of the most promising currently is the use of microwave or radio frequency energy assisted CVI due to the ability to create an inverse thermal gradient profile, Fig. 11f, compared to conventional heating, Fig. 11a. This greatly reduces the process times, whilst retaining all of the advantages of the fundamental CVI process. However, it should be noted that this process is still limited to laboratory scale and so further work is needed before it can be commercialised. Currently there is no published literature showing fully dense UHTCMCs but such work is currently underway throughout the world [254].

Slurry impregnation process

The slurry impregnation process (SIP) is perhaps the most common technique used to produce continuous fibre-reinforced ceramic composites. This process involves impregnating the fibres / woven fabrics by introducing a slurry made out of matrix powder. The slurry is generally prepared by ball milling the powder along with a binder and dispersant in a suitable solvent (aqueous or non-aqueous) using appropriate milling media that matches with the matrix material in terms of composition (to reduce deleterious impurities) and hardness [255]. After impregnation, the organics are removed in the drying stage and, if required because the powder is a precursor, the 'green' composite can be pyrolysed at elevated temperatures in a controlled atmosphere to avoid fibre degradation. The powder introduced via the slurry to create the matrix could have one of several different compositions or a mixture of them, including SiC, UHTCs, or their precursors.

Lange et al. [256], reported that the impregnation of a dry, porous medium with slurry typically occurs by capillary forces and / or applied pressure. The flow of liquid into a porous medium by differential pressure, ΔP , is described by Darcy's law:

$$h = (2K\Delta P/\eta)^{1/2} t^{1/2} \quad (1)$$

where h is the distance the liquid penetrates in a time period t , K the permeability of the porous body and η is the viscosity of the slurry.

The permeability has been related with the pore size [257]:

$$K = \phi m^2 / k_0 \quad (2)$$

where ϕ is the pore fraction, m the mean hydraulic radius (pore fraction divided by the wetted surface area) and k_0 a constant.

Lange et al. [256] studied the factors influencing the infiltration of slurry into a porous structure, such as a fibrous preform, in detail and suggested that the particle-to-fibre diameter ratio plays a vital role in the packing density of the matrix powder around the fibres. The viscosity and the pore size of the preform are the key factors influencing the infiltration kinetics, which can be improved by increasing the capillarity and the external force applied. The latter can be achieved by either squeezing the fibres or preforms [18] or using pressure-assisted methods [10], [17], [258], but these techniques can open up undesirable voids between the fibres and/or deteriorate the homogeneity of the fibre orientations. To achieve a high enough densification level without risking damaging the structure of the porous body, several impregnation / pyrolysis sequences (typically 6 to 10 and sometimes even more) have therefore to be performed, which is time consuming and reduces the economics of the process.

When the required powder-to-fibre ratio is not met, the distribution of powder into the stacked fibres or preforms can fail to be sufficiently homogeneous across the sample; it is common for the powder to be concentrated in the first fabric layers at the surface. For example, Paul et al. [18] fabricated hybrid UHTC composites using 2.5D C-fibre preforms (containing 23 vol% fibres) using vacuum impregnation but only succeeded in getting ~7 mm of UHTC powder penetration into 17 mm thick samples, Fig. 12 [17], whilst Tang et al. [10] only obtained ~2 mm of penetration for 28 – 30 vol% fibre preforms, Fig. 13 [10]. Lee et al. [258] developed a modified infiltration technique using a mould with a deformable foil at the bottom, Fig. 14 [258]. When using conventional pressure casting, the relative density of the samples decreased with increasing slurry solids loading, a consequence of the incomplete infiltration of the slurry, but when the fabrics were subjected to deformation casting, the density increased even with increasing solid loading. Concentrated slurries with solids loading of up to 43 vol% have been successfully injected homogeneously into the fabrics [258].

A slurry injection method has been used by multiple authors to produce components of high ceramic homogeneity in fibre reinforcements characteristically

difficult to impregnate[61], [179], [186]. Very recently, Hu et al. [61] impregnated a 3D needle punched preform with an ethanol-based ZrC and SiC slurry to a green body relative density of 42% via this method, though the porosity distribution was not presented in detail, nor were the original fibre volume of the preforms reported. Extensive work done at the University of Birmingham[179], [186] has characterised the injection process for UHTCMCs, showing clearly with X-ray computed tomography (micro-CT) the development of the ceramic distribution via the injection method and the required parameters to maximise the extent of impregnation for HfB₂ slurries in 2.5D C_f preforms.

Other methods

The primary processing methods used, such as PIP, RMI, CVI and SIP, to create fine-grained UHTC matrices in continuous fibre preforms have been discussed in the previous sections. As indicated, each has its advantages and disadvantages. A number of other processes have been investigated, however, including: sputter deposition [259]–[261]; electroplating / electrophoretic deposition (EPD) [259], [261], [262]; electron beam irradiation [260], [263]; liquid precursor methods [260], [264], [265]; slurry coating [260], [266]; chemical liquid vapour deposition (CLVD) [267]; and pack cementation [260], [268], [269]. Each method offers specific advantages in terms of control of material composition, deposit thickness or cost, enabling the development of a wide range of microstructures and configurations. As just one example, EPD requires only simple equipment and low cost operating conditions [262], [270], [271]. Nevertheless, these methods have not yet been explored extensively for UHTCMCs. A summary of the few available reports involving these techniques are briefly described below.

Pack cementation has been investigated by Li et al. [262], who incorporated a SiC nanowire – SiC – Si/SiC – ZrB₂ – ZrC matrix in a C/C composite via a three-step process involving pack cementation, EPD and a final pack cementation step. Meanwhile Tao et al. [272] prepared a ZrB₂ – SiC – Si/B-modified SiC coating on the surface of carbon/carbon composites by a two-step pack cementation process at 1900°C and Yao et al. [273] prepared a ZrB₂ – SiC coating on carbon/carbon composites also using a pack cementation process with Si, ZrB₂, and B₂O₃ powders at 1900–2200°C.

Corral et al. [274] developed UHTC coatings on C/C composites using inorganic–organic precursor solutions for infiltration and heat treatment at high temperatures (up to 2300°C) to convert them to borides and carbides. Zou et al. [230] infiltrated Zr melt into porous C/C to form ZrC coatings whilst Jayaseelan et al. [260] reported using a reactive infiltration process (RIP) to infiltrate porous carbon fibre reinforced carbon (C/C) composite hollow tubes with ZrB₂ particles by using inorganic–organic hybrid precursors of zirconium oxychloride (ZrOCl₂·8H₂O), boric acid and phenolic resin. He et al. [267] recently reported a CLVD process to prepare C/C – ZrC composites by using the precursors [(C₄H₈O)Zr₂]_n and liquid xylene (C₈H₁₀) in the temperature range of 800–1100°C and obtained a density of ~90% of theoretical.

Although these techniques enable the infiltration of nano-size particles and pure phase compounds, a major limitation is in achieving sufficient penetration of liquid precursors into preforms and hence the achievement of full densities. Many times, further densification has to be carried out by hot pressing, spark plasma sintering (SPS), CVI, etc. in order to obtain the required degree of densification. For example, Galizia et al. [275] produced C_f/ZrB₂ UHTCMCs by electrophoretic deposition (EPD) of ZrB₂ on unidirectional carbon fibers followed by ZrB₂ infiltration and hot pressing. More details on densification of UHTCMCs by hot pressing (HP), SPS, pressureless sintering (PS) and hot isostatic pressing (HIP) are given in the next section.

Sintering approaches

HP, SPS, HIP and pressureless

As applied to UHTCMCs, the hot pressing (HP) technique comprises three main steps [221]:

- 1) The continuous fibrous reinforcement is coated with interphase layers, typically pyrolytic carbon [276] or ceramic [275], [277] to enhance the fracture toughness of the composite and protect the fibres during pressing.

- 2) The continuous fibres are impregnated with UHTC particles in the form of slurry and consolidated by vacuum bagging [276], [278]–[280], or cold compaction/lamination [276], [277]. If short fibres are used as reinforcement [92], [95], [113], [114], [118] a

more traditional approach is the use of ball milling of the UHTC powders and short fibres as a slurry, followed by drying and uniaxial cold pressing.

3) The assembly is sintered at high temperature (1600-2100°C) and pressure (~20-100 MPa) by HP, HP, SPS or PS.

As a result of the high refractoriness of UHTCs, the temperature and the pressure applied need to be much higher compared to other manufacturing processes, e.g. CVI and PIP. One advantage is that the matrix is sintered and thus can contribute to the structural properties and act as thermal barrier for the carbon fibres; another is that the fibre content can be up to 70 vol% [279]. A high relative density is usually achieved (>90%) [278], [281] leading to a high modulus and strength to rupture.

The process is typically fast, taking approximately one working day for the production of the green composite and a few hours for sintering [279]. The high temperature and pressure involved during the sintering stage, however, are reported to be responsible for fibre degradation and chemical interaction between the fibres and matrix, which leads to the formation of strong but brittle phases at the interfaces [92]. As an example, the creation of carbides were ascribed to the carboreduction of the oxides impurities (ZrO_2 and SiO_2), naturally present in the UHTC powders, promoted by the carbon fibres [92], [95], [113] (see Fig. [113]). These phases dictate the mechanical behaviour of the UHTCMCs.

As a result, one of the main efforts has been to reduce the sintering conditions by using sintering aids. The use of, for example, 5 vol% of Si_3N_4 or 10 vol% of ZrSi_2 , TaSi_2 or MoSi_2 has been investigated because of their proved efficacy in promoting densification and oxidation resistance [95], [113]. Sintering temperature onset was shown to lie in the range 1550-1580°C, compared to at least 1900°C for the ZrB_2 [33]. Despite the reduction of the sintering temperature, the formation of SiC and ZrC surrounding the fibres was still observed. However, as discussed by Zoli et al. [281], despite the formation of brittle phases, pull-out still occurs because of the onion-like structure of the carbon fibres. It has also been reported that other mechanisms of toughening are activated, either crack deflection [275] or, in weak matrix composites such as porous $\text{C}_f\text{-ZrB}_2$ [279], with a fracture mechanism similar to that which occurs in oxide-oxide CMCs [282]. Table 9 [275], [276], [278], [279], [281], [283] summarises

the thermomechanical behaviour achieved by hot pressed UHTCMCs, including microstructural and physical properties.

The sintering stage has also been carried out by spark plasma sintering (SPS) [110], [284], [285]. This enables the sintering of ceramics in a short time because of the high heating ramp rate ($\sim 1000^{\circ}\text{C}/\text{min}$) and reduced dwell time (a few minutes), potentially diminishing the interaction time of the fibre with the matrix [110]. The relative density of 96.7% achieved for samples of $\text{ZrB}_2 - \text{C}_f$ sintered at 1900°C was significantly higher than for analogous specimens produced by conventional hot pressing, which achieved only 85% of their theoretical density. Lee et al. [284] investigated the effect of temperature on the integrity of composites made of SiC fibres (Hi-Nicalon Type S with 200 nm of BN coating) in a matrix of ZrB_2 with MoSi_2 , B_4C and carbon additives. Brittleness of the composite was observed when sintering occurred above 1600°C ; it was ascribed to fibre degradation, growth of the ZrB_2 grains into the rather soft BN and the decomposition of BN due to the reaction with ZrO_2 , B_4C and C.

Relatively little work has been done on hot isostatic pressing, HIP, and pressureless sintering: temperatures as high as 2000°C have been employed for $\text{C}_f\text{-ZrB}_2$ with 20 vol% of SiC and a pressure of 105 MPa for $\text{C}_f\text{-TaC}$ sintered by HIP [277]. Nasiri et al. [117] used pressureless sintering for $\text{C}_f\text{-ZrB}_2$ composites but using temperatures in excess of 2100°C . Tallon has also used pressureless sintering for porous UHTCs [286], though these are not composites and hence will not be discussed further here.

In summary, hot pressing is the most common route for the processing of UHTCMCs and it both reduces the processing times and allows high densities to be achieved. However, the high pressure and temperature involved are detrimental for the integrity of the reinforcement. Use of sintering aids alleviate the sintering conditions, but they are often responsible of the formation of brittle phases at the interface fibre-matrix and, hence, only a marginal increase in the fracture toughness of the material is observed when they are used. SPS promotes densification at lower temperatures and in shorter times, but additives, external pressure and high temperatures (if compared to other manufacturing process such as RMI and CVI) are still required. Relatively few projects have explored the use of pressureless sintering and HIP for UHTCMCs although they have the advantage of manufacturing near-net shape components.

Material characterisation

The quality of the fabricated UHTCMCs can be determined by microstructural characterisation and the evaluation of mechanical and thermal properties. The influences of various methods of fabrication and the type of matrix and second phase on these properties are described in this section.

Microstructural characterisation

No matter which shaping approach is adopted, composites with fine grains and well distributed secondary phases are generally desired for the particulate / chopped fibre reinforced UHTCs [33]. The elimination of large agglomerates is helpful to reduce the size of the critical flaws and therefore improve the strength and reliability of the ceramics [287]. However, in practice, microstructures of UHTCMCs can be inhomogeneous and are highly dependent on the processing methods and preform used. For example, typical defects in the as-sintered 1D - C_f/ZrB_2 composite (stacked cross - ply 0 – 90°, Fig. 16) include lenticular-shaped voids and vertical cracks in the ceramic layer, Fig. 16a [279]. Further investigation indicated that micro- and macro-cracks generated by the TEC mismatch between the fibre and matrix could be reduced if the C_f bundles were aligned unidirectionally at the adjacent layers, Fig. 16b [281]. Moreover, the elimination of such defects could be realized by optimizing the green forming approach, although no details have been reported [288].

For the C_f - UHTC powder composites prepared by SIP technology (see section on SIP), the distribution of UHTC powder was related to the porosity in the preform, the direction of infiltration and the rheological properties of the slurry [10], [18], [179], [289]. Taking 2.5D - C_f preforms as an example, UHTCs powders were found to concentrate at the regions near the surface where the slurry infiltration occurred, Fig. 13a [10]. The as-infiltrated green body was subsequently subjected to an isothermal CVI process and the pyrolytic carbon (PyC) deposited on the fibre could be clearly seen, as shown in Fig. 17 [10]. The PyC was infiltrated into the voids between the carbon fibres and the UHTC particles, integrating the particles into the composites, Fig. 17. It worth noting that the powders prefer concentrating into the area near the surface and the random layers in the preform, Fig. 18 [18], during SIP, the random layer with larger

pore size and higher porosity was generated as result of the Surface Transform's needling process.

Typical microstructures for UHTCMCs prepared by PIP (see section on PIP) are similar to those of composites made using SIP. However, much finer UHTC particles (down to $\sim 1 \mu\text{m}$) could be seen in the sample produced by PIP due to the nature of the process; PIP involves pyrolysis of precursors [290], [291]. Taking a C/C–ZrB₂–ZrC–SiC composite as an example, submicron-sized ZrB₂, SiC and ZrC particles were found to pack loosely in the voids between the carbon fibre bundles, Fig. 19a [290]. Large agglomeration with a core (ZrB₂) - shell (ZrC-SiC) structure can also be seen in this sample, Fig. 19b [290]. Since the viscosity of the precursor is lower than that of typical powder-based slurries, the particles infiltrated deeper during PIP processing.

As described in section on sintering, HP & SPS are normally used to further densify green bodies prepared by SIP or PIP to reduce the porosity in the UHTCMCs. Fig. 20 [289] shows a typical interface in C_f/ZrB₂–SiC composites densified by SIP and HIP. Elemental mappings indicate that, apart from limited ZrO₂ particles, no other phase from the reaction between fibre and matrix were observed, Fig. 20 [289]. The interfacial reaction was avoided by impregnation of the slurry prepared from nano-sized ZrB₂ into the C_f preform. Benefiting from the better sinterability of nano-sized powders, the post - sintering temperature for such composites was reduced to 1400°C [292].

Although reports of ZrC and ZrB₂ CVD coatings on the C_f preforms exist [293], investigations into the use of CVI to deposit a UHTC matrix in fibre preforms are rather limited.[249]. The most widely infiltrated substances during CVI are C and SiC. The effect of the interface with the carbon fibre and its influence on ZrC powder infiltration and the subsequent SiC - CVI process was investigated by Wang et al. [294]. The resulting images with different interfaces are compared in Fig. 21 [294]. Carbon deposition (or C - SiC deposition) on the carbon filaments facilitated the connection of the fibres, which retarded the further infiltration of ZrC particles into the wrapped carbon bundle. Therefore, a higher ZrC percentage was realized in the composite without a carbon interface, Fig. 21a.

Typical microstructures of UHTCMCs densified by RMI are compared in Fig. 22 [295]–[297]. Firstly, as indicated previously, RMI normally results in a high relative

density for the UHTCMC, hence, as expected, limited porosity can be observed in either the C_f/ZrC [295] or $C_f/ZrC-SiC$ [296] composites. Secondly, according to the different reactions during RMI, trace amount of unreacted materials with lower melting temperature are typically found as the residual phase in the final samples, e.g. α - Zr in C_f/Zr , Fig. 22a, and $ZrSi_2$ in $C_f/ZrB_2-SiC-ZrC$, Fig. 22c & d. In a recent study [297], $(Ti, Zr)C$ formed from a metal melt of $Ti_{0.8}Zr_{0.2}$ and PyC during RMI could be further converted into $Zr_{0.8}Ti_{0.2}C_{0.74}B_{0.26}$. The microstructure of this novel composite was composed of a surface $Ti-Zr-B-C$ coating and $C_f/Ti-Zr-B-C-SiC$ matrix, as shown in Fig. 22e. PIP could also be combined with both RMI and CVI in order to achieve better microstructures for improved desired properties [294]. $C_f/ZrC-SiC$ composites were fabricated via RMI of Si into $C_f/ZrC-C$ preforms [296]. The protective PyC coating on the C_f was generated by CVI, whilst the slurry infiltrated ZrC particles consumed the molten Si during the RMI process, which resulted in forming $ZrSi_2$ and SiC products and a much denser and finer microstructure was obtained, Fig. 22c & d.

In summary, as expected, the microstructure obtained depends very strongly on the process route used to prepare the UHTCMCs and the microstructure, as well as the composition, directly affects the resultant properties. Hence it is essential to design the microstructure and then select the best processing route to achieve it if the targeted properties are to be obtained. To achieve this with UHTCMCs, a combination of two or more techniques, yielding a hybrid process route, may be the best route forward [249].

Mechanical Properties

As a baseline material for UHTCs, the strength, fracture toughness and hardness of ZrB_2-SiC particle reinforced composites (ZS_p) have been the most investigated [33]. Results have shown that the fracture strength of ZS_p at room temperature has more relied on the grain size of the SiC rather than that of the ZrB_2 ; when the SiC particle size increased in ZrB_2-SiC systems, both the strength and toughness of the ceramics decreased accordingly [298]. The high temperature strength of UHTCs has been found to be related to the grain boundary phase; the softening of these phases causes the strength degradation at elevated temperatures [188], [299]–[302]. By removing the oxide impurities via adding WC in ZrB_2-SiC , strong $ZrB_2-SiC-WC$ ceramics without strength degradation up to 2000°C have been successfully developed [303]–[305]. The

mechanical properties of monolithic and particulate reinforced UHTCs have been well reviewed; interested readers can find more information from [33]. This chapter will therefore focus mainly on the mechanical properties of UHTCMCs.

The flexural strength and elastic modulus of selected UHTCMCs are compared in Table 10 [179], [192], [227], [279], [281], [294]–[296], [306]–[308], together with the open porosity. It can be seen that samples produced using RMI result in lower open porosity, typically <10% [191], [227], [296], [306]. When an additional and subsequent hot-pressing stage was utilised, even lower open porosity, <5%, was observed [281]. The pore / filler size and its distribution in the porous preforms are also very important for reducing the voids in composites, since they are related to the capillary pressure driving force for the melt during RMI. It is worth noting, however, that lower open porosity doesn't always mean higher flexural strength. In fact, the flexural strength values of many UHTCMCs, especially those produced by RMI, are typically less than 200 MPa. Low strengths have also been observed for samples made by hot pressing (HP) stacked 1D or 2D fabrics [279]; detailed investigations showed that defects such as cracks and voids were readily observed in these samples [191], [227], [279], [295], [307]. For both the RMI and HP, the low strengths probably result from the presence of residual stresses, which, in turn, will arise during cooling after densification as a result of CTE mismatch between the matrix, fibre and / or unreacted alloy. Defects are most likely to occur in the dense samples where there is no free space to release the stress, reinforcing the reason why the strengths are typically lower for composites made by RMI and HP compared to materials formed by a combination of PIP and CVI [294]. A detailed discussion about the effects of residual stresses on thermal damage accumulation in C_f reinforced UHTCs can be found elsewhere [309].

Interestingly, $C_f/ZrC-SiC$ samples obtained by a modified RMI route (infiltration of Si into nano-porous $C_f/ZrC-C$ preforms prepared by colloidal processing) show a much higher strength of ~380 MPa [296]. The authors argued that the excellent mechanical performance could be attributed to a denser microstructure, limited Si or C residue, no interphase degradation and some reinforced elements in the matrix. By carefully reducing the volume of large defects, UHTCMCs densified by post-HP have also been shown to exhibit excellent mechanical properties and non-brittle behaviour during flexure up to 1500°C [281].

For C_f-UHTC composites in which densification was achieved using CVI to deposit a carbon matrix within carbon fibre preforms containing impregnated (and unsintered) UHTC powder, a comprehensive understanding of the mechanical performance has been provided by Rubio et al. [179]. Whether under bending, compression or shear test, C_f plies with 0° orientation exhibited higher resistance to the stress than the 90° plies and the random orientation layers. Also, no tensile strength degradation was found for these composites up to 1000°C.

Although the fractural toughness is important for monolithic ceramics, its value hasn't been reported for UHTCMCs very often, especially for composites not densified by sintering. It should be noted that K_{IC} refers to the critical value of the Mode I stress intensity factor that is measured when the plane strain condition is satisfied at the crack tip [310]. However, due to the different fibre arrangements, the existence of interfaces and the fracture of the fibre & matrix, different fracture modes for cracks, including but not limited to mode I, mixed I / II and mode II, might coexist during a fracture toughness test [311], [312]. Therefore, in UHTCMCs, the definition of K_{IC} has generally not been strictly followed, nevertheless, the limited results available show that the incorporations of continuous fibres into UHTCs do significantly improves K_{IC}. For example, the fracture toughness (determined by the chevron notched beam method) for 2D-C_f/ZrB₂ – SiC – Si₃N₄ fabricated by slurry infiltration and hot-pressing reached $9.6 \pm 0.7 \text{ MPa m}^{1/2}$ [281], a much higher value than that for ZrB₂-SiC ceramics hot-pressed under similar conditions ($3 - 5 \text{ MPa m}^{1/2}$) [313], [314]. Even the K_{IC} of 1D-C_f/ZrB₂ – SiC composites [288] varied from 4.75 to 8.35 MPa m^{1/2}. The load-displacement curves of all the samples during the toughness measurements displayed quasi-brittle fracture behaviour and significant fibre bundle pull-out, whilst individual fibre pull-out was observed for samples with a higher K_{IC} and weaker fibre / matrix interface. This work, however, is mainly focused on toughness arising from crack initiation resistance, which can be regarded as rather simplistic. Compared to the particulate reinforced composites, fibre reinforced composites are expected to exhibit significant extrinsic toughening resulting from the pull-out of fibre with the crack propagation. Hence, initiation toughness may not be very useful as a design parameter. Unfortunately, the crack resistance curve, or R curve (material resistance as a function of crack extension [315], hasn't been well explored in the field of UHTCMCs. Limited results from fibre-glass composites [316] show that the crack resistance is dominated by frictional dissipation

upon the pull-out of fibres, which fracture in the wake of the crack plane. Even when the initial toughness was at a similar level, a significant increase in crack resistance was observed in the composite when fibre pull-out was extensive. This suggests that, as for other composites, both the crack initiation and crack propagation resistance of UHTCMCs can be further improved by optimising the interface between the fibre and the matrix. A thorough analysis of the crack resistance curve for UHTCMCs is necessary to develop the understanding of their fracture toughness.

According to the above discussion, it is clear that controlling the fibre pull-out in a fibre-reinforced material is crucial to maximizing their mechanical performance. The latter occurs when crack deflection along a fibre/matrix interface becomes easier than its penetration through the fibre. He & Hutchison [317], [318] found that this competition was reliant on the ratio of the fracture energy of the interface (G_c^i) and the fibre (G_c), as illustrated in Fig. 23 [124]. The Dundurs' parameter (α) in the x - axis could be calculated based on the plane strain modulus for the fibre and matrix, according to Eq. (3-5).

$$\alpha = \frac{\overline{E_f} - \overline{E_m}}{\overline{E_f} + \overline{E_m}} \quad (3)$$

$$\overline{E_f} = E_f (1 - \nu_f^2) \quad (4)$$

$$\overline{E_m} = E_m (1 - \nu_m^2) \quad (5)$$

Here, subscripts f and m refer to the fibre and the matrix, respectively. \overline{E} is the plane strain modulus for the phase x ; E_x and ν_x are the elastic moduli and Poisson's ratio for the fibre and matrix.

According to Fig. 23, when the fibre modulus is significantly larger than that of the matrix, crack deflection along an interface is favourable for a wide range of G_c^i/G_c values and so the relative strength of the interface is not critical. Porous UHTCMCs can be classified in this way, since the modulus of the porous matrix (porosity up to about 50 – 60 vol%) is likely to be lower than that of the carbon fibre. However, if the modulus of the fibre is similar to or smaller than that of the matrix, the ratio G_c^i/G_c must

be small enough (on the order of 0.25-0.5) in order to facilitate fibre pull-out [124]. Pressure-sintered UHTCMCs and composites densified by RMI usually have a denser matrix and hence a higher modulus (e.g., the modulus of TORAYCA® T700 C_f and dense ZrB₂-SiC ceramics are 230 and ~450 GPa, respectively) and thus belong to this category. Therefore, a weak interface must be created between the fibre and matrix to reduce the G_{ic}, this is usually achieved using either amorphous carbon or *h*-BN [124]. Such an interface engineering strategy has been well developed for the processing of CMCs [124] and has recently also been applied in the field of UHTCMCs. Silvestroni *et al.* [319] found using Si doped BN-coatings on Hi-Nicalon fibres within 25 vol% continuous SiC_f reinforced 65 vol% ZrB₂- 10 vol% ZrSi₂ composites results in a much higher inelastic work of fracture ($108 \pm 21 \text{ J/m}^2$) compared to their counterparts without the coating ($30 \pm 8 \text{ J/m}^2$). Hu *et al.* [320] also found that C_f/ZrC-SiC composites with a PyC coating on the C_f exhibited a much higher work of fracture and fracture toughness at room temperature compared to the same composites without the coating although the existence of such a soft interphase slightly lowered the fracture strength of the composite [319], [320]. In addition, it is essential to avoid any possible reactions between the fibre and matrix during post-processing and the service of the composites since this can undo any benefits gained by controlling the fibre / matrix interface strength. In both of Silvestroni's [319] and Hu's [320] work, the interfaces, either in the form of BN or PyC, were found to effectively hinder the fibre degradation during processing by reducing the reactions between the fibre and the matrix.

Residual stresses and their distribution within the composite can also affect fibre pull-out and the degree of toughening achieved. Residual stresses can accumulate in any ceramic matrix composites during cooling from the processing temperature as a result of the thermal expansion mismatch between the fibres and the matrix. In pressure-sintered UHTCMCs that have achieved high density, residual stresses can occur both in the direction normal and parallel to the fibre. In order to facilitate the pull-out of the fibre, tensile stresses in the radial direction should exist at the fibre-matrix interface; such condition can be met when the thermal contraction of the fibers is higher than that of the matrix. Unfortunately, C_f has a negative coefficient of longitudinal thermal expansion. Its axial CTE values depend on the modulus, e.g. CTE values of carbon fibre with moduli of 200-300 GPa and 700-900 GPa are $0.4\text{-}0.8 \times 10^{-6}/^\circ\text{C}$ and $1.6 \times 10^{-6}/^\circ\text{C}$, respectively [321]. Such values are much smaller than those for the UHTC matrix, e.g.

6.8 $\times 10^{-6}/^{\circ}\text{C}$ for ZrB_2 [322]. Therefore, an interface layer must be coated onto the fibres to alter the compressive radial stresses developed in them.

Understanding the mechanical properties of UHTCMCs at elevated temperatures is essential for understanding their performance in the service environment. Although very limited results have been reported to date, some have been very encouraging [281], [323]. For example, Zoli et al. [281] found the flexural strength of $\text{C}_f/\text{ZrB}_2\text{-SiC-Si}_3\text{N}_4$ increased from 360 MPa at RT to 550 MPa at 1500°C , this composite also exhibited excellent thermal shock resistance. Very recently, Ding et al. [323] reported that the interphase between fibre and matrix played an important role on the high temperature strength of C_f/SiBCN . A SiC / PyC coating on the fibre effectively avoided the degradation of the interphase and enhanced the load transfer between the fibre and matrix, therefore the strength of $\text{C}_f/\text{Si-B-C-N}$ was maintained to 1600°C . The importance of interphase on the mechanical properties of UHTCMCs has also been highlighted elsewhere [294].

The long-time-service properties of materials subjected to cyclic (fatigue) and constant (creep) loading are critical for certain applications of CMCs, for example SiC_f/SiC composites [324], though no results have been found to date for UHTCMCs. The reason for the latter may be because much of the focus of the present work is on applications that only need short service lives, typically seconds to a few minutes [18], [183], [325]. As applications are considered that require much longer service lives, it is likely that more attention will be given to these properties. It is assumed that, as for other CMCs, these properties are likely to be highly reliant on the performance of the fibre, the crack initiation resistance of the matrix and the sliding resistance between the fibre and the matrix [33].

Thermal and electrical properties

Properties such as thermal conductivity, specific heat capacity (C_p), coefficient of thermal expansion (CTE) and electrical conductivity are important for many high temperature applications and these can be significantly influenced by the presence of second phases. In addition, continuous fibre reinforced composites often exhibit anisotropy, especially in their thermal conductivity and CTE, and the thermal and electrical properties can be significantly affected by the level of residual porosity

present. Thus, for many applications where the thermal and electrical properties are critical, the chemical composition, fibre preform structure and the densification route of the UHTCMCs will all need to be strictly controlled. Details on a range of properties are given in Table 11 [38], [58], [98], [116], [118], [205], [210], [221], [322], [326]–[343].

Coefficient of Thermal Expansion (CTE)

In general, UHTCs and UHTCMCs are need to have a small coefficient of thermal expansion (CTE) because a large value can cause instability on the local surface at high temperature as a result of an imbalance in internal thermal stresses. Comparing the data in Table 11, the CTE of each UHTC fluctuates near $7 \times 10^{-6} \text{ K}^{-1}$, the variation with temperature being relatively small and the difference between transition metal carbides and borides not very large. From the energy point of view, generally stronger bonds between atoms can result in lower CTE. The CTE of the monolithic UHTCs can be affected by the presence of doped second phases such as MoSi_2 , TaSi_2 , ZrSi_2 and SiC . Pienti et al. [98], [333] found that doping with SiC significantly reduced the CTE of HfC and TaC because of the lower CTE of SiC ; whilst doping with TaSi_2 or MoSi_2 caused only a minor change in value. It was also observed that residual porosity increased the CTE, so achieving a denser UHTC reduced the CTE. Zimmermann et al. [322] also reported that the addition of 30 vol% SiC to ZrB_2 resulted in a decrease in CTE, however only at higher temperatures (1300 – 1675 K), whilst at lower temperatures (300 – 1300 K) this effect was not observed.

The CTE of UHTCMCs is significantly lower than that for the corresponding UHTCs due to the much lower CTE of the carbon fibres (C_f), Table 11. The presence of C_f can also cause anisotropy; Paul et al. [183] showed that in the plane of the C_f , the CTE reflects the value for C_f whilst perpendicular to the C_f the CTE depends more on the matrix and the presence of porosity and cracks. The large difference in CTE between carbon fibre and UHTC matrix can also yield residual stresses, as discussed in the mechanical properties section above.

Thermal Conductivity (k_{TH})

At present, obtaining values for the thermal conductivity of UHTCs or UHTCMCs mainly relies on experimental determination since there is no theoretical equation with sufficient accuracy. It can be seen from Table 11 that the K_{TH} of the borides is higher than that of the carbides, this is due to the lower atomic weight yielding a higher Debye temperature. However, the K_{TH} of the two types of UHTC are inversely related to the temperature; increasing temperature causes the K_{TH} of borides to decrease whilst that of carbides increases. Like CTE, the K_{TH} of the materials can be modified by addition of second phases. For example, Guo et al. [339] indicated that introducing $MoSi_2$ into ZrB_2 leads to a decrease in K_{TH} , whilst 5-30 vol% SiC increases K_{TH} , a result also found by Mallik et al. [334], [344].

A range of reports [333], [340], [343], [345], [346] have indicated that the presence of defects, such as porosity, can significantly reduce K_{TH} . This is partly because the K_{TH} of gases is close to zero and partly due to phonon scattering, thus denser materials, as expected, have higher K_{TH} values.

Specific Heat Capacity (C_p)

It is well known that the specific heat capacity (C_p) is one of the basic properties of matter, depending on the composition of the material. Since carbon atoms are larger and heavier than boron atoms, the C_p of borides is larger than for the corresponding carbides at the same temperature. Addition of second phases with higher C_p values also therefore increases the C_p for UHTCs and UHTCMCs. For example, both Guo et al. [339] and Tian et al. [346] showed that introducing SiC raises the C_p of UHTCs.

Electrical conductivity

Carbon fibres are considered to be a medium electrical conductor with electrical conductivities in the order of $10^{-3} \Omega \text{ cm}$ [347] and many studies have focused on improving the electrical properties of composite materials; however, this is currently not a major research direction for UHTCMCs. Temperature and doping level are two parameters that can significantly affect the electrical properties of the materials. For UHTCs and UHTCMCs, the most effective way to increase electrical conductivity is doping and literature values are given in Table 12 [339], [348]–[350]. Guo et al. [339] studied the introduction of different proportions of $MoSi_2$ and SiC into ZrB_2 and found

that the electrical conductivity decreased with an increase in MoSi₂ or SiC content, which was due to the lower intrinsic electrical conductivities of the dopants. Similar studies by Mallik et al. [334] and Zhang et al. [348] on ZrB₂-SiC and HfB₂-SiC also reported that the resistivity of composites increased with increasing volume content of SiC across the range 5 – 40 vol%.

From a structural point of view, a denser and less defective material can achieve higher electrical conductivity since defects such as porosity, cracks and interfaces all reduce the conduction path, a result confirmed by Guo. et al. [328]. The electrical conductivity of UHTCMCs is also likely to be anisotropic due to the use of C_f; the conductivity is higher in the plane of the C_f tows for 2D and 2.5D-based composites.

Emissivity

The modification of the emissivity of the material is a method for actively increasing the heat transfer rate of the surface of the material. Current doping studies for UHTCs focus on two major directions, one of them is the use of rare earth doping [351], [352] whilst the other branch involves using transition metal silicides [353]–[356]. The work to date, however, has only focused on the modification of UHTCs rather than UHTCMCs. Nevertheless, the same principles will apply and hence there is the possibility to change the overall emissivity of the composites by changing the ceramic phase composition or using a high emissivity coating [353].

For UHTCs, Tan et al. [351], [352] have indicated that samarium doping can increase the emissivity of ZrB₂ – 20 vol% SiC, although the trend varied with temperature. Doping with 5 mol% Sm(NO₃)₃ yielded the highest emissivity ($\epsilon=0.91$) though the results should be treated with caution since they were obtained from UHTCs subject to oxidation and ablation and hence a change of surface topography. Balat-Pichelin et al. [353] pointed out that doping with 5% Si₃N₄ can be beneficial to increasing the emissivity of the base material ZrB₂ – 15% SiC_f and the emissivity increased with temperature (~0.75 at 1200 K and ~0.90 at 1750 K). Du et al.'s [354] research on TaSi₂-based and MoSi₂-based coatings showed that increasing material density is beneficial with respect to increasing the emissivity and that it is necessary to prevent the oxidation of the coating to maintain the emissivity. Shao et al. [356] had similar results from research on WSi₂ – MoSi₂ – Si – SiB₆-borosilicate glass coatings.

Ablation and Oxidation

Testing methods and ablation

Table 13 [18], [109], [181], [182], [187], [197], [198], [207], [209], [210], [222], [227], [229], [357]–[371] summarises the methods used for testing UHTCs and their composites under conditions simulating launch and re-entry environments to different degrees. Typical re-entry conditions can include: heat flux enthalpies of 20 MJ kg^{-1} , speeds of Mach 7 to 9, mass flow rates of 75 g s^{-1} [45], combined with plasmonic and dissociating environments. The goal is to understand the underpinning thermal ablation mechanisms so that improved materials can be developed. Different test methods include: laser ablation methods [372], [373], arc jet [45], [374], [375], scramjet [376], high velocity oxyflame (HVOF) [109] and oxyacetylene torch (OAT) testing [17]. Amongst the test methods, HVOF and OAT are the relatively cost-effective screening techniques, whilst the others are costlier and available only in a few select locations in a handful of countries. It is extremely difficult to simulate the exact re-entry / hypersonic conditions at ground level, in a single method. Scramjet and arc jet methods are the closest to real use, but are extremely expensive tests to run. Oxyacetylene (OAT) and oxypropane (OPT) testing can reach similar temperatures and heat fluxes but the gas velocities are an order of magnitude too slow. They do form fast, cheap test methods though, that can be used for initial screening.

Laser ablation testing has been used to evaluate the ablation resistance of UHTCs in rapid tests that vaporise the UHTCs in a controlled atmosphere. The approach uses both continuous [372] and pulsed lasers [227] as a heat source and is able to test the materials at extreme heat fluxes of around 100 MW m^{-2} [377], enabling temperatures of about 3200°C to be achieved very rapidly. Whilst laser ablation can create extreme heat fluxes, the gas chemistries and high flow velocities of real applications are much more difficult to add in during testing, which is a significant disadvantage.

In HVOF testing, whilst the flame can reach supersonic velocities, e.g. Mach 2.5, which can induce useful mechanical stresses [109], the gas composition and heat fluxes do not approach those of real applications; e.g. a heat flux of only 2.5 MW m^{-2} was achieved. The required large sample dimensions are also a limiting factor.

Free-jet facilities have been used for high temperature testing in a sublimation regime [378]. It is an integrated testing system comprised of a hypersonic wind tunnel and arc / plasma heater [379] and is primarily designed to evaluate gas intake and engine performance in a supersonic / hypersonic flow. In this method, a conical nozzle is used to expand the preheated gas from where it is passed into a test section where the samples are mounted tangentially. The surface temperatures are measured using pyrometers; a stagnation temperature of 2400°C has been measured [380] and a heat flux of 4 – 6 MW m⁻² achieved [381]. The main disadvantage is the requirement of large, and expensive, test facility.

Similar to the free-jet method, the arc jet and scram jet tests are the best ground-based techniques, both of which simulate re-entry conditions reasonably well. The scram jet reproduces aerothermal conditions similar to actual flight, however, the gas chemistries are different from the atmosphere, since the temperature is not enough for the dissociation of gases to occur. It uses natural gases as the source in a combustion heater and the supersonic nozzle accelerates the test gas to a maximum speed of Mach 7. It provides opportunities to test both oxidation behaviour and the thermal stresses under extreme conditions, reaching test velocities of Mach 5 – 7 at heat fluxes of up to 12 MW m⁻². Arc jet testing simulates the most aggressive conditions to study the response of materials suitable for thermal protection systems, it also accounts for high fluid velocities and catalytic recombination effects [376]. It uses a plasma torch of typically 20 – 80 kW with inert gases (N₂ and Ar); the atmospheric air composition is simulated by adding O₂ into the test chamber. When the stream of plasma containing N₂/Ar enters the chamber at Mach 3, with an enthalpy of 20 MJ kg⁻¹, it reacts with O₂ to form disassociated mixtures of NO, N₂ and O at a low pressure of between 100 – 500 Pa. This allows the test samples to experience something close to the re-entry conditions of around 2000°C with a heat flux of 16 MW m⁻². However, the facilities are very expensive and not widely available.

OAT and OPT testing has therefore been developed, to determine the oxidation and erosion behaviour of UHTC materials. OAT testing can reach temperatures up to 3000°C and heat fluxes up to 17 MW m⁻² [187], whilst the equivalent figures for the OPT test are 2500°C and 6 MW m⁻² [187]. Interestingly, the gas velocity for both systems, which has been directly measured [382], were very similar at Mach ~0.6. The

flames involved can also be manipulated by varying the gas chemistry to be either oxidising, reducing or neutral and the distance between the flame and the sample and the angle the flame makes on contact with the sample can all be varied. As indicated, the disadvantages of this method are the absence of a plasma environment and hypersonic flow velocities, but measurements can be done very rapidly and at very low cost.

Oxidation

Most ultra-high temperature applications also involve exposure to oxidizing and corrosive environments, which demands resistance to oxidation, ablation and corrosion [53], [383]. The oxidation behaviour of non-oxide ceramics depends highly on the properties of the oxidation product and on the combination of physical and chemical processes taking place on the surface exposed to the oxygen containing atmosphere. In general, the chemical composition, structure and texture of an oxidized surface define the oxidation stability of a ceramic material [1]. However, the rapid oxidation of borides and carbides at $\sim 600^{\circ}\text{C}$ results in the formation of B_2O_3 , which evaporates at $\sim 1000^{\circ}\text{C}$, or CO/CO_2 [11], [53], [316]. It is reported that ZrB_2 is more protective compared to ZrC with respect to oxidation at up to 1200°C due to the formation of ZrO_2 containing a molten layer of boron oxide, whereas only porous ZrO_2 forms for ZrC , which is not protective to further ingress of oxygen [42]. A history of studies on the oxidation of diborides has been presented by Opeka et al. and others [30].

Over the past decade, researchers across the globe have investigated the oxidation behaviour of UHTCs (ZrB_2 , HfB_2 , ZrC , HfC , etc.) [22], [77], [386]–[390]. Modification of the chemical composition of the oxide surface layer, leading to decreased inward diffusion of oxygen, is one of the ways of controlling oxidation resistance of non-oxide ceramics. This modification can be accomplished by changing the bulk composition, or applying suitable coatings [1].

The poor oxidation resistance of ZrC is considered as a great restriction in applications at high temperatures in the presence of oxygen. Numerous studies [391]–[396] have been reported on the oxidation behaviour of ZrC and HfC with respect to the effect of temperature, time, oxygen partial pressures and sintering aids (type and its quantity). In general, the oxidation of ZrC is diffusion controlled as for other UHTCs

and oxidation appears preferentially along grain boundaries in sintered compounds [395]. It has been reported that the starting temperature of oxidation should be at 300°C for stoichiometric or nearly stoichiometric ZrC, independent of oxygen pressures [392]. Before the formation of zirconia, a thin intermediate layer of oxycarbide is believed to form owing to oxygen diffusion [391], [397]. At elevated temperatures, the crystalline oxycarbide layer can become amorphous, from which the cubic / tetragonal zirconia nanocrystals will subsequently form. The cubic ZrO-like oxide was also reported to form after low-temperature oxidation, as confirmed by measurements involving photoelectron spectroscopy [396], [398]. It is known that additions of higher valence metals into the ZrO₂ lattice will reduce oxygen vacancy concentration and diffusion, which reduce oxygen transport through the skeleton phase and so this may improve the oxidation / ablation resistance as well [1].

Relatively little research has been undertaken into the oxidation performance of UHTCMCs compared to UHTCs, mainly because UHTCMCs are still relatively new materials. There has been some work on the oxidation / thermoablation behaviour of UHTCMCs [254] and one of the primary goals has been to protect the fibres, and hence the fibre / matrix interfaces, from the oxidative environment since fracture toughness is one of the main properties of UHTCMCs. Fibre interface coatings can serve as reaction and diffusion barriers in aggressive operating conditions, protecting the underlying fibres from the oxidation [123], [399]. It is critically important that all the fibres are uniformly coated since poorly or uncoated fibres can bond to the matrix, increasing the fibre / matrix interface strength and hence reducing the likelihood of the crack deviating along the interface as discussed earlier. Oxidation of the fibre surfaces will also degrade the fibre properties leading to losses in fibre and hence composite strength [399].

A multi-layer SiC – Si – ZrB₂ coating, deposited by pack cementation on C/C composites [273], was reported to offer excellent oxidation resistance at 1500°C for more than 386 h due to the formation of an integrated layer of SiO₂-ZrSiO₄. The retention of 84% of the flexural strength after 20 thermal shocks between 1500°C and room temperature was also reported. A SiC nanowire – SiC – Si/SiC – ZrB₂ – ZrC coating was also deposited on C/C composites by a combination process of pack cementation and EPD [262] with a view to improving the oxidation resistance. Compared to a SiC – ZrB₂ – ZrC coating without nanowires, the EPD-SiC nanowire-

1 toughened coating showed a remarkably improved resistance for oxidation and thermal
2 shock, which was ascribed to the smaller size of cracks that were formed. It was
3 believed that the latter occurred by the nanowires helping to alleviate the thermal
4 stresses developed and increasing the coating toughness [262]. A combination of ZrB₂
5 or HfB₂ and SiC coated by CVD onto C/C composites exhibited protection against
6 oxidation, even in wet air [266].
7
8
9

10
11 Since the role of the second phase on oxidation behaviour remains
12 fundamentally the same irrespective of whether the material is a UHTC or a UHTCMC,
13 the majority of the discussion below is based on reports of the oxidation behaviour of
14 UHTCs.
15
16
17
18
19

20 The addition of silica formers or rare earth elements, notably silicides, SiC,
21 Si₃N₄, Ti₃SiC₂, Y, La, Eu, Ce and Yb, can reduce the oxidation rate through the
22 formation of a more stable borosilicate glass / rare earth (RE) oxides up to ~1600°C (for
23 Si formers) and >2000°C (for RE oxides) [67], [210], [221], [292], [300], [301], [314],
24 [316]–[318], [323]–[331]. Several groups have studied the effects of SiC additions on
25 the behaviour of Zr and Hf diborides or carbides when exposed to air at elevated
26 temperatures [325], [389], [390], [400]–[403]. The isothermal oxidised surface of the
27 ZrB₂-SiC-ZrC ceramic was oxidized to a white ZrO₂ phase, which was partially covered
28 with a thin SiO₂-rich layer at 1600 ± 15°C in 2 min. The thickness of the oxide layer
29 increased as the oxidation time increased to 40 min, with an accompanying increase of
30 the quantity of pores in the oxide layer [404]. Shaffer [405] and Pastor and Meyer [406]
31 evaluated the oxidation resistance of ZrB₂ with additions of the silicides of Ta, Nb, W,
32 Cr, Mo, Zr, Mo_{0.5}Ta_{0.5} and Mo_{0.8}Ta_{0.2}. Oxidation experiments with varying proportions
33 of MoSi₂ (1 to 20 mol%) were studied at 1950°C and the reported optimum composition
34 was 10 mol% for ZrB₂. The ZrB₂ + 10 mol% MoSi₂ composition was marketed by the
35 company Carborundum, USA, under the Trade name “Boride Z” [1], [405]. ZrB₂ + 15
36 wt% CrSi₂ composition was reported to be the most oxidation resistant by Pastor and
37 Meyer [406]. The flexural strength of the ZrB₂-SiC-ZrC **ceramics** oxidised specimens at
38 1400°C for 30 min were measured as 660 MPa, which is higher than that of the room
39 temperature value of 580 MPa [407]. The formation of the oxide layers resulted in: (i)
40 healing of the surface flaws, (ii) an increase in flexural strength, (iii) the formation of a
41 compressive stress zone beneath the surface oxide layers, (iv) a decrease in thermal
42
43
44
45
46
47
48
49
50
51
52
53
54
55
56
57
58
59
60
61
62
63
64
65

stress and (v) the consumption of thermal stress. These five aspects improved the thermal shock resistance of ZrB₂-SiC-ZrC ceramics. Thus the thin oxide layer formed acted as a passivation layer and prevented further oxidation, also healing defects and flaws [407].

One of the key findings based on Zr and Hf borides and carbides with Si-based additives up to temperatures of 1500°C are the formation of different grades of oxide layer, including: (1) a SiO₂-rich glassy layer on the surface (top layer), (2) a thin Zr/HfO₂-SiO₂ layer (intermediate layer) and (3) a Si-depleted matrix phase (beneath the above layer) and (4) the unaffected matrix phase [390], [401], [403], [404], [408]–[413]. The oxidation behaviour of TaC- and HfC-based composites was investigated with the addition of 15 vol% short SiC Tyranno SA3 fibres [98]. Several oxidation studies have been reported on continuous / chopped carbon / SiC fibre-reinforced UHTC composites with the additions of Si-based additives such as SiC, silicides [221], [274], [278], [279], [283], [414]–[426]. The oxidation behaviour of continuous carbon fibre reinforced ZrB₂-SiC ceramic composites was reported to reveal that above 15 vol% SiC content was required to form an homogeneous protective borosilicate glass that covered the entire sample and minimized fibre burnout [427]. A dense UHTC matrix ZrB₂ accompanied by a relatively strong C_f interface and SiC was reported to provide good oxidation protection [283]. The presence of 8 mol% W in ZrB₂ formed a WO₃ / B₂O₃ interface oxide layer that enhanced the ZrO₂ oxide scale adhesion to the composite [428]. Talmy et al. [429] reported that TaB₂ additions to ZrB₂-20 vol% SiC were more effective in improving oxidation resistance at temperatures between 1200 and 1400°C than additions of other group IV–VI transition metal borides, including Cr, Nb, Ti and V.

Similarly, addition of rare earths in the form of its borides (NdB₆, LaB₆, EuB₆) to ZrB₂ are also reported to improve the oxidation resistance compared to monolithic ZrB₂ [48], [82]. LaB₆ was also identified as a beneficial additive to ZrB₂-SiC based on its ability to act as a modifier for the ZrO₂, which stabilised the formation of the tetragonal phase [48], [389]. The oxidation behaviour of directly solidified eutectic LaB₆-ZrB₂ in situ composites was studied by Chen et al. [430], who reported the parabolic rate constant (kp) to be $9.71 \times 10^{-3} \exp(-31000/RT) \text{ mg}^2 \text{ cm}^{-4} \text{ min}^{-1}$ in the range 912-1094°C. Above 1094°C, rapid oxidation kinetics were observed with formation of

enriched La_2O_3 and B_2O_3 constituent with ZrO_2 deficiency in the outer scale [431], [432]. The pyrochlore phases associated with ZrO_2 and rare earth oxides are also known to exhibit significantly lower oxygen diffusion than ZrO_2 [1], [433].

It is well known that texture influences the mechanical properties and it is also reported that texture plays an important role in oxidation resistance. For example, Ni et al. [434] reported that a textured HfB_2 -based material exhibited much better oxidation resistance by forming a rich SiO_2 glassy layer on the particular-oriented matrix. Similar observations were not seen in ZrB_2 - SiC composites, however [434]. Further work is required in this area if the underpinning mechanisms are to be understood and hence the effect of texture elucidated, allowing the design of composite structures to be optimised.

The oxidation behaviour of HfB_2 with the addition of SiC and other silicides has also been reported in the literature [435]–[438]. The oxidation behaviour of HfB_2 - TaSi_2 is similar to that of diborides with MoSi_2 additions for temperatures up to 1900°C [374]. Although additions of SiB_6 (10 and 20 vol%) to HfB_2 were found to increase oxidation resistance, they were no better than SiC additions [1]. Oxidation of the modifying diborides resulted in the formation of the corresponding oxides in the surface borosilicate glass. TaB_2 -doped HfB_2 was synthesized by a boro/carbothermal reduction reaction, with an initial co-precipitation route to promote mixing [439]. It was believed that the Ta atom from the dopants substituted for the Hf atom in the HfB_2 lattice to form a solid solution of $(\text{Hf}, \text{Ta})\text{B}_2$, which played a key role in stabilising the oxidation products of HfB_2 in the tetragonal phase. The results of static furnace oxidation testing at 1400 – 1600°C showed that the addition of the Ta dopants inhibited the formation of monoclinic HfB_2 and almost fully stabilized the oxide scale of HfB_2 in the tetragonal phase. This meant that the volume change due to the tetragonal to monoclinic HfO_2 phase transformation was avoided, resulting in a denser oxide layer.

It is known from the literature that borate and silicate glasses containing transition / rare earth metal oxides show a strong tendency to phase separate as a result of immiscibility in the phase diagram [440]. Systems exhibiting such immiscibility are characterized by steeply rising liquidus temperatures and increased viscosity. As demonstrated by the Stokes–Einstein relationship [441], the latter decreases the oxygen diffusion rate through the oxide surface scale, since the diffusivity is inversely proportional to viscosity. Another potential benefit of increased viscosity, as well as

increased liquidus temperature, is the suppression of boria evaporation from the glass [1]. A survey of oxidation resistance of the diborides of Hf, Zr, Ti, Ta, and Nb from 1200 to 2200°C using inductively heated samples in flowing He-O₂ mixtures, revealed that HfB₂ was the most oxidation resistant, followed by ZrB₂ [1], [442] and then the other diborides such as TiB₂, TaB₂ and NbB₂ [389], [443]. Opila et al. [1] also reported that the addition of 20 vol% TaSi₂ improved the oxidation behaviour of ZrB₂-SiC up to 1627°C in air, however, its addition did not show any improvement in the HfB₂-SiC system. When WC and WB containing HfB₂-SiC samples were oxidized at 1600 and 1800°C, the resulting oxide scales were reported to be the same thickness as the base materials, suggesting that the oxidation resistance was not modified. However, when the samples were oxidized at 2000°C, a 30% reduction in scale thickness was reported due to the formation of a more viscous phase-separated glass in the outermost regions of the scale and a denser inner HfO₂ that restricted oxygen penetration to the sample [436]. Similar observations of improved oxidation resistance with the addition of W-based compounds were reported for ZrB₂ also by Zhang et.al [428], [444]. In-situ formed SiC whiskers (SiC_w) have been shown to improve the oxidation resistance of HfB₂-based composites [445], while HfB₂-SiC-Si / SiC coatings deposited by CVD on C / C composites improved the oxidation resistance and alleviated the thermal stresses present. Finally, the use of nitride additives has been shown to lead to rupture of the oxide scale and loss of protective behaviour at temperatures as low as 1400°C [389], [410].

In summary, the oxidation resistance of UHTCMCs can be significantly enhanced by compositional design leading to the formation of a surface layer of immiscible, multicomponent glass. The resulting increased liquidus temperatures and viscosities, as well as decreased oxygen diffusivities, in the immiscible glasses are considered responsible for the observed improvement in the oxidation resistance of the composites. It is beneficial to optimise the type and quantity of glass-forming elements in the form of additives in the UHTCMCs to obtain superior oxidation & ablation resistance for ultrahigh temperature applications. Although addition of second phases may improve the oxidation resistance, there is also a need to optimise the type and quantity of the second phase in order to optimise and balance the components' inherent properties (mechanical, physical, thermal) to best suit the end user application.

However, there is limited information available on the texture effects of oxidation resistance of UHTCMCs.

Summary and Outlook

Composites are, in general, a rapidly evolving and growing technical field with a very wide range of applications across the aerospace, defence, energy, medical and transport sectors as a result of their superior mechanical and physical properties. Ultra-high temperature ceramic matrix composites, UHTCMCs, are a new subfield within the wider grouping of CMCs that offer applications in rocket and hypersonic vehicle components, particularly nozzles, leading edges and engine components [2], [17].

Whilst UTHCs have some excellent properties as single phase monolithic components in structural applications, they are severely limited by their low fracture toughness, which makes them highly susceptible to thermal shock, hindering both their short-term and long-term use as external thermal protection systems on leading edges and propulsion systems. This has led to the utilisation of reinforcement, most typically in the form of a continuous fibrous phase. Reinforcing fibres symbiotically operate with the UHTC matrix to increase the toughness of the monolithic phase, whilst they are, in turn, protected by the matrix. Their addition permits the tailoring of the mechanical and thermal properties for use in different end use components via consideration of fibre architecture, fibre type and volume fractions of phases in the composite, in addition to choosing the most suitable processing method to obtain the desired microstructure [13], [183]. Techniques such as chemical vapour infiltration (CVI), reactive melt infiltration (RMI) and precursor infiltration and pyrolysis (PIP) are all being investigated, together with the more conventional slurry impregnation (SIP) followed by sintering, typically involving the pressure-based approaches of hot pressing or spark plasma sintering.

The selection of the matrix phases used is highly dependent upon both the properties desired for a component with respect to its intended operability window, but also on the fabrication techniques at the fabricator's disposal. This latter will set limits on the material quality, maximum density achievable and the process routes possible.

Although particulate second phases can improve the sinterability of UHTCs and enhance fracture toughness by up to around 100% compared to the baseline monolithic,

the absolute values of fracture toughness are still only $\leq 5 \text{ MPa m}^{1/2}$; values that are still very low compared to most structural engineering materials [56], [62]. Researchers have also explored other types of second phase reinforcement, including carbon nanotubes, graphene, a range of chopped fibres and whiskers. However, these types of additives still only improve the toughness to $\sim 8 \text{ MPa m}^{1/2}$ and failure is still predominantly catastrophic [99], [111]. Continuous fibre reinforcement using a range of different fibres, including C, SiC and even UHTC fibres, can improve the fracture toughness and strength to the point where they begin to meet the structural requirements.

Structure-texture and properties are all correlated with each other, hence learning how to obtain tailored structures and textures is crucial if the required mechanical & thermal properties are to be achieved. The processing method and process conditions all play a role and the required control needs to be identified and learnt. Precursor infiltration and pyrolysis (PIP) [195], [196] and slurry impregnation process (SIP) [255], [256] are green-forming procedures used to produce continuous fibre-reinforced ceramic composites. Hot pressing & spark plasma sintering can reduce the processing times and enable high densities to be achieved. However, the high pressure and temperature involved are detrimental for the integrity of the reinforcement. Use of sintering aids reduce the sintering conditions, but they can be responsible of the formation of brittle phases at the fibre-matrix interface, which, in turn, reduce the benefits to be gained in terms of the fracture toughness. The reactive melt infiltration (RMI) process is attractive for fabricating continuous fibre reinforced UHTC composites without the fibres being too significantly damaged, whilst still being able to obtain high densities [215], [217]. However, this process also has limitations including the presence of residual metal phases and liquid metal corrosion of fibres, amongst others. The use of chemical vapour infiltration (CVI) to deposit UHTC matrices is still very much a developing processing technique in the densification of UHTCMCs. It is useful in that it yields reasonably dense, complex-shaped components at low processing temperatures that do not damage the fibres used for reinforcement [189], [246]. However, it is an intrinsically slow process and therefore the product can be expensive. Amongst the different variations developed to overcome the limitations, one of the most promising currently is the use of microwave or radio frequency energy assisted CVI due to the ability to create an inverse thermal gradient profile, compared to conventional heating. This greatly reduces the process times, from ~ 2000 hours down to < 100 , whilst

retaining all of the advantages of the fundamental CVI process. However, it should be noted that this process is still limited to the laboratory scale, but further work is ongoing that will hopefully lead to it being commercialised.

The soundness of the fabricated UHTCMCs can be determined by microstructural characterisation and evaluation of mechanical and thermal properties, the latter including oxidation & ablation. As indicated, the microstructural features of the UHTCMCs are highly reliant on the processing method used and hence it is essential to select the correct process in order to achieve the required microstructure, which will, in turn, yield the targeted properties of the composites. To achieve this with UHTCMCs, the possibility of combining of two or more technologies from among CVI, SIP, RMI, PIP, HP and SPS becomes an interesting concept, allowing the whole process – microstructure – property relationship to be designed. Furthermore, the advanced characterization of UHTCMCs, with ability for atomic scale resolution, especially at the matrix and fibre interface, is also critical to developing an understanding of the toughening mechanisms in UHTCMCs in depth.

The flexural strength values of many UHTCMCs, especially those produced by RMI and HP, are typically less than 200 MPa [179], [191]. For both the RMI and HP processes, the low strengths probably result from the presence of residual stresses, which, in turn, arise during cooling after densification as a result of CTE mismatch between the matrix, fibre and/or unreacted alloy. UHTCMCs densified by post-HP exhibit excellent mechanical properties and non-brittle behaviour during flexure up to 1500°C. Although the fractural toughness is important for monolithic ceramics, its value hasn't been reported for UHTCMCs very often, especially for composites not densified by sintering. Understanding the mechanical properties of UHTCMCs at elevated temperatures is essential for understanding their performance in the service environment. Unfortunately, very limited results have been reported to date.

Amongst the thermal ablation methods, arc jet and scram jet testing are the best ground-based techniques since they simulate actual re-entry conditions the closest. The oxidation resistance of UHTCMCs can be significantly enhanced by compositional design leading to the formation of a surface layer of immiscible multicomponent glass. The resulting increased liquidus temperatures and viscosities, as well as decreased oxygen diffusivities, in the immiscible glasses are considered responsible for the

observed improvement in the oxidation resistance of the composites. It is beneficial to optimise the type and quantity of glass-forming elements in the form of additives in the UHTCMCs to obtain superior oxidation & ablation resistance for ultrahigh temperature applications. Although addition of second phases may improve the oxidation resistance, there is also a need to optimise the type and quantity of the second phase in order to optimise / balance the components inherent properties (mechanical, physical, thermal) to best suit the end user application [206], [357]. Moreover, there is limited information available on the texture effects of oxidation resistance of the UHTCMCs.

As is well known, the development of new materials offers tremendous opportunities for realizing many of the new advanced technologies that are required by mankind to meet our global demands. UHTCMCs will undoubtedly play a useful role in some of these technologies, including aerospace and energy, the latter including solar power, fission and fusion [446], since the factor that they have in common is that they generate fairly extreme environments. Meeting such aggressive requirements will necessitate the design of components with a suitable matrix, fibre reinforcement and interphase coating(s) and the development and exploitation of micro- and macrostructure control with increasing complexity at multiple length scales. The technically and economically successful manufacturing of components from these materials is currently a challenge and therefore provides fertile ground for innovation [446].

The main interest in fibre reinforced ceramic matrix composites in general arises from their non-brittle mechanical behaviour and improved reliability compared to their unreinforced counterparts [123], [124], [245]. However, this non-brittle character is observed only for well-processed materials, i.e. when i) the fibres are not damaged (etched, corroded, degraded, eroded, etc.) during processing [123]; ii) the fibres are weakly bonded to the matrix as a result of interfacial engineering by adopting techniques as shown in Fig. 6; [123], [246] and iii) both the fibres and interphases are protected against environmental effects, e.g. by use of coatings [123], [246], [447] or doping the UHTC matrix [18], [183], [448]. Each of these helps to ensure that the toughening mechanism(s) provided by the fibres is not degraded and so helps to maximise the properties of the composite.

1 Composition, micro- and macrostructures all need to be *designed* to yield the
2 required properties and then sophisticated processing techniques need to be explored
3 further in order to make viable components. This includes learning how to densify the
4 materials at temperatures low enough to avoid damaging the fibres, whilst fast enough
5 to keep costs down and without generating any brittle reaction products at the matrix /
6 fibre interface. The solution might be the creation of ‘hybrid’ processes that combine
7 elements of two – or more – existing process routes. Strength, toughness and oxidation /
8 ablation resistance can also be tailored by introducing carefully selected fillers into the
9 composites. For real applications, it is also essential to be able to join these new
10 materials, so reliable and user-friendly joining methods are required to allow the
11 assembly of potentially complex structures that can withstand the extreme environments
12 required by the end applications. Relatively little work has been done in this area to
13 date.
14
15
16
17
18
19
20
21
22
23

24 Multiscale modelling is going to be essential, both of the individual parts of the
25 materials and processes and the creation of models that link across between processing
26 and properties and that can be validated through extensive experimental work and
27 characterisation. This integrated selection–design–modelling–experiment–
28 manufacturing approach, spanning the ceramics–ensembles–component–system
29 hierarchy, embraces the integrated computational materials engineering and the
30 materials genome initiative paradigms [446]. Although not easy or low cost to create, in
31 the longer term they will significantly reduce the costs of manufacturing new materials
32 that offer the required combination of properties. In addition, new and ever-more
33 realistic testing is required – though it also can’t afford to be too expensive or new
34 materials will not be developed at a fast enough pace. So tests that can be done rapidly
35 and at low cost but which provide excellent guidance on the performance of the
36 materials and components under real environmental conditions are needed. Finally, we
37 need to ensure that we have a new generation of scientists and engineers with the
38 required skills – the ‘people pipeline’ is a key necessity for all new and expanding
39 research areas. Research organisations, universities and industry must all work together
40 to ensure that this happens smoothly and collaboration is the key; our planet is shrinking
41 by the day in terms of the ability to interact across borders and exchange workers and
42 best practice. We need to ensure that the development of skilled individuals remains at
43 the forefront of our thinking. UHTCMCs are poised to shape the future of aerospace
44
45
46
47
48
49
50
51
52
53
54
55
56
57
58
59
60
61
62
63
64
65

1 applications, but paradigm and culture shifts will be needed to accelerate their
2 development and take advantage of their full potential [446].
3
4
5
6
7

8 **Acknowledgements**

9

10
11 This work has been supported by a number of different research grants,
12 including:
13
14
15

16 *Materials systems for extreme environments (XMat)*, EPSRC research grant agreement
17 number EP/K008749/1-2 (2013-18).
18
19
20

21 *Ultra-high temperature ceramic materials*, MCM-ITP research grant agreement number
22 4700003222 (2014-16).
23
24
25

26 *Next generation ceramic composites for combustion harsh environments and space*
27 *(C3HarME)*, EU Horizon 2020 research grant agreement number GA 685594 (2016-20).
28
29
30

31 *Effect of rare-earth doping elements on the mechanical and oxidation resistance*
32 *performance of SiC coated C fibre / ZrC composites for high temperature applications*
33 *(EREMOZ)*, EU Horizon 2020 research grant agreement number 748568 (2018-20).
34
35
36

37 *UK's Engineering and Physical Science Research Council entitled 'Materials Systems*
38 *for Extreme Environments'*, grant number EP/K008749/2 and *'Multiscale tuning of*
39 *interfaces and surfaces for energy applications'*, grant number EP/P007821/1
40
41
42
43
44
45
46
47
48
49
50
51
52
53
54
55
56
57
58
59
60
61
62
63
64
65

List of Figures

- Fig. 1 Schematic on the effect of the shape of the leading edge on the shock wave propagation on the surface of the structure.
- Fig. 2 Some summary data for common UHTCs ubiquitous in literature; HfB₂, ZrB₂, ZrC, HfC, TaC, TiB₂, SiC is provided for contrast, due to its frequent inclusion as a secondary matrix component [13], [29]–[35].
- Fig. 3 a) Classification of the carbon fibres (value based on available commercial fibres of Table 2 and their use, b) different applications and properties [128], [134]–[141].
- Fig. 4 Microstructural features of three generations of SiC fibres: reprinted with permission from John Wiley and Sons, Macromolecular Materials and Engineering, 297(6), Fig.16 in p. 512 [144].
- Fig. 5 Structure of the 2.5 D carbon fibre preform bought from Surface Transforms, UK
- Fig. 6 Process flow sheet summarises the different methods of process for obtaining the UHTCMCs (CVI-chemical vapour infiltration, CVD-chemical vapour deposition, ED-Electro deposition, EPD- Electrophoretic deposition, PIP-precursor infiltration and pyrolysis, RMI - reactive melt infiltration, SIP - slurry impregnation process, HP – hot pressing, PS- pressureless sintering, SPS – spark plasma sintering, HIP – hot isostatic pressing)
- Fig. 7 The steps involved in the production of a composite via PIP. (a) A liquid precursor impregnated fabric dries, leaving residual porosity; (b) pyrolysis begins, resulting in an evolution of gaseous by-products and volume shrinkage from the polymer-ceramic transition; (c) a porous microstructure, with microcracks and pores shown in the matrix phases.
- Fig. 8 The precursor used by Xie et al for a ZrB₂/ ZrC matrix: reprinted with permission from Elsevier, Ceramics International, 2015, 41[5], Eq. 1 in p. 6228 [194].
- Fig. 9 (a) The reactive melt infiltration process and (b) residual free metal phase: reprinted with permission from Jeff Crompton, <https://uk.comsol.com/blogs/multiphysics-analysis-advanced-materials-ceramic-matrix-composites/> [216].

- Fig. 10 Schematic showing the growth of ceramic deposit on the cross section of the fibres to the point of full densification by CVI method.
- Fig. 11 a) Isothermal chemical vapour infiltration (ICVI), b) Thermal gradient (TGCVI), c) Isothermal forced flow CVI (FFCVI), d) Forced Flow Thermal Gradient CVI, e) Laser Chemical Vapour Infiltration (LCVI), f) Thermal gradient of Microwave and Radio Frequency CVI (MCVI and RFCVI) and g) pulse pressure CVI (PCVI).
- Fig. 12 3D micro-CT cross section of a UHTC composite prepared by squeeze impregnation showing powder penetration: reprinted with permission from Am. Ceram. Soc. Bull. 91, (2012), Fig.11 in p. 26 [17].
- Fig. 13 Backscattered electron images of particles distribution in C / C-UHTC composites: (a) C / C - ZrB₂, (b) C / C - 4ZrB₂ - 1SiC, and (c) C / C - 1ZrB₂ - 2SiC - 2HfC: reprinted with permission from Elsevier, Mater. Sci. Eng. A 465, (2007) Fig.1 in p. 3 [10].
- Fig. 14 Schematics of moulds for conventional vacuum-assisted pressure casting and a new deformation process. (a, b) The conventional fixture of a firm mould. Woven fabric suppresses the infiltration of slurry. (c) Mould with a deformable foil during initial infiltration. The fabrics are pressed by the difference of pressure (ΔP) inside and outside of the mould. (d) The onset of outward deformation of the foil by the slurry. (e) Completion of the full deformation and infiltration of the slurry. (f) Removal of excess slurry by squeezing the mould: reprinted with permission from John Wiley and Sons, *J. Am. Ceram. Soc.* 90, (2007) Fig.1 in p. 2658 [258].
- Fig. 15 a) Cross section of C_f-ZrB₂ composite using ZrSi₂ as a sintering aid. b) and c) Details of the fibre / matrix interface show the formation of brittle phases of SiC and ZrC: reprinted with permission from Elsevier, Journal of the European Ceramic Society 36 (2016) Fig.3 in p. 19 [113].
- Fig.16 (a) Cross section of C_f - ZrB₂ composites produced by vacuum bagging followed by hot pressing at 1700°C for 20 mins: reprinted with permission from Elsevier, Materials & Design 85 (2015) Fig.3d in p. 130 [279]. (b) Cross section of C_f - ZrB₂ composites, which was prepared by the infiltrate of ZrB₂ into unidirectional fabrics that were stacked in 0 - 0° configuration. The

- sample was densified at 1800 - 1900°C for 30 – 40 mins: reprinted with permission from iStec, Scientific Reports 8[9148] (2018) Fig.2a in p. 3[281].
- Fig. 17 The local microstructure of (Fig. 12a) after a carbon CVI at a higher magnification: reprinted with permission from Elsevier, Materials Science and Engineering: A 465 (2007) Fig.2 in p. 3 [281].
- Fig. 18 Powder distribution of a UHTC composite produced by slurry infiltration (a) The detailed microstructure of the top (b) and bottom of the composite (c): reprinted with permission from Elsevier, J. Eur. Ceram. Soc., 33[2], Fig.2 in p. 425 [288].
- Fig. 19 BSE images (a) (b) on the cross section of the C/C–ZrB₂–ZrC–SiC composites prepared by PIP at different magnifications: reprinted with permission from Elsevier, Corros. Sci., 98, Fig. 4 in p. 554 [290].
- Fig. 20 A tight and clean interface on the C_f/ZrB₂-SiC composite prepared by SIP and hot pressing, and corresponding elemental distributions: reprinted with permission from Elsevier, Journal of the European Ceramic Society, 39 (2019), Fig. 6 in p. 802 [289].
- Fig. 21 The polished surface of C_f/ZrC-SiC produced by PIP+CVI with different interfaces (a) none; (b) PyC; (c) PyC+SiC: reprinted with permission from John Wiley and Sons, J. Am. Ceram. Soc., **91[10]**, Fig.1 in p. 3435 [294].
- Fig. 22 The microstructure of C_f/ZrC (a,b): reprinted with permission from John Wiley and Sons, Int. J. Appl. Ceram. Technol., vol. 8, no. 2, Fig.6a & Fig.7b in p. 324 & 335 [295]; C_f/ZrC-SiC(c,d): reprinted with permission from John Wiley and Sons, J. Am. Ceram. Soc., vol. 101, no. 8, Fig.1B and Fig.3A in p. 3255 & 3256 [296]; C_f/Zr-Ti-B-C (e) composite densified by RMI: reprinted with permission from Author, Nat. Commun., vol. 8, 15836, Fig.4a in p.4 [297].
- Fig. 23 Debonding map showing crack penetration and crack deflection regimes as a function of Dundurs's parameter [124].

List of Tables

- Table 1 UHTCMCs reinforced with Chopped fibre / whisker / CNT / graphene reinforcement [57], [84]–[121].
- Table 2 Mechanical properties of carbon fibres produced by PAN and Pitch precursor [128].
- Table 3 Physical, mechanical and thermal properties of the commercially available SiC fibres [144]–[147].
- Table 4 Different preform types, manufacturing techniques, advantages and disadvantages. [193] – reference for one last figure
- Table 5 Summary of the advantages and disadvantages of various densification / consolidation methods
- Table 6 Literature reported data on RMI of UHTCMCs [207], [220], [224]–[232].
- Table 7 Precursors and the conditions needed for the deposition of oxide / non-oxide ceramics [236], [237].
- Table 8 Chemical vapour infiltration variants w.r.t. temperature, pressure, heating [242].
- Table 9 Mechanical properties, density achieved and sintering conditions of UHTCMCs processed by hot pressing [275], [276], [278], [279], [281], [283]
- Table 10 Properties of carbon fibre reinforced ultra-high temperature ceramic matrix composites prepared by different approaches [179], [192], [227], [279], [281], [294]–[296], [306]–[308].
- Table 11 Thermal properties (melting point, CTE, thermal conductivity, diffusivity, Cp) of UHTCs and UHTCMCs [38], [58], [98], [116], [118], [205], [210], [221], [322], [326]–[343].
- Table 12 Electrical properties of UHTCMCs reported in the literature [339], [348]–[350].
- Table 13 Thermal ablative methods and properties of various UHTCMCs [18], [109], [181], [182], [187], [197], [198], [207], [209], [210], [222], [227], [229], [357]–[371]

References

- [1] M. M. Opeka, I. G. Talmy, and J. A. Zaykoski, "Oxidation-based materials selection for 2000°C + hypersonic aerosurfaces: Theoretical considerations and historical experience," *J. Mater. Sci.*, vol. 39, no. 19, pp. 5887–5904, Oct. 2004.
- [2] P. L. Moses, V. L. Rausch, L. T. Nguyen, and J. R. Hill, "NASA hypersonic flight demonstrators—overview, status, and future plans," *Acta Astronaut.*, vol. 55, no. 3–9, pp. 619–630, Aug. 2004.
- [3] N. R. Council, *Evaluation of the National Aerospace Initiative*. Washington, D.C.: National Academies Press, 2004.
- [4] M. Holden, "A review of aerothermal problems associated with hypersonic flight," in *24th Aerospace Sciences Meeting*, 1986.
- [5] M.L. Rasmussen, *Hypersonic Flow*. New York: John Wiley and Sons Ltd, 1994.
- [6] John D. Anderson Jr., *Hypersonic and High-Temperature Gas Dynamics, Second Edition*, Second. Virginia: American Institute of Aeronautics and Astronautics, Inc., 2006.
- [7] J. L. Stollery, "Hypersonic viscous interaction on curved surfaces," *J. Fluid Mech.*, vol. 43, no. 3, pp. 497–511, Sep. 1970.
- [8] J. L. Stollery, "Hypersonic Flight," *Nature*, vol. 240, no. 5377, pp. 133–135, Nov. 1972.
- [9] R. Courant and K. O. Friedrichs, *Supersonic flow and shock waves*. Springer-Verlag, 1976.
- [10] S. Tang, J. Deng, S. Wang, W. Liu, and K. Yang, "Ablation behaviors of ultra-high temperature ceramic composites," *Mater. Sci. Eng. A*, vol. 465, no. 1–2, pp. 1–7, Sep. 2007.
- [11] T. A. Parthasarathy, R. A. Rapp, M. Opeka, and R. J. Kerans, "A model for the oxidation of ZrB₂, HfB₂ and TiB₂," *Acta Mater.*, vol. 55, no. 17, pp. 5999–6010, Oct. 2007.
- [12] R. Savino, M. De Stefano Fumo, D. Paterna, and M. Serpico, "Aerothermodynamic study of UHTC-based thermal protection systems," *Aerosp. Sci. Technol.*, vol. 9, no. 2, pp. 151–160, Mar. 2005.
- [13] W. G. Fahrenholtz, E. J. Wuchina, W. E. Lee, Y. Zhou, and G. Geiger, *Ultra-High Temperature Ceramics*. Hoboken, NJ: John Wiley & Sons, Inc, 2014.
- [14] P. Rogl and P. E. Potter, "A critical review and thermodynamic calculation of the binary system: Zirconium-boron," *Calphad*, vol. 12, no. 2, pp. 191–204, Apr. 1988.
- [15] F. W. Glaser and B. Post, "System Zirconium-Boron," *JOM*, vol. 5, no. 9, pp. 1117–1118, Sep. 1953.
- [16] J. Han, P. Hu, X. Zhang, S. Meng, and W. Han, "Oxidation-resistant ZrB₂-SiC composites at 2200°C," *Compos. Sci. Technol.*, vol. 68, no. 3–4, pp. 799–806, Mar. 2008.
- [17] P. Paul, A., Venugopal, S., Binner, J., Vaidhyanathan, B., Jayaseelan, D.D., Zapata-Solvas, E., Lee, W.E., Heaton, A., Brown, "UHTC composites for hypersonic applications," *Am. Ceram. Soc. Bull.*, vol. 91, no. 1, pp. 22–28, Oct. 2012.
- [18] A. Paul, S. Venugopal, J. G. P. Binner, B. Vaidhyanathan, A. C. J. Heaton, and P. M. Brown, "UHTC-carbon fibre composites: Preparation, oxyacetylene torch testing and characterisation," *J. Eur. Ceram. Soc.*, vol. 33, no. 2, pp. 423–432, Feb. 2013.
- [19] Tim Bowler, "Carbon fibre planes: Lighter and stronger by design - BBC News,"

- BBC, 2014. [Online]. Available: <https://www.bbc.co.uk/news/business-25833264>. [Accessed: 04-Jan-2019].
- [20] J. M. Quenisset, "Carbon combinations. Carbon/Carbon composites," *Adv. Mater.*, vol. 6, no. 2, pp. 176–177, Feb. 1994.
 - [21] T. S. Reinhart, F. H. Froes, and Society for the Advancement of Material and Process Engineering., "Stability Characterization of diboride Composites Under High-Velocity Atmospheric Flight Conditions," in *Advanced materials : meeting the economic challenge : 24th International SAMPE Technical Conference : Westin Harbour Castle Hotel, Toronto, Canada, October 20-22, 1992*, 1992, p. 718.
 - [22] T. S. R. C. Murthy, J. K. Sonber, K. Sairam, R. D. Bedse, and J. K. Chakarvartty, "Development of Refractory and Rare Earth Metal Borides & Carbides for High Temperature Applications," *Mater. Today Proc.*, vol. 3, no. 9, pp. 3104–3113, 2016.
 - [23] A. Bhattacharya *et al.*, "Nano-scale microstructure damage by neutron irradiations in a novel Boron-11 enriched TiB₂ ultra-high temperature ceramic," *Acta Mater.*, vol. 165, pp. 26–39, Feb. 2019.
 - [24] S. C. Middleburgh, D. C. Parfitt, P. R. Blair, and R. W. Grimes, "Atomic Scale Modeling of Point Defects in Zirconium Diboride," *J. Am. Ceram. Soc.*, vol. 94, no. 7, pp. 2225–2229, Jul. 2011.
 - [25] G. Gutierrez *et al.*, "Thermal behaviour of xenon in zirconium carbide at high temperature: Role of residual zirconia and free carbon," *J. Nucl. Mater.*, vol. 416, no. 1–2, pp. 94–98, Sep. 2011.
 - [26] E. Wuchina *et al.*, "UHTCs: Ultra-High Temperature Ceramic Materials for Extreme Environment Applications," *Electrochem. Soc. Interface*, vol. 16, no. 4, pp. 30–36, 2007.
 - [27] C. Mroz, "Minerals Review: Zirconium Diboride," *Am. Ceram. Soc. Bull.*, vol. 74, no. 6, pp. 164–165, 1995.
 - [28] E. Sani, L. Mercatelli, M. Meucci, A. Balbo, L. Silvestroni, and D. Sciti, "Compositional dependence of optical properties of zirconium, hafnium and tantalum carbides for solar absorber applications," *Sol. Energy*, vol. 131, pp. 199–207, Jun. 2016.
 - [29] K. Gürçan and E. Ayas, "In-situ synthesis and densification of HfB₂ ceramics by the spark plasma sintering technique," *Ceram. Int.*, vol. 43, no. 4, pp. 3547–3555, 2017.
 - [30] M. M. Opeka, I. G. Talmy, E. J. Wuchina, J. A. Zaykoski, and S. J. Causey, "Mechanical, Thermal, and Oxidation Properties of Refractory Hafnium and zirconium Compounds," *J. Eur. Ceram. Soc.*, vol. 19, no. 13–14, pp. 2405–2414, Oct. 1999.
 - [31] Netschz, "Thermal Properties of Ceramics." Netschz, 2012.
 - [32] A. L. Chamberlain, W. G. Fahrenholtz, G. E. Hilmas, and D. T. Ellerby, "High-Strength Zirconium Diboride-Based Ceramics," *J. Am. Ceram. Soc.*, vol. 87, no. 6, pp. 1170–1172, Jun. 2004.
 - [33] W. G. Fahrenholtz, G. E. Hilmas, I. G. Talmy, and J. A. Zaykoski, "Refractory Diborides of Zirconium and Hafnium," *J. Am. Ceram. Soc.*, vol. 90, no. 5, pp. 1347–1364, May 2007.
 - [34] P. Schwarzkopf and R. Kieffer, *Refractory Hard Metals: Borides, Carbides, Nitrides and Silicides*. New York: Macmillan Company, 1953.
 - [35] H. S. Hong and K. S. Lee, "Thermodynamic evaluation of the Ta–O system from pure tantalum to tantalum pentoxide," *J. Alloys Compd.*, vol. 360, no. 1, pp. 198–

204, 2003.

- [36] R. Wang and W. Li, "Characterization models for thermal shock resistance and fracture strength of ultra-high temperature ceramics at high temperatures," *Theor. Appl. Fract. Mech.*, vol. 90, pp. 1–13, 2017.
- [37] M. W. D. Van, J. D. G. Drewry, D. E. King, and C. M. Hudson, "The hypersonic environment: Required operating conditions and design challenges," *J. Mater. Sci.*, vol. 39, no. 19, pp. 5915–5924, Oct. 2004.
- [38] E. Wuchina *et al.*, "Designing for ultrahigh-temperature applications: The mechanical and thermal properties of HfB_2 , HfC_x , HfN_x and Hf(N) ," *J. Mater. Sci.*, vol. 39, no. 19, pp. 5939–5949, Oct. 2004.
- [39] R. J. Irving and I. G. Worsley, "The oxidation of titanium diboride and zirconium diboride at high temperatures," *J. Less Common Met.*, vol. 16, no. 2, pp. 103–112, 1968.
- [40] L. G.-Q. Han Ke-Chang Dong Chuang, Tai Kai-Ping, "Influence of Nitrogen Vacancy Concentration on Mechanical and Electrical Properties of Rocksalt Zirconium Nitride Films," *Acta Metall. Sin. Lett.*, vol. 30, no. 11, pp. 1100–1108, 2017.
- [41] L. Silvestroni, S. Failla, I. Neshpor, and O. Grigoriev, "Method to improve the oxidation resistance of ZrB_2 -based ceramics for reusable space systems," *J. Eur. Ceram. Soc.*, vol. 38, no. 6, pp. 2467–2476, 2018.
- [42] A. K. Kuriakose and J. L. Margrave, "The Oxidation Kinetics of Zirconium Diboride and Zirconium Carbide at High Temperatures," *J. Electrochem. Soc.*, vol. 111, no. 7, p. 827, 1964.
- [43] M. Desmaison Brut, J. Montintin, F. Valin, and M. Boncoeur, "Mechanical properties and oxidation behaviour of HIPed hafnium nitride ceramics," *J. Eur. Ceram. Soc.*, vol. 13, no. 4, pp. 379–386, Jan. 1994.
- [44] P. Patsalas *et al.*, "Conductive nitrides: Growth principles, optical and electronic properties, and their perspectives in photonics and plasmonics," *Mater. Sci. Eng. R Reports*, vol. 123, pp. 1–55, 2018.
- [45] R. Savino, M. De Stefano Fumo, D. Paterna, A. Di Maso, and F. Monteverde, "Arc-jet testing of ultra-high-temperature-ceramics," *Aerosp. Sci. Technol.*, vol. 14, no. 3, pp. 178–187, Apr. 2010.
- [46] D. L. Poerschke, M. D. Novak, N. Abdul-Jabbar, S. Krämer, and C. G. Levi, "Selective active oxidation in hafnium boride-silicon carbide composites above 2000°C ," *J. Eur. Ceram. Soc.*, vol. 36, no. 15, pp. 3697–3707, 2016.
- [47] V. V Kurbatkina, E. I. Patsera, E. A. Levashov, and A. N. Timofeev, "Self-propagating high-temperature synthesis of refractory boride ceramics $(\text{Zr,Ta})\text{B}_2$ with superior properties," *J. Eur. Ceram. Soc.*, vol. 38, no. 4, pp. 1118–1127, 2018.
- [48] X. Zhang, P. Hu, J. Han, L. Xu, and S. Meng, "The addition of lanthanum hexaboride to zirconium diboride for improved oxidation resistance," *Scr. Mater.*, vol. 57, no. 11, pp. 1036–1039, Dec. 2007.
- [49] C. Carney *et al.*, "Oxidation response of a SiC_t/SiC CMC with a HfB_2 -based coating in an arc jet test," *Adv. Appl. Ceram.*, vol. 117, no. sup1, pp. s19–s25, Oct. 2018.
- [50] P. Hu *et al.*, "Rolling compacted fabrication of carbon fiber reinforced ultra-high temperature ceramics with highly oriented architectures and exceptional mechanical feedback," *Ceram. Int.*, vol. 44, no. 12, pp. 14907–14912, Aug. 2018.
- [51] I. Akin, M. Hotta, F. C. Sahin, O. Yucel, G. Goller, and T. Goto, "Microstructure and densification of ZrB_2 -SiC composites prepared by spark plasma sintering,"

- J. Eur. Ceram. Soc.*, vol. 29, no. 11, pp. 2379–2385, Aug. 2009.
- [52] Muksin, D.-H. Yoon, and K. Raju, “Effects of Sc_2O_3 sintering aid for the densification and mechanical properties of SiC-ZrB_2 composites,” *Ceram. Int.*, vol. 42, no. 6, pp. 7300–7308, May 2016.
- [53] I.-M. M. Low, Y. (Yoshio) Sakka, and C. F. (Chunfeng) Hu, *MAX Phases and Ultra-High Temperature Ceramics for Extreme Environments*. IGI Global, 2013.
- [54] V. Rubio, P. Ramanujam, and J. Binner, “Ultra-high temperature ceramic composite,” *Adv. Appl. Ceram.*, vol. 117, no. sup1, pp. 56–61, Oct. 2018.
- [55] A. Purwar and B. Basu, “Thermo-structural design of ZrB_2 - SiC -based thermal protection system for hypersonic space vehicles,” *J. Am. Ceram. Soc.*, vol. 100, no. 4, pp. 1618–1633, Apr. 2017.
- [56] J. K. Sonber, T. S. R. C. Murthy, K. Sairam, A. Nagaraj, S. Majumdar, and V. Kain, “ ZrB_2 based novel composite with NiAl as reinforcement phase,” *Int. J. Refract. Met. Hard Mater.*, vol. 70, no. August 2017, pp. 56–65, Jan. 2018.
- [57] M. Shahedi Asl, B. Nayebi, and M. Shokouhimehr, “TEM characterization of spark plasma sintered ZrB_2 - SiC -graphene nanocomposite,” *Ceram. Int.*, vol. 44, no. 13, pp. 15269–15273, Sep. 2018.
- [58] R. Tu *et al.*, “Mechanical, electrical and thermal properties of ZrC-ZrB_2 - SiC ternary eutectic composites prepared by arc melting,” *J. Eur. Ceram. Soc.*, vol. 38, no. 11, pp. 3759–3766, Sep. 2018.
- [59] B. Xie *et al.*, “Influence of SiC on phase and microstructure of ZrB_2 powders synthesized via carbothermal reduction at different temperatures,” *Ceram. Int.*, vol. 44, no. 8, pp. 8795–8799, Jun. 2018.
- [60] V. Guérineau and A. Julian-Jankowiak, “Oxidation mechanisms under water vapour conditions of ZrB_2 - SiC and HfB_2 - SiC based materials up to 2400°C ,” *J. Eur. Ceram. Soc.*, vol. 38, no. 2, pp. 421–432, Feb. 2018.
- [61] P. Hu *et al.*, “Architectural engineering inspired method of preparing $\text{C}_2/\text{ZrC-SiC}$ with graceful mechanical responses,” *J. Am. Ceram. Soc.*, vol. 102, no. 1, pp. 70–78, Jan. 2019.
- [62] J. Ren, Y. Zhang, Y. Fu, P. Zhang, S. Tian, and L. Zhang, “Effects of the second phase on the microstructure and ablation resistance of HfC coating on C/C composites,” *Surf. Coatings Technol.*, vol. 344, pp. 250–258, Jun. 2018.
- [63] Y. Jing, H. Yuan, and Z. Lian, “Microstructure and Mechanical Properties of ZrB_2 - HfC Ceramics Influenced by HfC Addition,” *Materials (Basel)*, vol. 11, no. 10, p. 2046, Oct. 2018.
- [64] J. K. Sonber *et al.*, “Friction and wear properties of zirconium diboride in sliding against WC ball,” *Int. J. Refract. Met. Hard Mater.*, vol. 76, no. 0, pp. 41–48, Nov. 2018.
- [65] E. Castle, T. Csanádi, S. Grasso, J. Dusza, and M. Reece, “Processing and Properties of High-Entropy Ultra-High Temperature Carbides,” *Sci. Rep.*, vol. 8, no. 1, pp. 1–12, 2018.
- [66] A. Vinci, L. Zoli, D. Sciti, J. Watts, G. E. Hilmas, and W. G. Fahrenholtz, “Mechanical behaviour of carbon fibre reinforced TaC/SiC and ZrC/SiC composites up to 2100°C ,” *J. Eur. Ceram. Soc.*, vol. 39, no. 4, pp. 780–787, Apr. 2019.
- [67] D. Wu, G. Huangfu, D. Wang, B. Wei, Y. Wang, and Y. Zhou, “Microstructure and mechanical properties of ZrC-TaC composite fabricated by displacive compensation of porosity at 1300°C ,” *Ceram. Int.*, vol. 44, no. 1, pp. 246–253, Jan. 2018.
- [68] J. K. Sonber, “Studies on synthesis, densification and oxidation of zirconium

- diboride based materials,” PhD thesis Homi Bhabha National Institute, 2015.
- [69] J. K. Sonber and A. K. Suri, “Synthesis and consolidation of zirconium diboride: review,” *Adv. Appl. Ceram.*, vol. 110, no. 6, pp. 321–334, Aug. 2011.
- [70] T S R C Murthy, “Effect of Sinter Additives on the Consolidation and Properties of Titanium Diboride Composites,” PhD thesis, Homi Bhabha National Institute, 2012.
- [71] A. Mukhopadhyay, G. B. Raju, and B. Basu, “Ultra High Temperature Ceramics,” in *MAX Phases and Ultra-High Temperature Ceramics for Extreme Environments*, IGI Global, 2013, pp. 49–99.
- [72] E. Ghasali and M. Shahedi Asl, “Microstructural development during spark plasma sintering of ZrB_2 –SiC–Ti composite,” *Ceram. Int.*, vol. 44, no. 15, pp. 18078–18083, Oct. 2018.
- [73] M. T. S. R. Ch., B. Basu, R. Balasubramaniam, A. K. Suri, C. Subramanian, and R. K. Fotedar, “Processing and Properties of TiB_2 with $MoSi_2$ Sinter-additive: A First Report,” *J. Am. Ceram. Soc.*, vol. 89, no. 1, pp. 131–138, Jan. 2006.
- [74] T. S. R. C. Murthy, B. Basu, A. Srivastava, R. Balasubramaniam, and A. K. Suri, “Tribological properties of TiB_2 and TiB_2 – $MoSi_2$ ceramic composites,” *J. Eur. Ceram. Soc.*, vol. 26, no. 7, pp. 1293–1300, Jan. 2006.
- [75] T. S. R. C. Murthy *et al.*, “Preparation and property evaluation of TiB_2 + $TiSi_2$ composite,” *Int. J. Refract. Met. Hard Mater.*, vol. 27, no. 3, pp. 629–636, May 2009.
- [76] T. S. R. C. Murthy *et al.*, “A new TiB_2 + $CrSi_2$ composite – Densification, characterization and oxidation studies,” *Int. J. Refract. Met. Hard Mater.*, vol. 28, no. 4, pp. 529–540, Jul. 2010.
- [77] J. K. Sonber, T. S. R. C. Murthy, C. Subramanian, R. C. Hubli, R. K. Fotedar, and A. K. Suri, “Effect of WSi_2 addition on densification and properties of ZrB_2 ,” *Adv. Appl. Ceram.*, vol. 113, no. 2, pp. 114–119, Feb. 2014.
- [78] V. Reddy *et al.*, “Densification and mechanical properties of CrB_2 + $MoSi_2$ based novel composites,” *Ceram. Int.*, vol. 41, no. 6, pp. 7611–7617, Jul. 2015.
- [79] T. S. R. C. Murthy, J. K. Sonber, K. Sairam, and R. D. Bedse, “Development and Characterization of (Ti,Cr) B_2 based Composites,” *BARC Newsl.*, vol. January-Fe, no. February, pp. 1–10, 2016.
- [80] E. P. Simonenko, N. P. Simonenko, E. K. Papynov, E. A. Gridasova, V. G. Sevastyanov, and N. T. Kuznetsov, “Production of HfB_2 –SiC (10–65 vol % SiC) Ultra-High-Temperature Ceramics by Hot Pressing of HfB_2 –(SiO_2 –C) Composite Powder Synthesized by the Sol–Gel Method,” *Russ. J. Inorg. Chem.*, vol. 63, no. 1, pp. 1–15, Jan. 2018.
- [81] S. Guo, “High-temperature mechanical behavior of ZrB_2 -based composites with micrometer- and nano-sized SiC particles,” *J. Am. Ceram. Soc.*, vol. 101, no. 7, pp. 2707–2711, 2018.
- [82] J. K. Sonber, “Effect of NdB_6 addition on Densification and Properties Of ZrB_2 ,” *Ceram. - Silikaty*, vol. 60, no. 1, pp. 41–47, Mar. 2016.
- [83] E. Zapata Solvas, D. Gómez García, A. Domínguez Rodríguez, and W. E. Lee, “High temperature creep of 20 vol%. SiC– HfB_2 UHTCs up to 2000°C and the effect of La_2O_3 addition,” *J. Eur. Ceram. Soc.*, vol. 38, no. 1, pp. 47–56, Jan. 2018.
- [84] W.-W. Wu, M. Estili, G.-J. Zhang, and Y. Sakka, “Dispersion and structural evolution of multi-walled carbon nanotubes in ZrB_2 matrix,” *Ceram. Int.*, vol. 43, no. 13, pp. 10533–10539, Sep. 2017.
- [85] S. Zhou, Z. Wang, and W. Zhang, “Effect of graphite flake orientation on

- microstructure and mechanical properties of ZrB₂–SiC–graphite composite,” *J. Alloys Compd.*, vol. 485, no. 1–2, pp. 181–185, Oct. 2009.
- [86] G. B. Yadukulakrishnan, S. Karumuri, A. Rahman, R. P. Singh, A. Kaan Kalkan, and S. P. Harimkar, “Spark plasma sintering of graphene reinforced zirconium diboride ultra-high temperature ceramic composites,” *Ceram. Int.*, vol. 39, no. 6, pp. 6637–6646, Aug. 2013.
- [87] H. Jin, S. Meng, W. Xie, C. Xu, and J. Niu, “HfB₂-CNTs composites with enhanced mechanical properties prepared by spark plasma sintering,” *Ceram. Int.*, vol. 43, no. 2, pp. 2170–2173, 2017.
- [88] X. Zhang, Y. An, J. Han, W. Han, G. Zhao, and X. Jin, “Graphene nanosheet reinforced ZrB₂–SiC ceramic composite by thermal reduction of graphene oxide,” *RSC Adv.*, vol. 5, no. 58, pp. 47060–47065, 2015.
- [89] M. Shahedi Asl and M. Ghassemi Kakroudi, “Characterization of hot-pressed graphene reinforced ZrB₂-SiC composite,” *Mater. Sci. Eng. A*, vol. 625, pp. 385–392, 2015.
- [90] Y. Cheng, P. Hu, S. Zhou, X. Zhang, and W. Han, “Using macroporous graphene networks to toughen ZrC–SiC ceramic,” *J. Eur. Ceram. Soc.*, vol. 38, no. 11, pp. 3752–3758, Sep. 2018.
- [91] I. Akin and G. Goller, “Spark Plasma Sintering of Zirconia-Toughened Alumina Composites and Ultra-High Temperature Ceramics Reinforced with Carbon Nanotubes,” in *Research and Innovation in Carbon Nanotube-Based Composites*, no. December, D. B. Attaf, Ed. Hong Kong: The World Academic Publishing Co. Ltd., 2015, pp. 85–101.
- [92] D. Sciti and L. Silvestroni, “Processing, sintering and oxidation behavior of SiC fibers reinforced ZrB₂ composites,” *J. Eur. Ceram. Soc.*, vol. 32, no. 9, pp. 1933–1940, Jul. 2012.
- [93] L. Silvestroni, D. D. Fabbriche, and D. Sciti, “Tyranno SA3 fiber–ZrB₂ composites. Part I: Microstructure and densification,” *Mater. Des.*, vol. 65, pp. 1253–1263, Jan. 2015.
- [94] L. Pienti, D. Sciti, L. Silvestroni, and S. Guicciardi, “Effect of milling on the mechanical properties of chopped SiC fiber-reinforced ZrB₂,” *Materials (Basel)*, vol. 6, no. 5, pp. 1980–1993, 2013.
- [95] F. Yang, X. Zhang, J. Han, and S. Du, “Characterization of hot-pressed short carbon fiber reinforced ZrB₂–SiC ultra-high temperature ceramic composites,” *J. Alloys Compd.*, vol. 472, no. 1–2, pp. 395–399, Mar. 2009.
- [96] D. Sciti, S. Guicciardi, and L. Silvestroni, “SiC chopped fibers reinforced ZrB₂: Effect of the sintering aid,” *Scr. Mater.*, vol. 64, no. 8, pp. 769–772, Apr. 2011.
- [97] L. Silvestroni, S. Guicciardi, M. Nygren, C. Melandri, and D. Sciti, “Effect of the Sintering Additive on Microstructure and Mechanical Properties of Hi-Nicalon TM SiC Fibers in a HfB₂ Matrix,” *J. Am. Ceram. Soc.*, vol. 96, no. 2, pp. 643–650, Oct. 2012.
- [98] L. Pienti, L. Silvestroni, E. Landi, C. Melandri, and D. Sciti, “Microstructure, mechanical properties and oxidation behavior of TaC- and HfC-based materials containing short SiC fiber,” *Ceram. Int.*, vol. 41, no. 1, pp. 1367–1377, Jan. 2015.
- [99] S. R. Bakshi *et al.*, “Spark plasma sintered tantalum carbide–carbon nanotube composite: Effect of pressure, carbon nanotube length and dispersion technique on microstructure and mechanical properties,” *Mater. Sci. Eng. A*, vol. 528, no. 6, pp. 2538–2547, Mar. 2011.
- [100] Y. Wang, M. Zhu, L. Cheng, and L. Zhang, “Fabrication of SiCw reinforced

- ZrB_v-based ceramics,” *Ceram. Int.*, vol. 36, no. 6, pp. 1787–1790, Aug. 2010.
- [101] L. Jia, Z. Xinghong, W. Zhi, and H. Wenbo, “Microstructure and mechanical properties of ZrB₂-SiC-ZrO_{2f} ceramic,” *Scr. Mater.*, vol. 64, no. 9, pp. 872–875, May 2011.
- [102] M. Shahedi Asl, I. Farahbakhsh, and B. Nayebi, “Characteristics of multi-walled carbon nanotube toughened ZrB₂-SiC ceramic composite prepared by hot pressing,” *Ceram. Int.*, vol. 42, no. 1, pp. 1950–1958, 2016.
- [103] F. Y. Yang, “Preparation and Properties of ZrB₂-SiC Ceramic Composites Reinforced by Carbon Nanotubes,” *J. Inorg. Mater.*, vol. 23, no. 5, pp. 950–954, Oct. 2008.
- [104] J. Lin, Y. Huang, H. Zhang, Y. Yang, and N. Li, “Microstructure and mechanical properties of spark plasma sintered ZrB₂-SiC-MWCNT composites,” *Ceram. Int.*, vol. 41, no. 10, pp. 15261–15265, Dec. 2015.
- [105] G. B. Yadhukulakrishnan *et al.*, “Spark plasma sintering of silicon carbide and multi-walled carbon nanotube reinforced zirconium diboride ceramic composite,” *Mater. Sci. Eng. A*, vol. 552, pp. 125–133, Aug. 2012.
- [106] M. Shahedi Asl, F. Golmohammadi, M. Ghassemi Kakroudi, and M. Shokouhimehr, “Synergetic effects of SiC and Cs_f in ZrB₂-based ceramic composites. Part I: Densification behavior,” *Ceram. Int.*, vol. 42, no. 3, pp. 4498–4506, Feb. 2016.
- [107] R. B. Acicbe and G. Goller, “Densification behavior and mechanical properties of spark plasma-sintered ZrC-TiC and ZrC-TiC-CNT composites,” *J. Mater. Sci.*, vol. 48, no. 6, pp. 2388–2393, Mar. 2013.
- [108] G. Sagdic, S., Goller, “Densification behavior and mechanical properties of spark plasma sintered ZrC-SiC and ZrC-SiC-CNT composites,” *J. Aust. Ceram. Soc.*, vol. 50, no. 2, pp. 76–82, 2014.
- [109] D. Sciti, L. Zoli, L. Silvestroni, A. Cecere, G. D. Di Martino, and R. Savino, “Design, fabrication and high velocity oxy-fuel torch tests of a C_f-ZrB₂ - fiber nozzle to evaluate its potential in rocket motors,” *Mater. Des.*, vol. 109, pp. 709–717, Nov. 2016.
- [110] L. Zoli, A. Vinci, L. Silvestroni, D. Sciti, M. Reece, and S. Grasso, “Rapid spark plasma sintering to produce dense UHTCs reinforced with undamaged carbon fibres,” *Mater. Des.*, vol. 130, no. May, pp. 1–7, Sep. 2017.
- [111] J. Sha, J. Li, S. H. Wang, Y. Wang, Z. Zhang, and J. Dai, “Toughening effect of short carbon fibers in the ZrB₂-ZrSi₂ ceramic composites,” *Mater. Des.*, vol. 75, pp. 160–165, Jun. 2015.
- [112] J. J. Sha *et al.*, “ZrB₂-based composites toughened by as-received and heat-treated short carbon fibers,” *J. Eur. Ceram. Soc.*, vol. 37, no. 2, pp. 549–558, Feb. 2017.
- [113] L. Silvestroni, D. Dalle Fabbrie, C. Melandri, and D. Sciti, “Relationships between carbon fiber type and interfacial domain in ZrB₂ -based ceramics,” *J. Eur. Ceram. Soc.*, vol. 36, no. 1, pp. 17–24, Jan. 2016.
- [114] F. Yang, X. Zhang, J. Han, and S. Du, “Mechanical properties of short carbon fiber reinforced ZrB₂-SiC ceramic matrix composites,” *Mater. Lett.*, vol. 62, no. 17–18, pp. 2925–2927, Jun. 2008.
- [115] L. Silvestroni, D. Sciti, C. Melandri, and S. Guicciardi, “Tyranno SA3 fiber-ZrB₂ composites. Part II: Mechanical properties,” *Mater. Des.*, vol. 65, pp. 1264–1273, Jan. 2015.
- [116] W.-B. Tian, Y.-M. Kan, G.-J. Zhang, and P.-L. Wang, “Effect of carbon nanotubes on the properties of ZrB₂-SiC ceramics,” *Mater. Sci. Eng. A*, vol. 487,

- no. 1–2, pp. 568–573, Jul. 2008.
- [117] Z. Nasiri, M. Mashhadi, and A. Abdollahi, “Effect of short carbon fiber addition on pressureless densification and mechanical properties of $\text{ZrB}_2\text{--SiC--Csf}$ nanocomposite,” *Int. J. Refract. Met. Hard Mater.*, vol. 51, pp. 216–223, Jul. 2015.
- [118] S. Guo, K. Naito, and Y. Kagawa, “Mechanical and physical behaviors of short pitch-based carbon fiber-reinforced $\text{HfB}_2\text{--SiC}$ matrix composites,” *Ceram. Int.*, vol. 39, no. 2, pp. 1567–1574, Mar. 2013.
- [119] M. Shahedi Asl, M. Ghassemi Kakroudi, R. Abedi Kondolaji, and H. Nasiri, “Influence of graphite nano-flakes on densification and mechanical properties of hot-pressed $\text{ZrB}_2\text{--SiC}$ composite,” *Ceram. Int.*, vol. 41, no. 4, pp. 5843–5851, May 2015.
- [120] X. Zhang, Z. Wang, X. Sun, W. Han, and C. Hong, “Effect of graphite flake on the mechanical properties of hot pressed $\text{ZrB}_2\text{--SiC}$ ceramics,” *Mater. Lett.*, vol. 62, no. 28, pp. 4360–4362, Nov. 2008.
- [121] Z. Wang, C. Hong, X. Zhang, X. Sun, and J. Han, “Microstructure and thermal shock behavior of $\text{ZrB}_2\text{--SiC}$ –graphite composite,” *Mater. Chem. Phys.*, vol. 113, no. 1, pp. 338–341, Jan. 2009.
- [122] R. Alexander *et al.*, “Effect of graphene nano-platelet reinforcement on the mechanical properties of hot pressed boron carbide based composite,” *Ceram. Int.*, vol. 44, no. 8, pp. 9830–9838, Jun. 2018.
- [123] J. D. Kiser, R. Andrulonis, K. E. David, and C. Davies, *Composite Materials Handbook Volume 5 - Revision A*, vol. 5. SAE International, 2017.
- [124] K. T. Faber, “Ceramic Composite Interfaces: Properties and Design,” *Annu. Rev. Mater. Sci.*, vol. 27, no. 1, pp. 499–524, Aug. 1997.
- [125] J. Buckley, “Carbon-Carbon, An Overview,” *Am. Ceram. Soc. Bull.*, vol. 67, no. 2, pp. 364–368, 1988.
- [126] B. T. B. T. Kelly, *Physics of graphite*. Applied Science, 1981.
- [127] X. Huang, “Fabrication and Properties of Carbon Fibers,” *Materials (Basel)*, vol. 2, no. 4, pp. 2369–2403, Dec. 2009.
- [128] S. J. Park, *Carbon Fibers*, vol. 210. Dordrecht: Springer Netherlands, 2015.
- [129] E. Fitzer, “Pan-based carbon fibers—present state and trend of the technology from the viewpoint of possibilities and limits to influence and to control the fiber properties by the process parameters,” *Carbon N. Y.*, vol. 27, no. 5, pp. 621–645, Jan. 1989.
- [130] Akio Shindo, “Process for the preparation of carbon fibers,” US3529934A, 04-Jan-1968.
- [131] W. N. Reynolds and J. V. Sharp, “Crystal shear limit to carbon fibre strength,” *Carbon N. Y.*, vol. 12, no. 2, pp. 103–110, Apr. 1974.
- [132] X. Huang, “Fabrication and Properties of Carbon Fibers,” *Materials (Basel)*, vol. 2, no. 4, pp. 2369–2403, Dec. 2009.
- [133] P. Morgan, *Carbon fibers and their composites*. Taylor & Francis, 2005.
- [134] “Teijin Carbon – Tenax® Filament Yarn.” [Online]. Available: <https://www.tejincarbon.com/products/tenaxr-carbon-fiber/tenaxr-filament-yarn>. [Accessed: 24-Jan-2019].
- [135] “TORAYCA® yarn | TORAYCA® | TORAY.” [Online]. Available: http://www.torayca.com/en/lineup/product/pro_001_01.html. [Accessed: 24-Jan-2019].
- [136] “PAN Fiber - Mitsubishi Chemical Carbon Fiber Composites.” [Online]. Available: <http://mccfc.com/pan-fiber/>. [Accessed: 24-Jan-2019].

- [137] "Carbon Fiber DataSheet | Hexcel." [Online]. Available: <https://www.hexcel.com/Resources/DataSheets/Carbon-Fiber>. [Accessed: 24-Jan-2019].
- [138] "Search | Solvay." [Online]. Available: <https://www.solvay.com/en/search?f%5B0%5D=fsection%3AProducts>. [Accessed: 24-Jan-2019].
- [139] "Carbon Fiber." [Online]. Available: <http://www.formosa.co.kr/producs/carbon-fiber/#collapse-1-12662>. [Accessed: 24-Jan-2019].
- [140] "SIGRAFIL C PAN-based Carbon Fiber SGL CARBON." [Online]. Available: https://www.sglgroup.com/cms/international/products/product-groups/cf/carbon-fiber-continuous-tow/index.html?__locale=en. [Accessed: 24-Jan-2019].
- [141] "GRANOC Yarn | Nippon Graphite Fiber Corporation | Unique properties of GRANOC contribute to the development of advanced technology." [Online]. Available: http://www.ngfworld.com/en/en_product/en_yarn.html. [Accessed: 24-Jan-2019].
- [142] S. Yajima, Y. Hasegawa, K. Okamura, and T. Matsuzawa, "Development of high tensile strength silicon carbide fibre using an organosilicon polymer precursor," *Nature*, vol. 273, no. 5663, pp. 525–527, Jun. 1978.
- [143] W. Caputo, AJ (Caputo, Aj); Lackey, WJ (Lackey, "Continued Development of the Fabrication of Ceramic Fiber-Reinforced Ceramic Composites," *Am. Ceram. Soc. Bull.*, vol. 63, no. 12, pp. 1477–1477, 1984.
- [144] D. Schawaller, B. Clauß, and M. R. Buchmeiser, "Ceramic Filament Fibers - A Review," *Macromol. Mater. Eng.*, vol. 297, no. 6, pp. 502–522, Jun. 2012.
- [145] A. R. Bunsell and A. Piant, "A review of the development of three generations of small diameter silicon carbide fibres," *J. Mater. Sci.*, vol. 41, no. 3, pp. 823–839, Feb. 2006.
- [146] O. Flores, R. K. Bordia, D. Nestler, W. Krenkel, and G. Motz, "Ceramic Fibers Based on SiC and SiCN Systems: Current Research, Development, and Commercial Status," *Adv. Eng. Mater.*, vol. 16, no. 6, pp. 621–636, Jun. 2014.
- [147] J. A. DiCarlo and H.-M. Yun, "Non-oxide (Silicon Carbide) Fibers," in *Handbook of Ceramic Composites*, Springer, Boston, MA, 2005, pp. 33–52.
- [148] "Silicon Carbide Fibre| TISICS Ltd." [Online]. Available: <https://www.tisics.co.uk/Silicon-Carbide-Fibre>. [Accessed: 06-Jan-2019].
- [149] "Specialty Materials, Inc. - Boron Fiber, SCS Silicon Carbide Fibers and Boron Nanopowder." [Online]. Available: <http://specmaterials.com/>. [Accessed: 06-Jan-2019].
- [150] R. Leucht and H. J. Dudek, "Properties of SiC-fibre reinforced titanium alloys processed by fibre coating and hot isostatic pressing," *Mater. Sci. Eng. A*, vol. 188, no. 1–2, pp. 201–210, Nov. 1994.
- [151] S. Yajima, Y. Hasegawa, J. Hayashi, and M. Imura, "Synthesis of continuous silicon carbide fibre with high tensile strength and high Young's modulus," *J. Mater. Sci.*, vol. 13, no. 12, pp. 2569–2576, Dec. 1978.
- [152] N. P. Bansal, *Handbook of Ceramic Composites*. Springer US, 2005.
- [153] Y. Lipowitz, J., Rabe, J. A., Zangvil, A. & Xu, "Structure and Properties of SylramicTM Silicon Carbide Fiber—A Polycrystalline, Stoichiometric β - SiC Composition," in *Proceedings of the 21 st Annual Conference on Composites, Advanced Ceramics, Materials, and Structures-A*, 1997, vol. January 12-16, pp. 147–157.
- [154] J. DiCarlo, *Advances in SiC/SiC Composites for Aero-Propulsion in Ceramic matrix composites : materials, modeling and technology*. 2015.

- [155] “GE Aviation is fired up about CMCs! | The GE Aviation Blog | Aerospace & Flight News,” 2015. [Online]. Available: <https://blog.geaviation.com/manufacturing/ge-aviation-fired-up-about-cmcs/>. [Accessed: 30-Apr-2019].
- [156] R. Naslain *et al.*, “Boron Nitride Interphase in Ceramic-Matrix Composites,” *J. Am. Ceram. Soc.*, vol. 74, no. 10, pp. 2482–2488, Oct. 1991.
- [157] J. A. Dever, M. V. Nathal, and J. A. DiCarlo, “Research on High-Temperature Aerospace Materials at NASA Glenn Research Center,” *J. Aerosp. Eng.*, vol. 26, no. 2, pp. 500–514, Apr. 2013.
- [158] S. Johnson and M. Gasch, “Assessment of the State of the Art of Ultra High Temperature Ceramics,” Moffett Field, 2009.
- [159] C. Yan, R. Liu, C. Zhang, and Y. Cao, “Zirconium carbide, hafnium carbide and their ternary carbide nanoparticles by an in situ polymerization route,” *RSC Adv.*, vol. 5, no. 46, pp. 36520–36529, 2015.
- [160] K. Nakane, S. Matsuoka, S. Gao, S. Yonezawa, J. H. Kim, and N. Ogata, “Formation of inorganic nanofibers by heat-treatment of poly(vinyl alcohol)-zirconium compound hybrid nanofibers,” *J. Min. Metall. Sect. B Metall.*, vol. 49, no. 1, pp. 77–82, 2013.
- [161] X. M. Cui, Y. S. Nam, J. Y. Lee, and W. H. Park, “Fabrication of zirconium carbide (ZrC) ultra-thin fibers by electrospinning,” *Mater. Lett.*, vol. 62, no. 12–13, pp. 1961–1964, Apr. 2008.
- [162] R. Ghelich, R. Mehdiavaz Aghdam, F. S. Torknik, M. R. Jahannama, and M. Keyanpour-Rad, “Carbothermal reduction synthesis of ZrB₂ nanofibers via pre-oxidized electrospun zirconium n-propoxide,” *Ceram. Int.*, vol. 41, no. 5, pp. 6905–6911, Jun. 2015.
- [163] I. Hasegawa, Y. Fukuda, and M. Kajiwara, “Inorganic–organic hybrid route to synthesis of ZrC and Si–Zr–C fibres,” *Ceram. Int.*, vol. 25, no. 6, pp. 523–527, Aug. 1999.
- [164] X. Tao *et al.*, “A facile method to prepare ZrC nanofibers by electrospinning and pyrolysis of polymeric precursors,” *Ceram. Int.*, vol. 43, no. 4, pp. 3910–3914, Mar. 2017.
- [165] F. Li, Z. Kang, X. Huang, and G.-J. Zhang, “Fabrication of zirconium carbide nanofibers by electrospinning,” *Ceram. Int.*, vol. 40, no. 7, pp. 10137–10141, Aug. 2014.
- [166] J. S. Atchison, M. Zeiger, A. Tolosa, L. M. Funke, N. Jäckel, and V. Presser, “Electrospinning of ultrafine metal oxide/carbon and metal carbide/carbon nanocomposite fibers,” *RSC Adv.*, vol. 5, no. 45, pp. 35683–35692, 2015.
- [167] “MATECH | Military Advanced Technology.” [Online]. Available: <http://www.matech.net/>. [Accessed: 06-Jan-2019].
- [168] K. Pope, E.J.A. and Kratsch and Pope E.J.A and Kratsch K.M, “Preceramic polymers to hafnium carbide and hafnium nitride ceramic fibers and matrices,” 10/058,808, 2002.
- [169] E. J. A. Pope, “Ultra-High-Temperature Refractory Metal Carbide CMC’s,” in *29th Annual Conference on Composites, Materials and Structures (U.S. Only/ITAR restricted) (2005)*, 2005.
- [170] E. J. A. Pope, “Preceramic Polymers to Hafnium Carbide Fibres and Matrices,” in *National Space and Missile Materials Symposium (U.S. Only/ITAR restricted) (2004)*, 2004.
- [171] E. J. A. . Kratsch *et al.*, “High Temperature and Ultra-High temperature Ceramic Fibre Development and Applications,” in *(AFRL, 2009)*, 2009.

- [172] G. Metcalfe, E. N., W. B., and M. Opeka, "Oxidation Above 3300°C of Refractory Materials in an Aluminized Flame," in *4th, International Symposium on High Temperature Corrosion and Materials Chemistry Proceedings-Electrochemical Society Pv;*, 2003, pp. 420–430.
- [173] E. J. A. Pope, "TaC_f/TaC CMCs for Ultra-High-Temperature Applications.," in *29th Annual Conference on Composites, Materials and Composites (2005).*, 2005.
- [174] K. A. W. Maurlice James Evans, "Manufacture of carbon fibre preform Page," GB 2234989 A, 1999.
- [175] L. M. Manocha and O. P. Bahl, "Influence of carbon fiber type and weave pattern on the development of 2D carbon-carbon composites," *Carbon N. Y.*, vol. 26, no. 1, pp. 13–21, 1988.
- [176] C. C. M. Ma;, N. H. Tai;, W. C. Change;, and Y. P. Tsai, "Morphologies, Microstructure and Mechanical Properties of 2D Carbon/Carbon Composites during the CVI Densification Process," *Carbon N. Y.*, vol. 34, no. 10, pp. 1175–1179, 1996.
- [177] S. Berthon and G. Malé, "Infiltration of zirconium diboride by ICVI in porous materials," *Compos. Sci. Technol.*, vol. 57, no. 2, pp. 217–227, Jan. 1997.
- [178] U. Beier, F. Fischer, J. K. W. Sandler, V. Altstädt, C. Weimer, and W. Buchs, "Mechanical performance of carbon fibre-reinforced composites based on stitched preforms," *Compos. Part A Appl. Sci. Manuf.*, vol. 38, no. 7, pp. 1655–1663, Jul. 2007.
- [179] V. Rubio *et al.*, "Materials characterisation and mechanical properties of C_f-UHTC powder composites," *J. Eur. Ceram. Soc.*, vol. 39, no. 4, pp. 813–824, Apr. 2019.
- [180] P. M. Ajayan, L. S. Schadler, C. Giannaris, and A. Rubio, "Single-Walled Carbon Nanotube-Polymer Composites: Strength and Weakness," *Adv. Mater.*, vol. 12, no. 10, pp. 750–753, May 2000.
- [181] Y. Wang, W. Liu, L. Cheng, and L. Zhang, "Preparation and properties of 2D C/ZrB₂-SiC ultra high temperature ceramic composites," *Mater. Sci. Eng. A*, vol. 524, no. 1–2, pp. 129–133, Oct. 2009.
- [182] J. Xie, K. Li, H. Li, Q. Fu, and L. Guo, "Ablation behavior and mechanism of C/C–ZrC–SiC composites under an oxyacetylene torch at 3000°C," *Ceram. Int.*, vol. 39, no. 4, pp. 4171–4178, May 2013.
- [183] A. Paul, V. Rubio, J. Binner, B. Vaidhyanathan, A. Heaton, and P. Brown, "Evaluation of the high temperature performance of HfB₂ UHTC particulate filled C_f/C composites," *Int. J. Appl. Ceram. Technol.*, vol. 14, no. 3, pp. 344–353, May 2017.
- [184] J. P. Ai, S. S. Luo, W. K. Li, S. W. Wang, and G. H. Zhou, "Mechanical Properties and Microstructure of 2.5D C/ZrO₂ Composites Prepared by Precursor Infiltration and Pyrolysis," *Key Eng. Mater.*, vol. 697, pp. 639–643, Jul. 2016.
- [185] G. Boitier, J. Vicens, and J. . Chermant, "Understanding the creep behavior of a 2.5D C_f-SiC composite-I. Morphology and microstructure of the as-received material," *Mater. Sci. Eng. A*, vol. 279, no. 1–2, pp. 73–80, Feb. 2000.
- [186] I. D. B. Baker, V. Rubio, P. Ramanujam, J. Binner, A. Hussain, T. Ackerman, P. Brown, "Development of a slurry injection technique for continuous fibre ultra-high temperature ceramic matrix composites (UHTCMCs)," *J. Eur. Ceram. Soc.*, vol. Under revi, 2019.
- [187] A. Paul, J. G. P. Binner, B. Vaidhyanathan, A. C. J. Heaton, and P. M. Brown, "Heat flux mapping of oxyacetylene flames and their use to characterise C_f-HfB₂

- composites,” *Adv. Appl. Ceram.*, vol. 115, no. 3, pp. 158–165, Apr. 2016.
- [188] A. D’Angio’, J. Zou, J. Binner, H. Ma, G. E. Hilmas, and W. G. Fahrenholtz, “Mechanical properties and grain orientation evolution of zirconium diboride-zirconium carbide ceramics,” *J. Eur. Ceram. Soc.*, vol. 38, no. 2, pp. 391–402, Feb. 2018.
- [189] L. A. Timms, W. Westby, C. Prentice, D. Jaglin, R. A. Shatwell, and J. G. P. Binner, “Reducing chemical vapour infiltration time for ceramic matrix composites,” *J. Microsc.*, vol. 201, no. 2, pp. 316–323, Feb. 2001.
- [190] X. Chen, S. Dong, Y. Kan, H. Zhou, J. Hu, and D. Wang, “3D C_f/SiC-ZrC-ZrB₂ composites fabricated via sol-gel process combined with reactive melt infiltration,” *J. Eur. Ceram. Soc.*, vol. 36, no. 15, pp. 3607–3613, Nov. 2016.
- [191] J. Jiang, S. Wang, W. Li, Z. Chen, and Y. Zhu, “Preparation of 3D C_f/ZrC–SiC composites by joint processes of PIP and RMI,” *Mater. Sci. Eng. A*, vol. 607, pp. 334–340, Jun. 2014.
- [192] Q. Li *et al.*, “Fabrication and Properties of 3-D C_f/SiC-ZrC Composites, Using ZrC Precursor and Polycarbosilane,” *J. Am. Ceram. Soc.*, vol. 95, no. 4, pp. 1216–1219, Apr. 2012.
- [193] B. S. Sugun; and R. Sundaram, “3D Composites: Opportunities & Challenges,” *J. Indian Inst. Sci.*, vol. 95:3, no. Jul.–Sep., pp. 1–13, 2016.
- [194] Z. Xie, T. Zhou, and Y. Gou, “Synthesis and characterization of zirconium diboride ceramic precursor,” *Ceram. Int.*, vol. 41, no. 5, Part A, pp. 6226–6231, 2015.
- [195] A. Gao, C. Zhao, S. Luo, Y. Tong, and L. Xu, “Correlation between graphite crystallite distribution morphology and the mechanical properties of carbon fiber during heat treatment,” *Mater. Lett.*, vol. 65, no. 23, pp. 3444–3446, 2011.
- [196] Z. Xie, X. Deng, X. Suo, T. Zhou, and Y. Gou, “Synthesis and characterization of zirconium diboride precursor based on polycentric bridge bonds,” *Mater. Chem. Phys.*, vol. 159, pp. 178–184, 2015.
- [197] M. Zhang, K. zhi Li, X. hong Shi, and W. long Tan, “Effects of SiC interphase on the mechanical and ablation properties of C/C-ZrC-ZrB₂-SiC composites prepared by precursor infiltration and pyrolysis,” *Mater. Des.*, vol. 122, pp. 322–329, 2017.
- [198] X. Zhao, Y. Wang, L. Duan, L. Luo, and Y. Lu, “Improved ablation resistance of C/SiC-ZrB₂ composites via polymer precursor impregnation and pyrolysis,” *Ceram. Int.*, vol. 43, no. 15, pp. 12480–12489, 2017.
- [199] J. He, Y. Gao, Y. Wang, J. Fang, and L. An, “Synthesis of ZrB₂-SiC nanocomposite powder via polymeric precursor route,” *Ceram. Int.*, vol. 43, no. 1, pp. 1602–1607, Jan. 2017.
- [200] W. Zhang, C. Xie, M. Ge, and X. Wei, “C/C-ZrB₂-ZrC-SiC Composites Derived from Polymeric Precursor Infiltration and Pyrolysis Part I,” in *MAX Phases and Ultra-High Temperature Ceramics for Extreme Environments*, C. F. H. Low, I. M., Y. Sakka, Ed. United States of America: IGI Global, 2013, pp. 413–434.
- [201] X. Lv, S. Yu, M. Ge, Y. Tian, and W. Zhang, “Synthesis and microstructure of continuous composite ceramic fibres of ZrC/ZrB₂-SiC derived from polymeric precursors,” *Ceram. Int.*, vol. 42, no. 7, pp. 9299–9303, May 2016.
- [202] Y. Li, X. Tao, W. Qiu, J. Zhao, and T. Zhao, “Preparation of powdered zirconium diboride by a solution precursor conversion method,” *J. Beijing Univ. Chem. Technol. (Natural Sci. Ed.)*, vol. 37, no. 4, pp. 78–82, 2010.
- [203] G. Takahiro, Y. Hiroshi, H. Takaaki, B. K. Kyoko, and A. Yoshimoto, “Preparation of polyzirconoxane from zirconium oxychloride octahydrate and

- ethylene glycol as a precursor for zirconia ceramics,” *Appl. Organomet. Chem.*, vol. 14, no. 2, pp. 119–126, 2000.
- [204] Y. Abe, T. Kudo, H. Tomioka, T. Gunji, Y. Nagao, and Y. Abe, “Preparation of continuous zirconia fibres from polyzirconoxane synthesized by the facile one-pot reaction,” *J. Mater. Sci.*, vol. 33, no. 7, pp. 1863–1870, Apr. 1998.
- [205] N. Patra, N. Al Nasiri, D. D. Jayaseelan, and W. E. Lee, “Thermal properties of C_f/HfC and $C_f/HfC-SiC$ composites prepared by precursor infiltration and pyrolysis,” *J. Eur. Ceram. Soc.*, vol. 38, no. 5, pp. 2297–2303, May 2018.
- [206] M. Yan, H. Li, Q. Fu, J. Xie, L. Liu, and B. Feng, “Ablative Property of $C/C-SiC-HfC$ Composites Prepared via Precursor Infiltration and Pyrolysis under 3,000°C Oxyacetylene Torch,” *Acta Metall. Sin. (English Lett.)*, vol. 27, no. 6, pp. 981–987, Dec. 2014.
- [207] L. Duan, X. Zhao, and Y. Wang, “Comparative ablation behaviors of $C/SiC-HfC$ composites prepared by reactive melt infiltration and precursor infiltration and pyrolysis routes,” *Ceram. Int.*, vol. 43, no. 18, pp. 16114–16120, Dec. 2017.
- [208] D. Huang, M. Zhang, Q. Huang, L. Wang, and K. Tong, “Mechanical Property, Oxidation and Ablation Resistance of $C/C-ZrB_2-ZrC-SiC$ Composite Fabricated by Polymer Infiltration and Pyrolysis with Preform of C_f/ZrB_2 ,” *J. Mater. Sci. Technol.*, vol. 33, no. 5, pp. 481–486, 2017.
- [209] Q. Li, S. Dong, Z. Wang, and G. Shi, “Fabrication and properties of 3-D $C_f/ZrB_2-ZrC-SiC$ composites via polymer infiltration and pyrolysis,” *Ceram. Int.*, vol. 39, no. 5, pp. 5937–5941, Jul. 2013.
- [210] L. Zhuang, Q.-G. Fu, and T.-Y. Liu, “Ablation resistance of wedge-shaped $C/C-ZrB_2-ZrC-SiC$ composites exposed to an oxyacetylene torch,” *Corros. Sci.*, vol. 112, pp. 462–470, Nov. 2016.
- [211] G. Ziegler, I. Richter, and D. Suttor, “Fiber-reinforced composites with polymer-derived matrix: processing, matrix formation and properties,” *Compos. Part A Appl. Sci. Manuf.*, vol. 30, no. 4, pp. 411–417, 1999.
- [212] C. Yan, R. Liu, C. Zhang, Y. Cao, and X. Long, “Mechanical behaviour and microstructure of C_f/ZrC , C_f/SiC and $C_f/ZrC-SiC$ composites,” *Adv. Appl. Ceram.*, vol. 115, no. 7, pp. 391–395, 2016.
- [213] D. King, Z. Apostolov, T. Key, C. Carney, and M. Cinibulk, “Novel processing approach to polymer-derived ceramic matrix composites,” *Int. J. Appl. Ceram. Technol.*, vol. 15, no. 2, pp. 399–408, 2018.
- [214] “GE Aviation fired up on CMCs.” General Electric, Delaware, US, 2015.
- [215] W. B. Hillig *et al.*, “Fabrication of Ceramic Matrix Composites by Liquid Silicon Infiltration (LSI),” *Ceram. Int.*, vol. 38, no. 2, pp. 191–196, 2012.
- [216] Jeff Crompton and J. Compton, “Multiphysics Analysis of Advanced Materials: Ceramic Matrix Composites | COMSOL Blog,” *COMSOL BLOG*, 2014. [Online]. Available: <https://uk.comsol.com/blogs/multiphysics-analysis-advanced-materials-ceramic-matrix-composites/>. [Accessed: 04-Jan-2019].
- [217] E. O. Einset, “Analysis of reactive melt infiltration in the processing of ceramics and ceramic composites,” *Chem. Eng. Sci.*, vol. 53, no. 5, pp. 1027–1039, Feb. 1998.
- [218] L. Zhang, S. Dong, H. Zhou, Y. Kan, F. Zhou, and Z. Wang, “3D $C_f/ZrC-SiC$ composites fabricated with ZrC nanoparticles and $ZrSi_2$ alloy,” *Ceram. Int.*, vol. 40, no. 8, Part A, pp. 11795–11801, 2014.
- [219] X. Chen *et al.*, “Interphase degradation of three-dimensional $C_f/SiC-ZrC-ZrB_2$ composites fabricated via reactive melt infiltration,” *J. Am. Ceram. Soc.*, vol. 100, no. 10, pp. 4816–4826, Oct. 2017.

- [220] M. Küttemeyer, L. Schomer, T. Helmreich, S. Rosiwal, and D. Koch, "Fabrication of ultra high temperature ceramic matrix composites using a reactive melt infiltration process," *J. Eur. Ceram. Soc.*, vol. 36, no. 15, pp. 3647–3655, Nov. 2016.
- [221] S. Tang and C. Hu, "Design, Preparation and Properties of Carbon Fiber Reinforced Ultra-High Temperature Ceramic Composites for Aerospace Applications: A Review," *J. Mater. Sci. Technol.*, vol. 33, no. 2, pp. 117–130, Feb. 2017.
- [222] Y. Liu, Q. Fu, J. Zhang, L. Li, and L. Zhuang, "Erosion resistance of C/C-SiC-ZrB₂ composites exposed to oxyacetylene torch," *J. Eur. Ceram. Soc.*, vol. 36, no. 15, pp. 3815–3821, Nov. 2016.
- [223] W. B. Hillig, "Melt Infiltration Approach to Ceramic Matrix Composites," *J. Am. Ceram. Soc.*, vol. 71, no. 2, p. C- 96-C- 99, 1988.
- [224] Y. Tong, S. Bai, Y. Ye, H. Zhang, and Z. Yang, "Reactive melt infiltration of a ZrB₂ modified C/ZrC composite by a eutectic Zr-B alloy," *Mater. Lett.*, vol. 138, pp. 208–211, 2015.
- [225] S. Chen, C. Zhang, Y. Zhang, and H. Hu, "Preparation and properties of carbon fiber reinforced ZrC-ZrB₂ based composites via reactive melt infiltration," *Compos. Part B Eng.*, vol. 60, pp. 222–226, Apr. 2014.
- [226] M. Kutemeyer Helmreich, T., Koch, D., Rosiwal, S., "Influence of Zirconium-Based Alloys on Manufacturing and Mechanical-Properties of Ultra High Temperature Ceramic Matrix Composites," *Adv. Appl. Ceram. Struct. Funct. Bioceram.*, vol. Submitted, 2018.
- [227] Y. Tong, S. Bai, and K. Chen, "C/C-ZrC composite prepared by chemical vapor infiltration combined with alloyed reactive melt infiltration," *Ceram. Int.*, vol. 38, no. 7, pp. 5723–5730, 2012.
- [228] Z. Li, H. Li, S. Zhang, J. Wang, W. Li, and F. Sun, "Effect of reaction melt infiltration temperature on the ablation properties of 2D C/C-SiC-ZrC composites," *Corros. Sci.*, vol. 58, pp. 12–19, 2012.
- [229] Y. Wang, X. Zhu, L. Zhang, and L. Cheng, "Reaction kinetics and ablation properties of C/C-ZrC composites fabricated by reactive melt infiltration," *Ceram. Int.*, vol. 37, no. 4, pp. 1277–1283, 2011.
- [230] L. Zou, N. Wali, J.-M. Yang, and N. P. Bansal, "Microstructural development of a C_f/ZrC composite manufactured by reactive melt infiltration," *J. Eur. Ceram. Soc.*, vol. 30, no. 6, pp. 1527–1535, 2010.
- [231] H. Pi, S. Fan, and Y. Wang, "C/SiC-ZrB₂-ZrC composites fabricated by reactive melt infiltration with ZrSi₂ alloy," *Ceram. Int.*, vol. 38, no. 8, pp. 6541–6548, 2012.
- [232] X. Chen *et al.*, "Reaction mechanism and microstructure development of ZrSi₂ melt-infiltrated Cf/SiC-ZrC-ZrB₂ composites: The influence of preform pore structures," *J. Mater.*, vol. 4, no. 3, pp. 266–275, Sep. 2018.
- [233] M. . Muolo, E. Ferrera, R. Novakovic, and A. Passerone, "Wettability of zirconium diboride ceramics by Ag, Cu and their alloys with Zr," *Scr. Mater.*, vol. 48, no. 2, pp. 191–196, Jan. 2003.
- [234] Y. Wang, Q. Liu, J. Liu, L. Zhang, and L. Cheng, "Deposition Mechanism for Chemical Vapor Deposition of Zirconium Carbide Coatings," *J. Am. Ceram. Soc.*, vol. 91, no. 4, pp. 1249–1252, Apr. 2008.
- [235] A. Allemand *et al.*, "Protection against Oxydation by CVD or SPS Coatings of Hafnium Carbide and Silicon Carbide on Carbon/Carbon Composites," *Adv. Ceram. Coatings Mater. Extrem. Environ. II*, pp. 161-169., 2013.

- [236] H. O. Pierson, *Handbook of refractory carbides and nitrides: Properties, characteristics, processing and applications*. Noyes Publication, New York, NY (United States), 1997.
- [237] H. Pierson, *Handbook of Chemical Vapour Deposition: Principles, Technology and Applications*. New York: William Andrew Publishing, 1999.
- [238] J. Arnold, J. O., Y.K. Chen, T. Squire, D. Srivastava, G. Allen and E. V. and M. P. L. M. Stackpoole, H. E. Goldstein, "Nanostructured Thermal Protection Systems for Space Exploration Missions," 2004.
- [239] V. Wunder et al., "Multilayer coatings on CFC composites for high-temperature applications," *Surf. Coatings Technol.*, vol. 100, pp. 329-332., 1998.
- [240] C. Subramanian and K. N. Strafford, "Review of multicomponent and multilayer coatings for tribological applications," *Wear*, vol. 165, no. 1, pp. 85-95, 1993.
- [241] F. Smeacetto et al., "Protective coatings for carbon bonded carbon fibre composites," *Ceram. Int.*, 2008.
- [242] I. Golecki, "Rapid vapor-phase densification of refractory composites.," *Mater. Sci. Eng. R-Reports*, vol. 20, no. 2, pp. 37-124., 1997.
- [243] J. Y. Ofori; and S. V Sotirchos, "Optimal pressures and temperatures for isobaric, isothermal chemical vapor infiltration," *Aiche J.*, vol. 42, no. 10, pp. 2828-2840., 1996.
- [244] X. Ma Yin, X., Cao, X., Chen, L., Cheng, L., and Zhang, L., "Effect of heat treatment on the mechanical properties of SiC_f/BN/SiC fabricated by CVI," *Ceram. Int.*, vol. 42, no. 2, pp. 3652-3658., 2016.
- [245] R. Naslain Hannache, H., Heraud, L., Christin, F., Rossignol, J.Y., and Colmet, R., "Advanced Ceramic-Ceramic Composite-Materials from the CVI Process," *Am. Ceram. Soc. Bull.*, vol. 62, no. 11, 1983.
- [246] R. Naslain, F. Langlais, and R. Fedou, "The Cvi-Processing of Ceramic Matrix Composites," *Le J. Phys. Colloq.*, vol. 50, no. C5, pp. 191-207, May 1989.
- [247] K. Yee, "Protective coatings for metals by chemical vapour deposition," *Int. Met. Rev.*, vol. 23, no. 1, pp. 19-42., 1978.
- [248] H.-J. Li, H. Xue, Y.-J. Wang, Q.-G. Fu, and D.-J. Yao, "A MoSi₂-SiC-Si oxidation protective coating for carbon/carbon composites," *Surf. Coatings Technol.*, vol. 201, no. 24, pp. 9444-9447, Oct. 2007.
- [249] A. Lazzeri, "CVI Processing of Ceramic Matrix Composites," in *Ceramics and Composites Processing Methods*, Hoboken, NJ, USA: John Wiley & Sons, Inc., 2012, pp. 313-349.
- [250] G. Q. Lu, "Modelling the densification of porous structures in CVI ceramic composites processing," *J. Mater. Process. Technol.*, vol. 37, no. 1-4, pp. 487-498, Feb. 1993.
- [251] J. M. Rosas, J. Bedia-Matamoros, J. Rodríguez-Mirasol, and T. Cordero, "Kinetics of pyrolytic carbon infiltration for the preparation of ceramic/carbon and carbon/carbon composites," *Carbon N. Y.*, vol. 42, no. 7, pp. 1285-1290, Jan. 2004.
- [252] Y. S. Lin and A. J. Burggraaf, "Modelling and analysis of CVD processes in porous media for ceramic composite preparation," *Chem. Eng. Sci.*, vol. 46, no. 12, pp. 3067-3080, Jan. 1991.
- [253] J. P. Dekker, R. Moene, and J. Schoonman, "The influence of surface kinetics in modelling chemical vapour deposition processes in porous preforms," *J. Mater. Sci.*, vol. 31, pp. 3021-3033, 1996.
- [254] D. Sciti, L. Silvestroni, F. Monteverde, A. Vinci, and L. Zoli, "Introduction to H2020 project C 3 HARME – next generation ceramic composites for

- combustion harsh environment and space,” *Adv. Appl. Ceram.*, vol. 117, no. sup1, pp. 70–75, Oct. 2018.
- [255] M. Balasubramanian, *Composite Materials and Processing*. CRC Press, 2013.
- [256] F. F. Lange, W. C. Tu, and A. G. Evans, “Processing of damage-tolerant, oxidation-resistant ceramic matrix composites by a precursor infiltration and pyrolysis method,” *Mater. Sci. Eng. A*, vol. 195, pp. 145–150, Jun. 1995.
- [257] J. S. Reed, “Liquid Permeability of Packed Particles: Why Perpetuate the Carmen-Kozeny Model?,” *J. Am. Ceram. Soc.*, vol. 76, no. 2, pp. 547–548, Feb. 1993.
- [258] S.-H. Lee, M. Weinmann, and F. Aldinger, “Fabrication of Fiber-Reinforced Ceramic Composites by the Modified Slurry Infiltration Technique,” *J. Am. Ceram. Soc.*, vol. 90, no. 8, pp. 2657–2660, Aug. 2007.
- [259] A. V. Vasin *et al.*, “Amorphous SiO_xC_y (:Er) films deposited by RF-magnetron sputtering on ZrB_2 –SiC ceramics: Antioxidation and strengthening effects,” *Surf. Coatings Technol.*, vol. 343, pp. 11–16, Jun. 2018.
- [260] D. D. Jayaseelan, R. G. de Sá, P. Brown, and W. E. Lee, “Reactive infiltration processing (RIP) of ultra high temperature ceramics (UHTC) into porous C/C composite tubes,” *J. Eur. Ceram. Soc.*, vol. 31, no. 3, pp. 361–368, Mar. 2011.
- [261] J. D. Buckley and D. D. (Dan D. Edie, *Carbon-carbon materials and composites*. Noyes Publications, 1993.
- [262] L. Li, H. Li, Y. Li, X. Yin, Q. Shen, and Q. Fu, “A SiC– ZrB_2 –ZrC coating toughened by electrophoretically-deposited SiC nanowires to protect C/C composites against thermal shock and oxidation,” *Appl. Surf. Sci.*, vol. 349, pp. 465–471, Sep. 2015.
- [263] M. D. Alvey and P. M. George, “ ZrPt_3 as a high-temperature, reflective, oxidation-resistant coating for carbon-carbon composites,” *Carbon N. Y.*, vol. 29, no. 4–5, pp. 523–530, Jan. 1991.
- [264] Y. Yan, Z. Huang, S. Dong, and D. Jiang, “New Route to Synthesize Ultra-Fine Zirconium Diboride Powders Using Inorganic/Organic Hybrid Precursors,” *J. Am. Ceram. Soc.*, vol. 89, no. 11, pp. 3585–3588, Nov. 2006.
- [265] J. A. Jensen, J. E. Gozum, D. M. Pollina, and G. S. Girolami, “Titanium, zirconium, and hafnium tetrahydroborates as ‘tailored’ CVD precursors for metal diboride thin films,” *J. Am. Chem. Soc.*, vol. 110, no. 5, pp. 1643–1644, Mar. 1988.
- [266] D. W. McKee, “Oxidation behavior and protection of carbon/carbon composites,” *Carbon N. Y.*, vol. 25, no. 4, pp. 551–557, Jan. 1987.
- [267] Q. He, H. Li, C. Wang, S. Chen, and J. Lu, “Densification behavior and ablation property of C/C–ZrC composites prepared by chemical liquid vapor deposition process at temperatures from 800 to 1100 °C,” *Ceram. Int.*, vol. 44, no. 7, pp. 7991–8004, May 2018.
- [268] J. Pourasad, N. Ehsani, and Z. Valefi, “Oxidation resistance of a SiC– ZrB_2 coating prepared by a novel pack cementation on SiC-coated graphite,” *J. Mater. Sci.*, vol. 52, no. 3, pp. 1639–1646, Feb. 2017.
- [269] J. Prakash, M. Gade, B. Paul, and K. Dasgupta, “A facile route for graded conversion of carbon fabric to silicon carbide fabric and its oxidation kinetics study in atmospheric high-temperature environment,” *Bull. Mater. Sci.*, vol. 41, no. 4, p. 108, Aug. 2018.
- [270] H. Mei, Q. Bai, T. Ji, H. Li, and L. Cheng, “Effect of carbon nanotubes electrophoretically-deposited on reinforcing carbon fibers on the strength and toughness of C/SiC composites,” *Compos. Sci. Technol.*, vol. 103, pp. 94–99,

Oct. 2014.

- [271] J. Guo and C. Lu, "Continuous preparation of multiscale reinforcement by electrophoretic deposition of carbon nanotubes onto carbon fiber tows," *Carbon N. Y.*, vol. 50, no. 8, pp. 3101–3103, Jul. 2012.
- [272] T. Feng, H.-J. Li, X.-H. Shi, X. Yang, and S.-L. Wang, "Oxidation and ablation resistance of $\text{ZrB}_2\text{--SiC--Si/B}$ -modified SiC coating for carbon/carbon composites," *Corros. Sci.*, vol. 67, pp. 292–297, Feb. 2013.
- [273] X. Yao, H. Li, Y. Zhang, H. Wu, and X. Qiang, "A SiC–Si– ZrB_2 multiphase oxidation protective ceramic coating for SiC-coated carbon/carbon composites," *Ceram. Int.*, vol. 38, no. 3, pp. 2095–2100, Apr. 2012.
- [274] E. L. Corral and R. E. Loehman, "Ultra-High-Temperature Ceramic Coatings for Oxidation Protection of Carbon–Carbon Composites," *J. Am. Ceram. Soc.*, vol. 91, no. 5, pp. 1495–1502, May 2008.
- [275] P. Galizia, S. Failla, L. Zoli, and D. Sciti, "Tough salami-inspired C_f/ZrB_2 UHTCMCs produced by electrophoretic deposition," *J. Eur. Ceram. Soc.*, vol. 38, no. 2, pp. 403–409, Feb. 2018.
- [276] K. Xiao, Q. Guo, Z. Liu, S. Zhao, and Y. Zhao, "Influence of fiber coating thickness on microstructure and mechanical properties of carbon fiber-reinforced zirconium diboride based composites," *Ceram. Int.*, vol. 40, no. 1, pp. 1539–1544, Jan. 2014.
- [277] C. Kim, D. S. Grummon, and G. Gottstein, "Processing and interface characteristics of graphite fiber reinforced tantalum carbide matrix composites," *Scr. Metall. Mater.*, vol. 25, no. 10, pp. 2351–2356, Oct. 1991.
- [278] L. Zoli, V. Medri, C. Melandri, and D. Sciti, "Continuous SiC fibers– ZrB_2 composites," *J. Eur. Ceram. Soc.*, vol. 35, no. 16, pp. 4371–4376, Dec. 2015.
- [279] D. Sciti, A. Natali Murri, V. Medri, and L. Zoli, "Continuous C fibre composites with a porous ZrB_2 Matrix," *Mater. Des.*, vol. 85, pp. 127–134, Nov. 2015.
- [280] D. Sciti, L. Pienti, A. Natali Murri, E. Landi, V. Medri, and L. Zoli, "From random chopped to oriented continuous SiC fibers– ZrB_2 composites," *Mater. Des.*, vol. 63, pp. 464–470, Nov. 2014.
- [281] L. Zoli, A. Vinci, P. Galizia, C. Melandri, and D. Sciti, "On the thermal shock resistance and mechanical properties of novel unidirectional UHTCMCs for extreme environments," *Sci. Rep.*, vol. 8, no. 1, p. 9148, Dec. 2018.
- [282] R. Naslain and W. Krenkel, *Ceramic Matrix Composites*, vol. 22-26 June, no. 13. Weinheim, Germany: Wiley-VCH Verlag GmbH & Co. KGaA, 2008.
- [283] L. Zoli and D. Sciti, "Efficacy of a $\text{ZrB}_2\text{--SiC}$ matrix in protecting C fibres from oxidation in novel UHTCMC materials," *Mater. Des.*, vol. 113, pp. 207–213, Jan. 2017.
- [284] S. H. Lee, H. D. Kim, and Y. Kagawa, "SiC– ZrB_2 Fiber-Reinforced Composites Prepared by Spark Plasma Sintering," in *ICCM17 proceedings*, 2017, pp. 1–10.
- [285] L. Silvestroni, M. Nygren, and D. Sciti, "Study of the interactions between HfB_2 and Hi-NicalonTM fiber," *J. Eur. Ceram. Soc.*, vol. 33, no. 15–16, pp. 2879–2888, Dec. 2013.
- [286] V. Rubio, J. Binner, A. T Ackerman, S. Cousinet, N. Pommepuy, and X. Bertrand, "Ultra high temperature ceramic composite materials," in *ECI Symposium Series, (2017)*, 2017.
- [287] J. Zou *et al.*, "A top-down approach to densify $\text{ZrB}_2\text{--SiC--BN}$ composites with deeper homogeneity and improved reliability," *Chem. Eng. J.*, vol. 249, pp. 93–101, Aug. 2014.
- [288] A. Vinci, L. Zoli, D. Sciti, C. Melandri, and S. Guicciardi, "Understanding the

- mechanical properties of novel UHTCMCs through random forest and regression tree analysis,” *Mater. Des.*, vol. 145, pp. 97–107, May 2018.
- [289] P. Hu, D. Zhang, S. Dong, Q. Qu, and X. Zhang, “A novel vibration-assisted slurry impregnation to fabricate C_f/ZrB_2 -SiC composite with enhanced mechanical properties,” *J. Eur. Ceram. Soc.*, vol. 39, no. 4, pp. 798–805, Apr. 2019.
- [290] D. Huang *et al.*, “Ablation mechanism of C/C- ZrB_2 -ZrC-SiC composite fabricated by polymer infiltration and pyrolysis with preform of C_f/ZrB_2 ,” *Corros. Sci.*, vol. 98, pp. 551–559, Sep. 2015.
- [291] D. Liu, W.-F. Qiu, T. Cai, Y. Sun, A.-J. Zhao, and T. Zhao, “Synthesis, Characterization, and Microstructure of ZrC/SiC Composite Ceramics via Liquid Precursor Conversion Method,” *J. Am. Ceram. Soc.*, vol. 97, no. 4, pp. 1242–1247, Apr. 2014.
- [292] P. Hu, K. Gui, W. Hong, X. Zhang, and S. Dong, “High-performance ZrB_2 -SiC- C_f composite prepared by low-temperature hot pressing using nanosized ZrB_2 powder,” *J. Eur. Ceram. Soc.*, vol. 37, no. 6, pp. 2317–2324, Jun. 2017.
- [293] Y. Zhu, L. Cheng, M. Li, B. Ma, Y. Liu, and L. Zhang, “The synthesis and characterization of CVD ZrB_2 coating from $ZrCl_4$ - BCl_3 - H_2 -Ar system,” *Ceram. Int.*, vol. 44, no. 2, pp. 2002–2010, Feb. 2018.
- [294] Z. Wang *et al.*, “Fabrication and Properties of C_f /SiC-ZrC Composites,” *J. Am. Ceram. Soc.*, vol. 91, no. 10, pp. 3434–3436, Oct. 2008.
- [295] L. Zou, N. Wali, J.-M. Yang, N. P. Bansal, and D. Yan, “Microstructural Characterization of a C_f /ZrC Composite Manufactured by Reactive Melt Infiltration,” *Int. J. Appl. Ceram. Technol.*, vol. 8, no. 2, pp. 329–341, Mar. 2011.
- [296] D.-W. Ni *et al.*, “Fabrication and properties of C_f /ZrC-SiC-based composites by an improved reactive melt infiltration,” *J. Am. Ceram. Soc.*, vol. 101, no. 8, pp. 3253–3258, Aug. 2018.
- [297] Y. Zeng *et al.*, “Ablation-resistant carbide $Zr_{0.8}Ti_{0.2}C_{0.74}B_{0.26}$ for oxidizing environments up to 3,000 °C,” *Nat. Commun.*, vol. 8, p. 15836, Jun. 2017.
- [298] A. Rezaie, W. G. Fahrenholtz, and G. E. Hilmas, “Effect of hot pressing time and temperature on the microstructure and mechanical properties of ZrB_2 -SiC,” *J. Mater. Sci.*, vol. 42, no. 8, pp. 2735–2744, Apr. 2007.
- [299] J. Zou *et al.*, “High-temperature bending strength, internal friction and stiffness of ZrB_2 -20vol% SiC ceramics,” *J. Eur. Ceram. Soc.*, vol. 32, no. 10, pp. 2519–2527, Aug. 2012.
- [300] E. W. Neuman, G. E. Hilmas, and W. G. Fahrenholtz, “Mechanical behavior of zirconium diboride-silicon carbide-boron carbide ceramics up to 2200°C,” *J. Eur. Ceram. Soc.*, vol. 35, no. 2, pp. 463–476, Feb. 2015.
- [301] J. Zou, G.-J. Zhang, J. Vleugels, and O. Van der Biest, “High temperature strength of hot pressed ZrB_2 -20vol% SiC ceramics based on ZrB_2 starting powders prepared by different carbo/boro-thermal reduction routes,” *J. Eur. Ceram. Soc.*, vol. 33, no. 10, pp. 1609–1614, Sep. 2013.
- [302] P. Hu and Z. Wang, “Flexural strength and fracture behavior of ZrB_2 -SiC ultra-high temperature ceramic composites at 1800°C,” *J. Eur. Ceram. Soc.*, vol. 30, no. 4, pp. 1021–1026, Mar. 2010.
- [303] J. Zou, H.-B. Ma, A. D’Angio, and G.-J. Zhang, “Tungsten carbide: A versatile additive to get trace alkaline-earth oxide impurities out of ZrB_2 based ceramics,” *Scr. Mater.*, vol. 147, pp. 40–44, Apr. 2018.
- [304] L. Silvestroni, H.-J. Kleebe, W. G. Fahrenholtz, and J. Watts, “Super-strong materials for temperatures exceeding 2000°C,” *Sci. Rep.*, vol. 7, no. 1, p. 40730,

- Feb. 2017.
- [305] J. Zou *et al.*, “Strong ZrB₂-SiC-WC Ceramics at 1600°C,” *J. Am. Ceram. Soc.*, vol. 95, no. 3, pp. 874–878, Feb. 2012.
 - [306] X. Chen *et al.*, “Microstructure and mechanical properties of three dimensional C_f/SiC-ZrC-ZrB₂ composites prepared by reactive melt infiltration method,” *J. Eur. Ceram. Soc.*, vol. 36, no. 16, pp. 3969–3976, Dec. 2016.
 - [307] D. Wang, Y. Wang, J. Rao, J. Ouyang, Y. Zhou, and G. Song, “Influence of reactive melt infiltration parameters on microstructure and properties of low temperature derived Cf/ZrC composites,” *Mater. Sci. Eng. A*, vol. 568, pp. 25–32, Apr. 2013.
 - [308] D. Zhao, C. Zhang, H. Hu, and Y. Zhang, “Preparation and characterization of three-dimensional carbon fiber reinforced zirconium carbide composite by precursor infiltration and pyrolysis process,” *Ceram. Int.*, vol. 37, no. 7, pp. 2089–2093, Sep. 2011.
 - [309] P. Galizia, L. Zoli, and D. Sciti, “Impact of residual stress on thermal damage accumulation, and Young’s modulus of fiber-reinforced ultra-high temperature ceramics,” *Mater. Des.*, vol. 160, pp. 803–809, Dec. 2018.
 - [310] Marc Meyers; and K. Chawla, *Mechanical Behaviour of Materials*, Second edi. Cambridge: Cambridge university press, 2008.
 - [311] S. V. Nair, T.-J. Gwo, N. M. Narbut, J. G. Kohl, and G. J. Sundberg, “Mechanical Behavior of a Continuous-SiC-Fiber-Reinforced RBSN-Matrix Composite,” *J. Am. Ceram. Soc.*, vol. 74, no. 10, pp. 2551–2558, Oct. 1991.
 - [312] N. M. Narbut, “Mechanical Behavior of a Continuous Fiber Reinforced SiC/RBSN Ceramic Composite,” University of Massachusetts Amherst, 1992.
 - [313] J. Zou, G.-J. Zhang, Y.-M. Kan, and P.-L. Wang, “Hot-Pressed ZrB₂- SiC Ceramics with VC Addition: Chemical Reactions, Microstructures, and Mechanical Properties,” *J. Am. Ceram. Soc.*, vol. 92, no. 12, pp. 2838–2846, Dec. 2009.
 - [314] J. Zou, G.-J. Zhang, H. Zhang, Z.-R. Huang, J. Vleugels, and O. Van der Biest, “Improving high temperature properties of hot pressed ZrB₂–20vol% SiC ceramic using high purity powders,” *Ceram. Int.*, vol. 39, no. 1, pp. 871–876, Jan. 2013.
 - [315] D. Munz, “What Can We Learn from R-Curve Measurements?,” *J. Am. Ceram. Soc.*, vol. 90, no. 1, pp. 1–15, Jan. 2007.
 - [316] F. Zok, O. Sbaizero, C. L. Hom, and A. G. Evans, “Mode I Fracture Resistance of a Laminated Fiber-Reinforced Ceramic,” *J. Am. Ceram. Soc.*, vol. 74, no. 1, pp. 187–193, Jan. 1991.
 - [317] H. Ming Yuan and J. W. Hutchinson, “Crack deflection at an interface between dissimilar elastic materials,” *Int. J. Solids Struct.*, vol. 25, no. 9, pp. 1053–1067, 1989.
 - [318] M. Y. He and J. W. Hutchinson, “Kinking of a Crack Out of an Interface,” *J. Appl. Mech.*, vol. 56, no. 2, p. 270, 1989.
 - [319] L. Silvestroni, D. Sciti, G. E. Hilmas, W. G. Fahrenholtz, and J. Watts, “Effect of a weak fiber interface coating in ZrB₂ reinforced with long SiC fibers,” *Mater. Des.*, vol. 88, pp. 610–618, Dec. 2015.
 - [320] P. Hu *et al.*, “Damage mechanism analysis to the carbon fiber and fiber-ceramic interface tailoring of C_f/ZrC-SiC using PyC coating,” *Ceram. Int.*, vol. 44, no. 15, pp. 19038–19043, Oct. 2018.
 - [321] M. Minus and S. Kumar, “The processing, properties, and structure of carbon fibers,” *JOM*, vol. 57, no. 2, pp. 52–58, Feb. 2005.

- [322] J. W. Zimmermann, G. E. Hilmas, W. G. Fahrenholtz, R. B. Dinwiddie, W. D. Porter, and H. Wang, "Thermophysical Properties of ZrB_2 and ZrB_2 -SiC Ceramics," *J. Am. Ceram. Soc.*, vol. 91, no. 5, pp. 1405–1411, May 2008.
- [323] Q. Ding *et al.*, "Mechanical properties and microstructure evolution of 3D C_f /SiBCN composites at elevated temperatures," *J. Am. Ceram. Soc.*, vol. 101, no. 10, pp. 4699–4707, Oct. 2018.
- [324] A. Raffray *et al.*, "Design and material issues for high performance SiC_f/SiC-based fusion power cores," *Fusion Eng. Des.*, vol. 55, no. 1, pp. 55–95, May 2001.
- [325] R. Loehman, E. Corral, H. P. Dumm, P. Kotula, and R. Tandon, "Ultra High Temperature Ceramics for Hypersonic Vehicle Applications," 2006.
- [326] Q. Fu, J. Jing, B. Tan, R. Yuan, L. Zhuang, and L. Li, "Nanowire-toughened transition layer to improve the oxidation resistance of SiC–MoSi₂–ZrB₂ coating for C/C composites," *Corros. Sci.*, vol. 111, pp. 259–266, Oct. 2016.
- [327] S. Tang, J. Deng, S. Wang, and W. Liu, "Comparison of thermal and ablation behaviors of C/SiC composites and C/ZrB₂-SiC composites," *Corros. Sci.*, vol. 51, no. 1, pp. 54–61, Jan. 2009.
- [328] S. Guo, "Thermal and electrical properties of hot-pressed short pitch-based carbon fiber-reinforced ZrB₂-SiC matrix composites," *Ceram. Int.*, vol. 39, no. 5, pp. 5733–5740, Jul. 2013.
- [329] C. Hu, S. Pang, S. Tang, Y. Wang, and H.-M. Cheng, "An integrated composite with a porous C_f/C-ZrB₂-SiC core between two compact outer layers of C_f/C-ZrB₂-SiC and C_f/C-SiC," *J. Eur. Ceram. Soc.*, vol. 35, no. 3, pp. 1113–1117, Mar. 2015.
- [330] R. Inoue, Y. Arai, Y. Kubota, K. Goto, and Y. Kogo, "Development of short- and continuous carbon fiber-reinforced ZrB₂-SiC-ZrC matrix composites for thermal protection systems," *Ceram. Int.*, vol. 44, no. 13, pp. 15859–15867, Sep. 2018.
- [331] L. F. He, Y. W. Bao, J. Y. Wang, M. S. Li, and Y. C. Zhou, "Microstructure and mechanical and thermal properties of ternary carbides in Hf–Al–C system," *Acta Mater.*, vol. 57, no. 9, pp. 2765–2774, May 2009.
- [332] O. Cedillos-Barraza, S. Grasso, N. Al Nasiri, D. D. Jayaseelan, M. J. Reece, and W. E. Lee, "Sintering behaviour, solid solution formation and characterisation of TaC, HfC and TaC–HfC fabricated by spark plasma sintering," *J. Eur. Ceram. Soc.*, vol. 36, no. 7, pp. 1539–1548, Jun. 2016.
- [333] L. Pienti, D. Sciti, L. Silvestroni, A. Cecere, and R. Savino, "Ablation tests on HfC- and TaC-based ceramics for aeropropulsive applications," *J. Eur. Ceram. Soc.*, vol. 35, no. 5, pp. 1401–1411, May 2015.
- [334] M. Mallik, A. J. Kailath, K. K. Ray, and R. Mitra, "Electrical and thermophysical properties of ZrB₂ and HfB₂ based composites," *J. Eur. Ceram. Soc.*, vol. 32, no. 10, pp. 2545–2555, Aug. 2012.
- [335] G. Shao *et al.*, "High emissivity MoSi₂-TaSi₂-borosilicate glass porous coating for fibrous ZrO₂ ceramic by a rapid sintering method," *J. Alloys Compd.*, vol. 690, pp. 63–71, Jan. 2017.
- [336] J. Kulczyk-Malecka *et al.*, "Thermo – mechanical properties of SPS produced self-healing thermal barrier coatings containing pure and alloyed MoSi₂ particles," *J. Eur. Ceram. Soc.*, vol. 38, no. 12, pp. 4268–4275, Sep. 2018.
- [337] S.-Q. Guo, Y. Kagawa, T. Nishimura, D. Chung, and J.-M. Yang, "Mechanical and physical behavior of spark plasma sintered ZrC–ZrB₂-SiC composites," *J. Eur. Ceram. Soc.*, vol. 28, no. 6, pp. 1279–1285, Jan. 2008.
- [338] R. W. Harrison and W. E. Lee, "Processing and properties of ZrC, ZrN and ZrCN

- ceramics: a review,” *Adv. Appl. Ceram.*, 2016.
- [339] S. Guo, Y. Kagawa, T. Nishimura, and H. Tanaka, “Thermal and Electric Properties in Hot-Pressed ZrB₂- MoSi₂ -SiC Composites,” *J. Am. Ceram. Soc.*, vol. 90, no. 7, pp. 2255–2258, Jul. 2007.
- [340] C. Li, K. Li, H. Li, H. Ouyang, Y. Zhang, and L. Guo, “Mechanical and thermophysical properties of carbon/carbon composites with hafnium carbide,” *Ceram. Int.*, vol. 39, no. 6, pp. 6769–6776, Aug. 2013.
- [341] J. Ren, Y. Zhang, P. Zhang, T. Li, J. Li, and Y. Yang, “Ablation resistance of HfC coating reinforced by HfC nanowires in cyclic ablation environment,” *J. Eur. Ceram. Soc.*, vol. 37, no. 8, pp. 2759–2768, Jul. 2017.
- [342] J. F. Justin and A. Jankowiak, “Ultra High Temperature Ceramics: Densification, Properties and Thermal Stability,” 2011.
- [343] D. Mikociak, A. Rudawski, and S. Blazewicz, “Mechanical and thermal properties of C/C composites modified with SiC nanofiller,” *Mater. Sci. Eng. A*, vol. 716, pp. 220–227, Feb. 2018.
- [344] M. Mallik, S. Roy, K. K. Ray, and R. Mitra, “Effect of SiC content, additives and process parameters on densification and structure-property relations of pressureless sintered ZrB₂-SiC composites,” *Ceram. Int.*, vol. 39, no. 3, pp. 2915–2932, 2013.
- [345] C. Pradere and C. Sauder, “Transverse and longitudinal coefficient of thermal expansion of carbon fibers at high temperatures (300–2500K),” *Carbon N. Y.*, vol. 46, no. 14, pp. 1874–1884, Nov. 2008.
- [346] R. Luo, T. Liu, J. Li, H. Zhang, Z. Chen, and G. Tian, “Thermophysical properties of carbon/carbon composites and physical mechanism of thermal expansion and thermal conductivity,” *Carbon N. Y.*, vol. 42, no. 14, pp. 2887–2895, Jan. 2004.
- [347] W. E. Org, S. Rebouillat, and M. E. G. Lyons, “Measuring the Electrical Conductivity of Single Fibres,” *Int. J. Electrochem. Sci*, vol. 6, pp. 5731–5740, 2011.
- [348] L. Zhang, D. A. Pejaković, J. Marschall, and M. Gasch, “Thermal and Electrical Transport Properties of Spark Plasma-Sintered HfB₂ and ZrB₂ Ceramics,” *J. Am. Ceram. Soc.*, vol. 94, no. 8, pp. 2562–2570, Aug. 2011.
- [349] M. Mallik, A. J. Kailath, K. K. Ray, and R. Mitra, “Effect of SiC content on electrical, thermal and ablative properties of pressureless sintered ZrB₂ -based ultrahigh temperature ceramic composites,” *J. Eur. Ceram. Soc.*, vol. 37, no. 2, pp. 559–572, Feb. 2017.
- [350] C. Hu *et al.*, “Microstructure and properties of ZrB₂-SiC and HfB₂-SiC composites fabricated by spark plasma sintering (SPS) using TaSi₂ as sintering aid,” *J. Ceram. Soc. Japan*, vol. 118, no. 1383, pp. 997–1001, Nov. 2010.
- [351] W. Tan, C. A. Petorak, and R. W. Trice, “Rare-earth modified zirconium diboride high emissivity coatings for hypersonic applications,” *J. Eur. Ceram. Soc.*, vol. 34, no. 1, pp. 1–11, Jan. 2014.
- [352] W. Tan, M. Adducci, C. Petorak, B. Thompson, A. E. Brenner, and R. W. Trice, “Effect of rare-earth dopant (Sm) concentration on total hemispherical emissivity and ablation resistance of ZrB₂ /SiC coatings,” *J. Eur. Ceram. Soc.*, vol. 36, no. 16, pp. 3833–3841, Dec. 2016.
- [353] M. Balat-Pichelin, E. Bêche, D. Sciti, and D. Alfano, “Emissivity, catalycity and microstructural characterization of ZrB₂-SiC fiber based UHTC at high temperature in a non-equilibrium air plasma flow,” *Ceram. Int.*, vol. 40, no. 7, pp. 9731–9742, Aug. 2014.

- [354] B. Du, S. Zhou, X. Zhang, C. Hong, and Q. Qu, "Preparation of a high spectral emissivity TaSi₂-based hybrid coating on SiOC-modified carbon-bonded carbon fiber composite by a flash sintering method," *Surf. Coatings Technol.*, vol. 350, pp. 146–153, Sep. 2018.
- [355] X. Tao *et al.*, "Effect of TaSi₂ content on the structure and properties of TaSi₂ - MoSi₂ -borosilicate glass coating on fibrous insulations for enhanced surficial thermal radiation," *Surf. Coatings Technol.*, vol. 316, pp. 122–130, Apr. 2017.
- [356] G. Shao, Y. Lu, D. A. H. Hanaor, S. Cui, J. Jiao, and X. Shen, "Improved oxidation resistance of high emissivity coatings on fibrous ceramic for reusable space systems," *Corros. Sci.*, vol. 146, pp. 233–246, Jan. 2019.
- [357] L. Luo, Y. Wang, L. Duan, L. Liu, and G. Wang, "Ablation behavior of C/SiC-HfC composites in the plasma wind tunnel," *J. Eur. Ceram. Soc.*, vol. 36, no. 15, pp. 3801–3807, Nov. 2016.
- [358] Q. Feng *et al.*, "Microstructure analysis of C_f/SiC–ZrC composites in both fabrication and plasma wind tunnel testing processes," *Ceram. Int.*, vol. 40, no. 1, pp. 1199–1204, Jan. 2014.
- [359] J. Li *et al.*, "Effect of ZrC–SiC content on microstructure and ablation properties of C/C composites," *Trans. Nonferrous Met. Soc. China*, vol. 26, no. 10, pp. 2653–2664, Oct. 2016.
- [360] S. Wang *et al.*, "Microstructure and ablation mechanism of C/C–ZrC–SiC composites in a plasma flame," *Ceram. Int.*, vol. 43, no. 14, pp. 10661–10667, Oct. 2017.
- [361] D. Zhao, C. Zhang, H. Hu, and Y. Zhang, "Ablation behavior and mechanism of 3D C/ZrC composite in oxyacetylene torch environment," *Compos. Sci. Technol.*, vol. 71, no. 11, pp. 1392–1396, Jul. 2011.
- [362] Y. Liu, Q. Fu, Y. Guan, B. Wang, and Q. Shen, "Ablation behavior of sharp-shape C/C–SiC–ZrB₂ composites under oxyacetylene flame," *J. Alloys Compd.*, vol. 713, pp. 19–27, Aug. 2017.
- [363] L. Zhuang *et al.*, "Ablation behaviour of C/C and C/C–ZrC–SiC composites with cone-shaped holes under an oxyacetylene flame," *Corros. Sci.*, vol. 102, pp. 84–92, Jan. 2016.
- [364] J. Lu *et al.*, "Ablation resistance of SiC–HfC–ZrC multiphase modified carbon/carbon composites," *Corros. Sci.*, vol. 103, pp. 1–9, Feb. 2016.
- [365] B. Feng, H. Li, Y. Zhang, L. Liu, and M. Yan, "Effect of SiC/ZrC ratio on the mechanical and ablation properties of C/C–SiC–ZrC composites," *Corros. Sci.*, vol. 82, pp. 27–35, May 2014.
- [366] Y. Jia, X. Yao, J. Sun, and H. Li, "Effect of ZrC particle size on the ablation resistance of C/C–ZrC–SiC composites," *Mater. Des.*, vol. 129, pp. 15–25, Sep. 2017.
- [367] C. Yan, R. Liu, B. Zha, and C. Zhang, "Fabrication and properties of 3-dimensional 4-directional C_f/HfC–SiC composites by precursor impregnation and pyrolysis process," *J. Alloys Compd.*, vol. 739, pp. 955–960, Mar. 2018.
- [368] S. Chen, G. Li, H. Hu, Y. Li, and M. Mei, "Microstructure and properties of ablative C/ZrC–SiC composites prepared by reactive melt infiltration of zirconium and vapour silicon infiltration," *Ceram. Int.*, vol. 43, no. 3, pp. 3439–3442, Feb. 2017.
- [369] J. P. Zhang, Q. G. Fu, and L. Wang, "Preparation, ablation behavior and thermal retardant ability of C/C–HfB₂–SiC composites," *Mater. Des.*, vol. 132, pp. 552–558, Oct. 2017.
- [370] L. Li, Y. Wang, L. Cheng, and L. Zhang, "Preparation and properties of 2D

- C/SiC–ZrB₂–TaC composites,” *Ceram. Int.*, vol. 37, no. 3, pp. 891–896, Apr. 2011.
- [371] Y. Liu, Q. Fu, B. Wang, T. Liu, and J. Sun, “The ablation behavior and mechanical property of C/C–SiC–ZrB₂ composites fabricated by reactive melt infiltration,” *Ceram. Int.*, vol. 43, no. 8, pp. 6138–6147, Jun. 2017.
- [372] X. Luan *et al.*, “Laser ablation behavior of Cf/SiHfBCN ceramic matrix composites,” *J. Eur. Ceram. Soc.*, vol. 36, no. 15, pp. 3761–3768, Nov. 2016.
- [373] L. Larrimbe *et al.*, “High Heat Flux Laser Testing of HfB₂ Cylinders,” *J. Am. Ceram. Soc.*, vol. 100, no. 1, pp. 293–303, Jan. 2017.
- [374] D. Sciti, V. Medri, and L. Silvestroni, “Oxidation behaviour of HfB₂–15 vol.% TaSi₂ at low, intermediate and high temperatures,” *Scr. Mater.*, vol. 63, no. 6, pp. 601–604, Sep. 2010.
- [375] X. Zhang, P. Hu, J. Han, and S. Meng, “Ablation behavior of ZrB₂–SiC ultra high temperature ceramics under simulated atmospheric re-entry conditions,” *Compos. Sci. Technol.*, vol. 68, no. 7–8, pp. 1718–1726, Jun. 2008.
- [376] T. A. Parthasarathy, M. D. Petry, G. Jefferson, M. K. Cinibulk, T. Mathur, and M. R. Gruber, “Development of a Test to Evaluate Aerothermal Response of Materials to Hypersonic Flow Using a Scramjet Wind Tunnel,” *Int. J. Appl. Ceram. Technol.*, vol. 8, no. 4, pp. 832–847, Jul. 2011.
- [377] L. Larrimbe *et al.*, “High Heat Flux Laser Testing of HfB₂ Cylinders,” *J. Am. Ceram. Soc.*, vol. 100, no. 1, pp. 293–303, Jan. 2017.
- [378] N. S. Diaconis, M. J. Engel, and J. W. Metzger, “Oxidation and sublimation of graphite in simulated re-entry environments,” *AIAA J.*, vol. 5, no. 3, pp. 451–460, Mar. 1967.
- [379] M. Funatsu, M. Ozawa, H. Shirai, and F. Takakusagi, “Experimental Study of Ablation Processes of SiC-based Materials in Air Plasma Freejets,” *Trans. Japan Soc. Aeronaut. Sp. Sci. Aerosp. Technol. Japan*, vol. 8, no. ists27, p. Pe_41–Pe_46, 2010.
- [380] E. R. Smart Michael, “Free-jet testing of a rest scramjet at off-design conditions,” in *25th AIAA Aerodynamic Measurement Technology and Ground Testing Conference*, 2006.
- [381] M. Funatsu, K. Konishi, M. Kawada, M. Ozawa, and F. Takakusagi, “Visualizations of SiC Ablations in Air Plasma Freejets,” *Trans. Japan Soc. Aeronaut. Sp. Sci. Aerosp. Technol. Japan*, vol. 12, no. 29, pp. 45–50, 2014.
- [382] B. J. R. V. and Presser S., “Measurement of the velocity of oxyacetylene and oxypropane torches for UHTC composite testing,” *to be Publ.*, 2019.
- [383] J. K. Sonber, T. S. R. Ch. Murthy, C. Subramanian, R. C. Hubli, and A. K. Suri, “Processing Methods for Ultra High Temperature Ceramics,” in *MAX Phases and Ultra-High Temperature Ceramics for Extreme Environments*, IGI Global, 2013, pp. 180–202.
- [384] J. B. Berkowitz-Mattuck, “High-Temperature Oxidation,” *J. Electrochem. Soc.*, vol. 113, no. 9, p. 908, Sep. 1966.
- [385] T. A. Parthasarathy, R. A. Rapp, M. Opeka, and R. J. Kerans, “A model for the oxidation of ZrB₂, HfB₂ and TiB₂,” *Acta Mater.*, vol. 55, no. 17, pp. 5999–6010, Oct. 2007.
- [386] D. Sciti, A. Balbo, and A. Bellosi, “Oxidation behaviour of a pressureless sintered HfB₂–MoSi₂ composite,” *J. Eur. Ceram. Soc.*, vol. 29, no. 9, pp. 1809–1815, Jun. 2009.
- [387] C.-M. Chen, L. T. Zhang, W. C. Zhou, and M. Q. Li, “High temperature oxidation of LaB₆–ZrB₂ eutectic in situ composite,” *Acta Mater.*, vol. 47, no. 6,

- pp. 1945–1952, Apr. 1999.
- [388] F. Monteverde and A. Bellosi, “Oxidation of ZrB_2 - Based Ceramics in Dry Air,” *J. Electrochem. Soc.*, vol. 150, no. 11, p. B552, 2003.
- [389] W. G. Fahrenholtz and G. E. Hilmas, “Oxidation of ultra-high temperature transition metal diboride ceramics,” *Int. Mater. Rev.*, vol. 57, no. 1, pp. 61–72, Jan. 2012.
- [390] W. G. Fahrenholtz, “Thermodynamic Analysis of ZrB_2 /SiC Oxidation: Formation of a SiC-Depleted Region,” *J. Am. Ceram. Soc.*, vol. 90, no. 1, pp. 143–148, Jan. 2007.
- [391] S. Shimada, M. Inagaki, and M. Suzuki, “Microstructural observation of the ZrC/ZrO_2 interface formed by oxidation of ZrC ,” *J. Mater. Res.*, vol. 11, no. 10, pp. 2594–2597, Oct. 1996.
- [392] S. Shimada and T. Ishil, “Oxidation Kinetics of Zirconium Carbide at Relatively Low Temperatures,” *J. Am. Ceram. Soc.*, vol. 73, no. 10, pp. 2804–2808, Oct. 1990.
- [393] S. Shimada, M. Nishisako, M. Inagaki, and K. Yamamoto, “Formation and Microstructure of Carbon-Containing Oxide Scales by Oxidation of Single Crystals of Zirconium Carbide,” *J. Am. Ceram. Soc.*, vol. 78, no. 1, pp. 41–48, Jan. 1995.
- [394] A. Bellucci, D. Gozzi, T. Kimura, T. Noda, and S. Otani, “Zirconia growth on zirconium carbide single crystals by oxidation,” *Surf. Coatings Technol.*, vol. 197, no. 2–3, pp. 294–302, Jul. 2005.
- [395] G. A. Rama Rao and V. Venugopal, “Kinetics and mechanism of the oxidation of ZrC ,” *J. Alloys Compd.*, vol. 206, no. 2, pp. 237–242, May 1994.
- [396] W. Hu, Y. Tian, and Z. Liu, “Carbon Vacancy Ordered Non-Stoichiometric $\text{ZrC}_{0.6}$,” in *MAX Phases and Ultra-High Temperature Ceramics for Extreme Environments*, IGI Global, 2013, pp. 478–508.
- [397] S. Shimada, “Oxidation and Mechanism of Single Crystal Carbides with Formation of Carbon,” *J. Ceram. Soc. Japan*, vol. 109, no. 1267, pp. S33–S42, 2001.
- [398] K. Edamoto, T. Nagayama, K. Ozawa, and S. Otani, “Angle-resolved and resonant photoemission study of the ZrO -like film on $\text{ZrC}(100)$,” *Surf. Sci.*, vol. 601, no. 21, pp. 5077–5082, Nov. 2007.
- [399] L. Casas and J. M. Martínez-Esnaola, “Modelling the effect of oxidation on the creep behaviour of fibre-reinforced ceramic matrix composites,” *Acta Mater.*, vol. 51, no. 13, pp. 3745–3757, Aug. 2003.
- [400] W. C. Tripp, H. H. Davis, and H. C. Graham, “Effect of an SiC addition on the oxidation of ZrB_2 ,” *Amer. Ceram. Soc. Bull.*, vol. 52, no. 8, pp. 612–616, 1973.
- [401] A. Rezaie, W. G. Fahrenholtz, and G. E. Hilmas, “Evolution of structure during the oxidation of zirconium diboride–silicon carbide in air up to 1500°C ,” *J. Eur. Ceram. Soc.*, vol. 27, no. 6, pp. 2495–2501, Jan. 2007.
- [402] K. Shugart, W. Jennings, and E. Opila, “Initial Stages of ZrB_2 -30 vol% SiC Oxidation at 1500°C ,” *J. Am. Ceram. Soc.*, vol. 97, no. 5, pp. 1645–1651, May 2014.
- [403] S. N. Karlsdottir and J. W. Halloran, “Rapid Oxidation Characterization of Ultra-High Temperature Ceramics,” *J. Am. Ceram. Soc.*, vol. 90, no. 10, pp. 3233–3238, Oct. 2007.
- [404] Z. Wang and Z. Wu, “Fabrication, Microstructure, and Properties of Zirconium Diboride Matrix Ceramic,” in *MAX Phases and Ultra-High Temperature Ceramics for Extreme Environments*, IGI Global, 2013, pp. 354–412.

- [405] S. P.T.B, "An Oxidation Resistant Boride Composition," *J. Name Am. Ceram. Soc. Bull. (U.S.)*, vol. 41, 1962.
- [406] R. Pastor, H.; Meyer, "An investigation of the effect of additions of metal silicides on titanium and zirconium borides from the point of view of their sintering behaviour and their resistance to oxidation at high temperature," *Rev. Int. Htes Temp. Refract. II*, vol. 11, no. 1, pp. 41–54, 1974.
- [407] Z. Wu, Z. Wang, G. Shi, and J. Sheng, "Effect of surface oxidation on thermal shock resistance of the $\text{ZrB}_2\text{-SiC-ZrC}$ ceramic," *Compos. Sci. Technol.*, vol. 71, no. 12, pp. 1501–1506, Aug. 2011.
- [408] F. Monteverde and A. Bellosi, "Microstructure and Properties of an $\text{HfB}_2\text{-SiC}$ Composite for Ultra High Temperature Applications," *Adv. Eng. Mater.*, vol. 6, no. 5, pp. 331–336, May 2004.
- [409] J. W. Hinze, "The High-Temperature Oxidation Behavior of a $\text{HfB}_2 + 20 \text{ vol\% SiC}$ Composite," *J. Electrochem. Soc.*, vol. 122, no. 9, p. 1249, Sep. 1975.
- [410] F. Monteverde, "The thermal stability in air of hot-pressed diboride matrix composites for uses at ultra-high temperatures," *Corros. Sci.*, vol. 47, no. 8, pp. 2020–2033, Aug. 2005.
- [411] M. Gasch, "Processing, Properties, and Arc Jet Oxidation of Hafnium Diboride/Silican Carbide Ultra-High Temperature Ceramics," vol. 39, no. 17, pp. 5925–5937, 2004.
- [412] E. J. Opila and M. C. Halbig, "Oxidation of $\text{ZrB}_2\text{-SiC}$," in *25th Annual Conference on Composites, Advanced Ceramics, Materials, and Structures: A: Ceramic Engineering and Science Proceedings, Volume 22, Issue 3*, Hoboken, NJ, USA: John Wiley & Sons, Inc., 2008, pp. 221–228.
- [413] X. W. Yin, L. F. Cheng, L. T. Zhang, N. Travitzky, and P. Greil, "Fibre-reinforced multifunctional SiC matrix composite materials," *Int. Mater. Rev.*, vol. 62, no. 3, pp. 117–172, Apr. 2017.
- [414] L. S. Walker and E. L. Corral, "Self-Generating High-Temperature Oxidation-Resistant Glass-Ceramic Coatings for C-C Composites Using UHTCs," *J. Am. Ceram. Soc.*, vol. 97, no. 9, pp. 3004–3011, Sep. 2014.
- [415] W. Lu, F. Qian-gang, and Z. Feng-ling, "A novel gradient $\text{SiC-ZrB}_2\text{-MoSi}_2$ coating for SiC coated C/C composites by supersonic plasma spraying," *Surf. Coatings Technol.*, vol. 313, pp. 63–72, Mar. 2017.
- [416] Y. L. Zhang, J. Ren, S. Tian, H. Li, X. Ren, and Z. Hu, "HfC nanowire-toughened $\text{TaSi}_2\text{-TaC-SiC-Si}$ multiphase coating for C/C composites against oxidation," *Corros. Sci.*, vol. 90, pp. 554–561, Jan. 2015.
- [417] X. Ren, H. Li, K. Li, and Q. Fu, "Preparation of oxidation protective $\text{Hf}_{0.2}\text{Ta}_{0.8}\text{B}_{2-x}\text{-SiC}$ coating by in-situ reaction method on SiC-coated carbon/carbon composites," *J. Alloys Compd.*, vol. 618, pp. 390–395, Jan. 2015.
- [418] T. Feng, H. Li, M. Hu, H. Lin, and L. Li, "Oxidation and ablation resistance of the $\text{ZrB}_2\text{-CrSi}_2\text{-Si/SiC}$ coating for C/C composites at high temperature," *J. Alloys Compd.*, vol. 662, pp. 302–307, Mar. 2016.
- [419] X. Ren, H. Li, Y. Chu, Q. Fu, and K. Li, "Ultra-High-Temperature Ceramic $\text{HfB}_2\text{-SiC}$ Coating for Oxidation Protection of SiC-Coated Carbon/Carbon Composites," *Int. J. Appl. Ceram. Technol.*, vol. 12, no. 3, pp. 560–567, May 2015.
- [420] M. Pavese, P. Fino, C. Badini, A. Ortona, and G. Marino, " $\text{HfB}_2\text{/SiC}$ as a protective coating for 2D $\text{C}_f\text{/SiC}$ composites: Effect of high temperature oxidation on mechanical properties," *Surf. Coatings Technol.*, vol. 202, no. 10, pp. 2059–2067, Feb. 2008.

- [421] D. Sciti, L. Silvestroni, G. Saccone, and D. Alfano, "Effect of different sintering aids on thermo-mechanical properties and oxidation of SiC fibers – Reinforced ZrB₂ composites," *Mater. Chem. Phys.*, vol. 137, no. 3, pp. 834–842, Jan. 2013.
- [422] L. Silvestroni and D. Sciti, "Oxidation of ZrB₂ Ceramics Containing SiC as Particles, Whiskers, or Short Fibers," *J. Am. Ceram. Soc.*, vol. 94, no. 9, pp. 2796–2799, Sep. 2011.
- [423] W. Z. Zhang, Y. Zeng, L. Gbologah, X. Xiong, and B. Y. Huang, "Preparation and oxidation property of ZrB₂-MoSi₂/SiC coating on carbon/carbon composites," *Trans. Nonferrous Met. Soc. China*, vol. 21, no. 7, pp. 1538–1544, Jul. 2011.
- [424] S. M. Johnson, "Ultra High Temperature Ceramics Application: Issues and Prospects," 2011.
- [425] A. Vinci, L. Zoli, E. Landi, and D. Sciti, "Oxidation behaviour of a continuous carbon fibre reinforced ZrB₂-SiC composite," *Corros. Sci.*, vol. 123, no. November 2016, pp. 129–138, Jul. 2017.
- [426] O. Haibo *et al.*, "Self-healing ZrB₂-SiO₂ oxidation resistance coating for SiC coated carbon/carbon composites," *Corros. Sci.*, vol. 110, pp. 265–272, Sep. 2016.
- [427] A. Vinci, L. Zoli, and D. Sciti, "Influence of SiC content on the oxidation of carbon fibre reinforced ZrB₂ /SiC composites at 1500 and 1650°C in air," *J. Eur. Ceram. Soc.*, vol. 38, no. 11, pp. 3767–3776, Sep. 2018.
- [428] S. C. Zhang, G. E. Hilmas, and W. G. Fahrenholtz, "Improved Oxidation Resistance of Zirconium Diboride by Tungsten Carbide Additions," *J. Am. Ceram. Soc.*, vol. 91, no. 11, pp. 3530–3535, Nov. 2008.
- [429] I. Talmy, J. Zaykoski, M. Opeka, and S. Dallek, "High temperature corrosion and materials chemistry III : proceedings of the International Symposium," in *High Temperature Corrosion and Materials Chemistry III*, M. McNallan, E. J. Opila, Electrochemical Society. High Temperature Materials Division., Electrochemical Society. Corrosion Division., and D. C. . Electrochemical Society. Meeting (199th : 2001 : Washington, Eds. Pennington, NJ, 2001: Electrochemical Society, 2001, p. 144.
- [430] C.-M. Chen, L. T. Zhang, W. C. Zhou, Z. Z. Hao, Y. J. Jiang, and S. L. Yang, "Microstructure, mechanical performance and oxidation mechanism of boride in situ composites," *Compos. Sci. Technol.*, vol. 61, no. 7, pp. 971–975, May 2001.
- [431] I. Bogomol and P. Loboda, "Directionally Solidified Ceramic Eutectics for High-Temperature Applications," in *MAX Phases and Ultra-High Temperature Ceramics for Extreme Environments*, C. I. M. Low (Curtin University, Perth, Australia); Y. Sakka (National Institute for Materials Science (NIMS), Japan); C. F. Hu (Chinese Academy of Sciences, Ed. Hershey, PA 17033-1240: IGI Global, 2013, pp. 303–322.
- [432] I. Bogomol, T. Nishimura, Y. Nesterenko, O. Vasylykiv, Y. Sakka, and P. Loboda, "The bending strength temperature dependence of the directionally solidified eutectic LaB₆-ZrB₂ composite," *J. Alloys Compd.*, vol. 509, no. 20, pp. 6123–6129, May 2011.
- [433] E. L. Courtright, H. C. Graham, A. P. Katz, and R. J. Kerans, "Ultrahigh Temperature Assessment Study: Ceramic Matrix Composites," 1992.
- [434] D.-W. Ni, G.-J. Zhang, Y.-M. Kan, and Y. Sakka, "Textured HfB₂-based ultrahigh-temperature ceramics with anisotropic oxidation behavior," *Scr. Mater.*, vol. 60, no. 10, pp. 913–916, May 2009.
- [435] C. M. Carney, P. Mogilvesky, and T. A. Parthasarathy, "Oxidation Behavior of

- Zirconium Diboride Silicon Carbide Produced by the Spark Plasma Sintering Method,” *J. Am. Ceram. Soc.*, vol. 92, no. 9, pp. 2046–2052, Sep. 2009.
- [436] C. M. Carney, T. A. Parthasarathy, and M. K. Cinibulk, “Oxidation Resistance of Hafnium Diboride Ceramics with Additions of Silicon Carbide and Tungsten Boride or Tungsten Carbide,” *J. Am. Ceram. Soc.*, vol. 94, no. 8, pp. 2600–2607, Aug. 2011.
- [437] C. M. Carney and T. S. Key, “Comparison of the oxidation protection of HfB₂ based ultra-high temperature ceramics by the addition of SiC or MoSi₂,” in *Ceramic Engineering and Science Proceedings*, 2014, pp. 261–273.
- [438] F. Monteverde, “Ultra-high temperature HfB₂-SiC ceramics consolidated by hot-pressing and spark plasma sintering,” *J. Alloys Compd.*, vol. 428, no. 1–2, pp. 197–205, 2007.
- [439] P. Zheng, B. Vaidhyanathan, S. Grasso, C. Carney, and J. Binner, “Synthesis, Sintering and Oxidation Testing of Ta-Doped HfB₂ Powders,” *Prep.*
- [440] W. Vogel, *Glass Chemistry*. Springer Berlin Heidelberg, 1994.
- [441] P. W. Atkins, *Physical Chemistry*. Oxford University Press, 1978.
- [442] L. Kaufman; and E. Clougherty, “Technical Report RTD-TDR-63-4096,” 1963.
- [443] M. J. Gasch, D. T. Ellerby, and S. M. Johnson, “Ultra High Temperature Ceramic Composites,” in *Handbook of Ceramic Composites*, Springer US, 2005, pp. 197–224.
- [444] S. C. Zhang, W. G. Fahrenholtz, and G. E. Hilmas, “Oxidation of ZrB₂ and ZrB₂-SiC Ceramics with Tungsten Additions,” in *ECS Transactions*, 2009, vol. 16, no. 44, pp. 137–145.
- [445] T. Wang and R. Luo, “Oxidation protection and mechanism of the HfB₂-SiC-Si/SiC coatings modified by in-situ strengthening of SiC whiskers for C/C composites,” *Ceram. Int.*, vol. 44, no. 11, pp. 12370–12380, Aug. 2018.
- [446] N. P. Padture, “Advanced structural ceramics in aerospace propulsion,” *Nat. Mater.*, vol. 15, no. 8, pp. 804–809, Aug. 2016.
- [447] S. Chand, “Review Carbon fibers for composites,” *J. Mater. Sci.*, vol. 35, no. 6, pp. 1303–1313, 2000.
- [448] A. Paul, J. Binner, and B. Vaidhyanathan, “UHTC Composites for Hypersonic Applications,” in *Ultra-High Temperature Ceramics*, W. G. Fahrenholtz, E. J. Wuchina, W. E. Lee, and Y. Zhou, Eds. Hoboken, NJ: John Wiley & Sons, Inc, 2014, pp. 144–166.

Design, Selection, Processing, Properties and Applications of Ultra-High Temperature Ceramic Matrix Composites, UHTCMCs - A Review

Total 23 figures

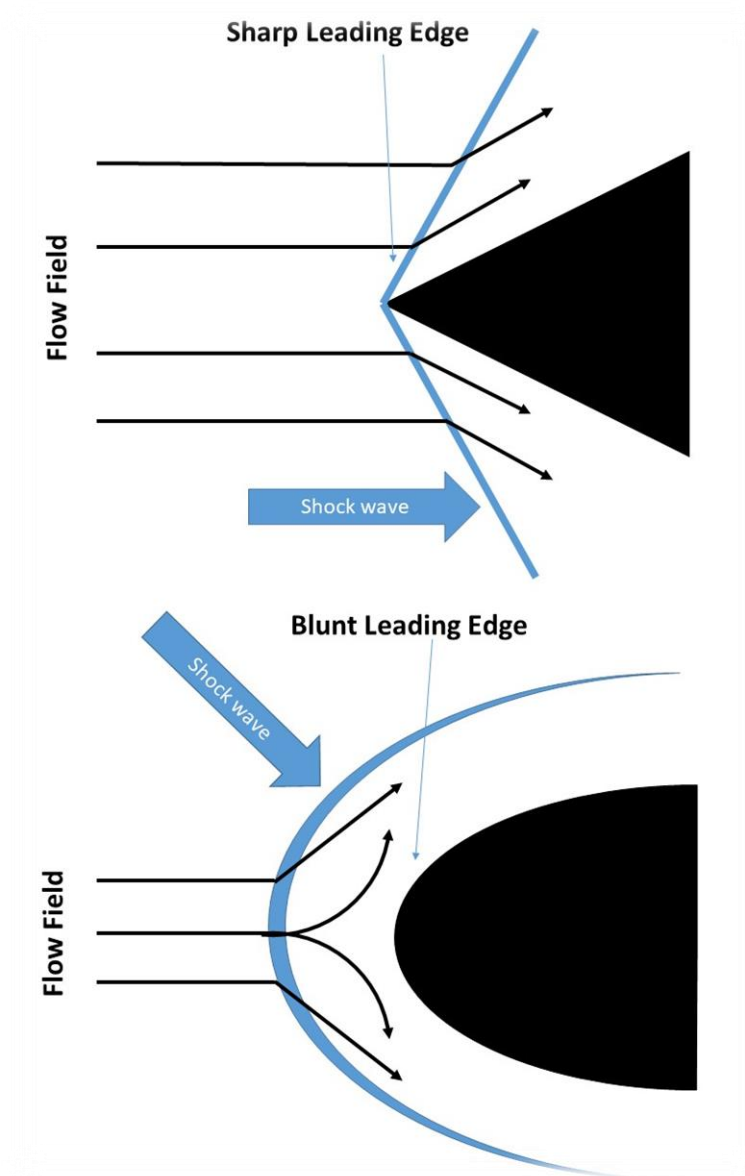


Fig. 1 Schematic on the effect of shape of leading edge on the shock wave propagation on the surface of the structure.

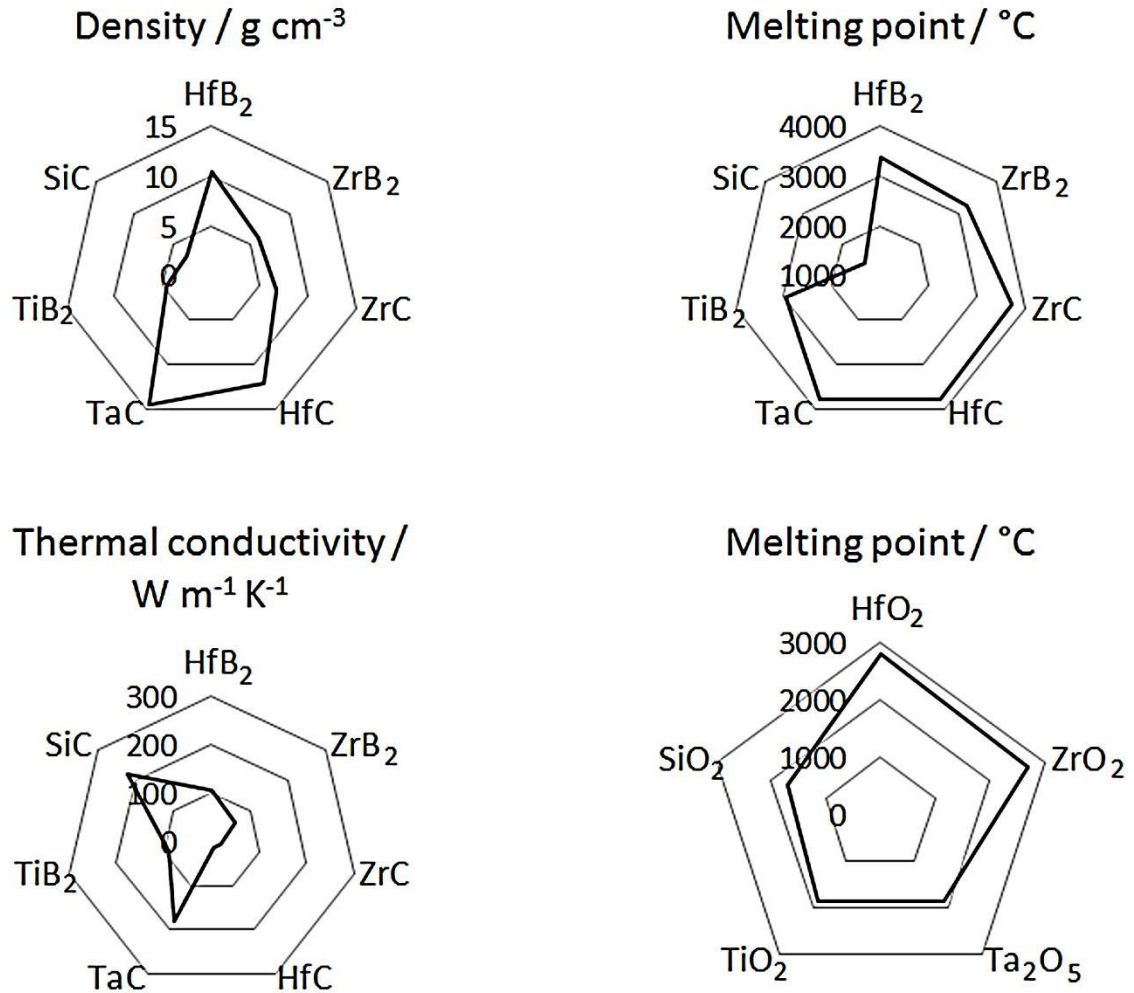


Fig. 2 Some summary data for common UHTCs ubiquitous in literature; HfB₂, ZrB₂, ZrC, HfC, TaC, TiB₂, SiC is provided for contrast, due to its frequent inclusion as a secondary matrix component [13], [29]–[35].

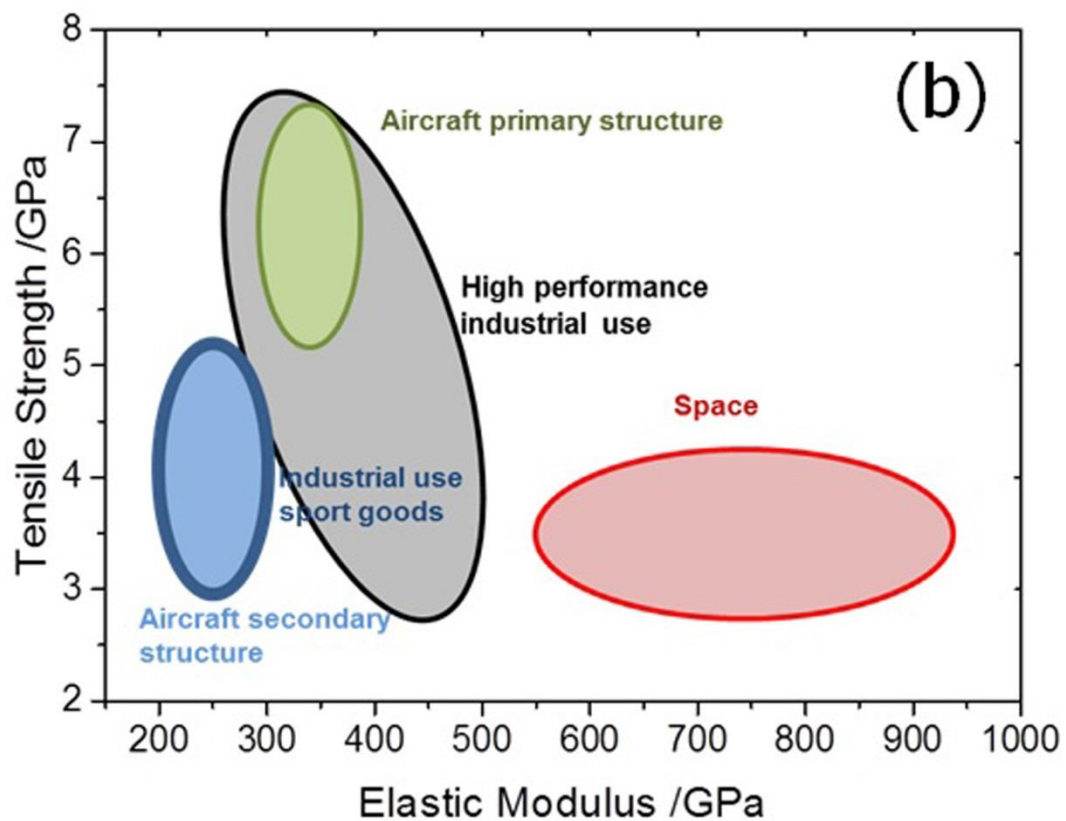
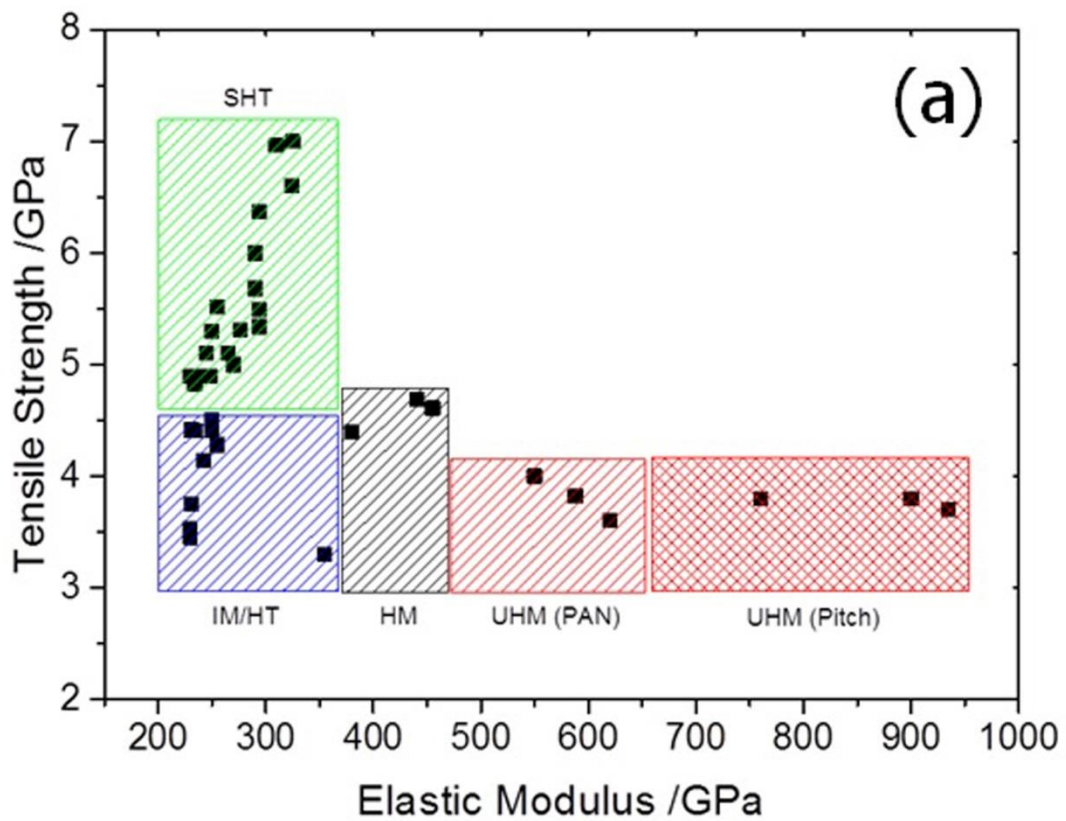


Fig. 3. a) Classification of the carbon fibres (value based on available commercial fibres of Error! Reference source not found. and their use, b) different applications with required properties range [128]

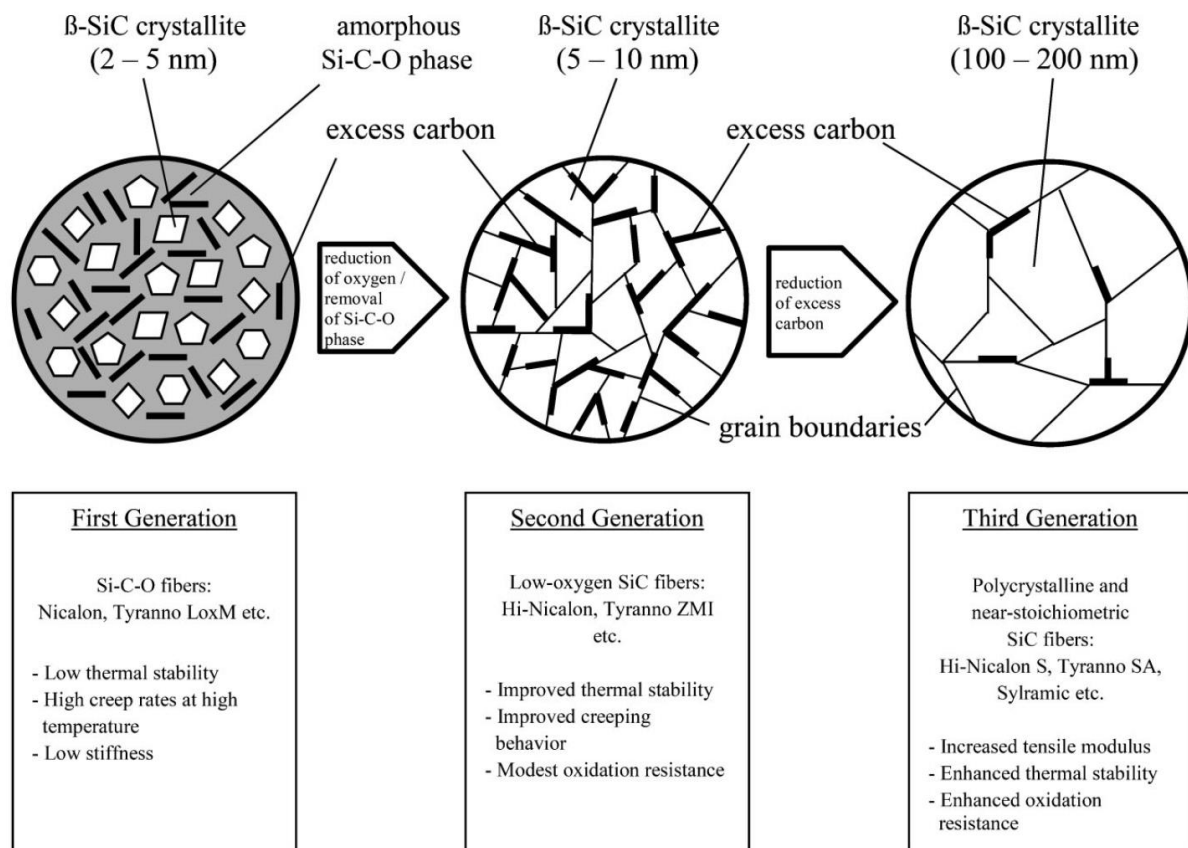


Fig. 4 Microstructural of the three generations of SiC fibres: reprinted with permission from John Wiley and Sons, Macromolecular Materials and Engineering, 297(6), Fig.16 in p. 512 [144].

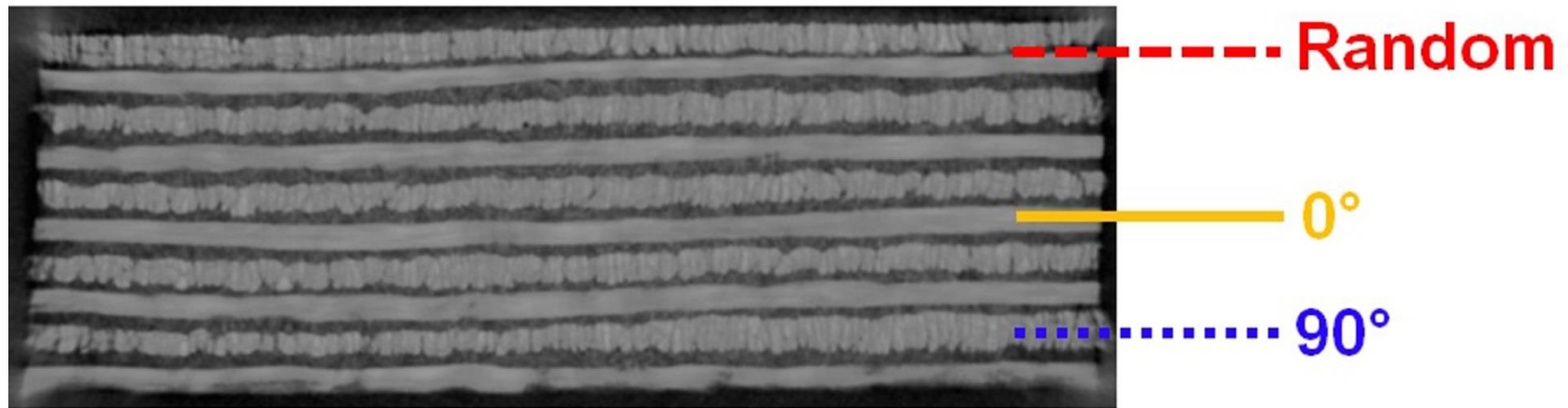


Fig. 5 Structure of the 2.5 D carbon fibre preform bought from Surface Transforms, UK (Structure: RO/90°/RO/0°/RO, 23% fibre, 77% porosity, bulk density: 0.36 g/cc, Random oriented (RO) arises from the needling process)

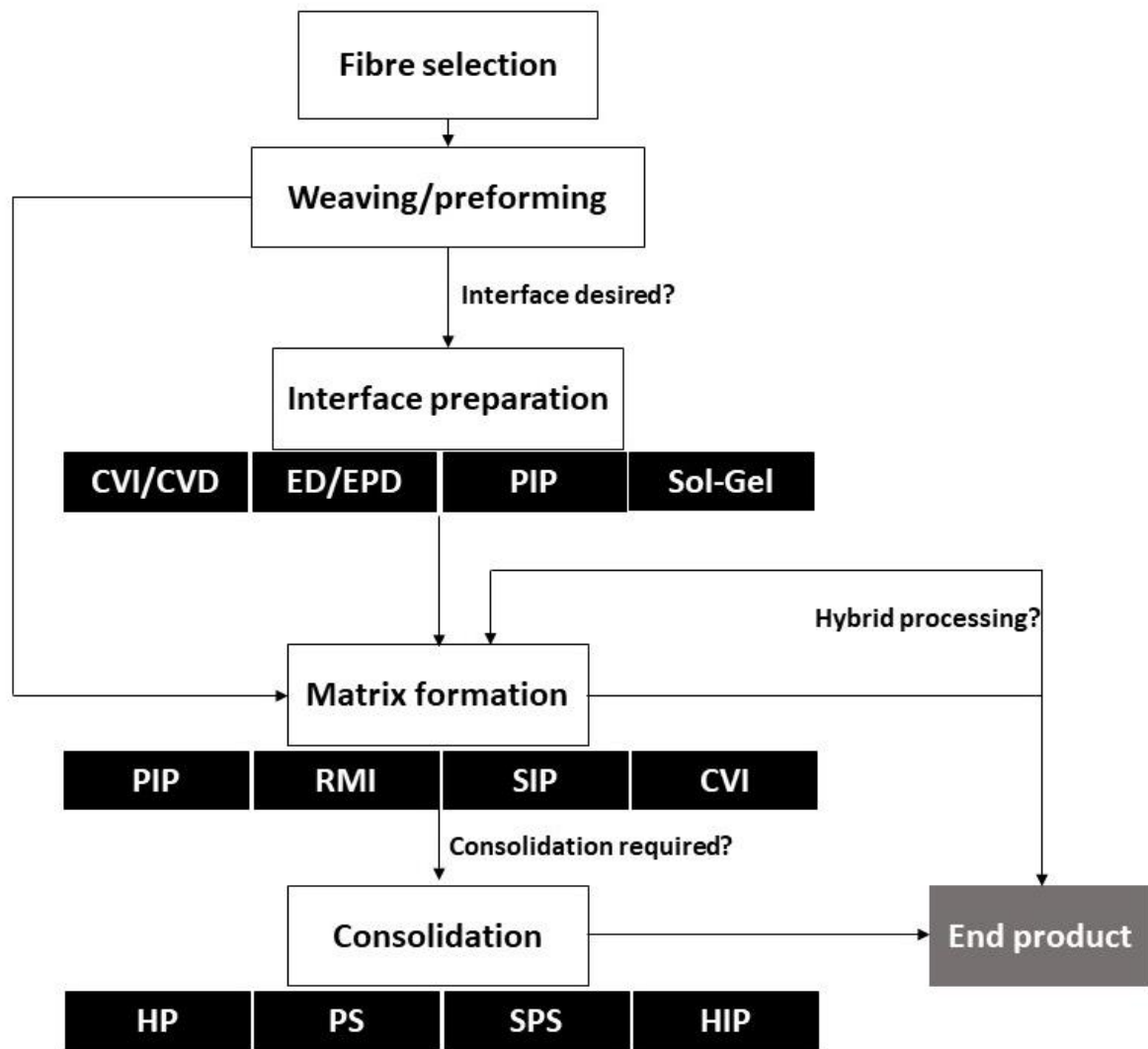


Fig. 6 Process flow sheet summarises the different methods of process for obtaining the UHTCMCs (CVI-chemical vapour infiltration, CVD-chemical vapour deposition, ED- Electro deposition, EPD- Electrophoretic deposition, PIP- precursor infiltration and pyrolysis, RMI - reactive melt infiltration, SIP - slurry impregnation process, HP – hot pressing, PS- pressureless sintering, SPS – spark plasma sintering, HIP – hot isostatic pressing)

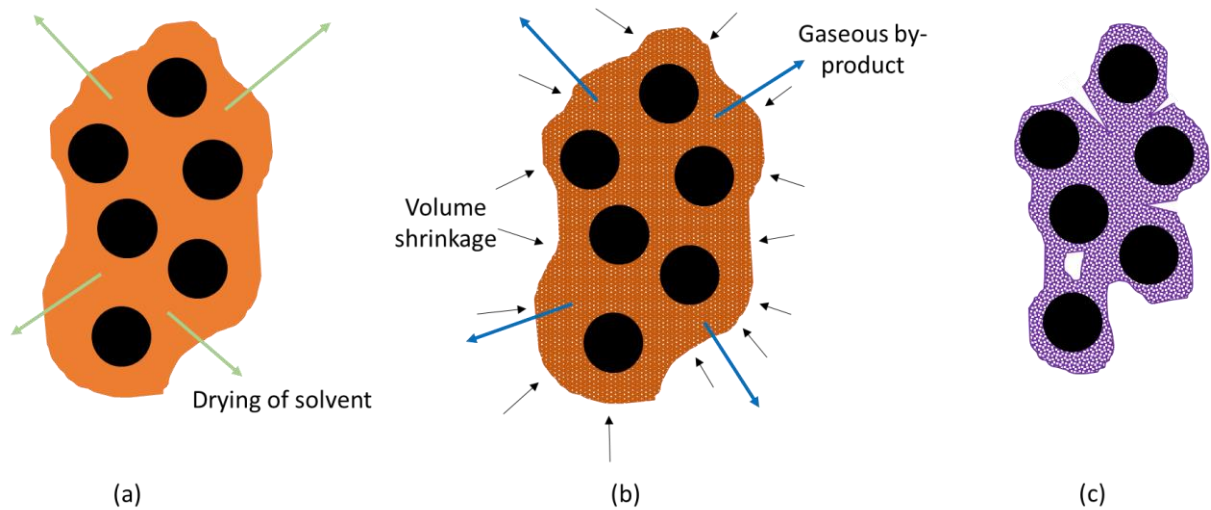


Fig. 7 The steps involved in production of a composite via PIP. (a) A liquid precursor impregnated fabric dries, leaving residual porosity; (b) pyrolysis begins, resulting in evolution of gaseous by-products and volume shrinkage from the polymer-ceramic transition; (c) a porous microstructure, with microcracks and pores shown in the matrix phases.

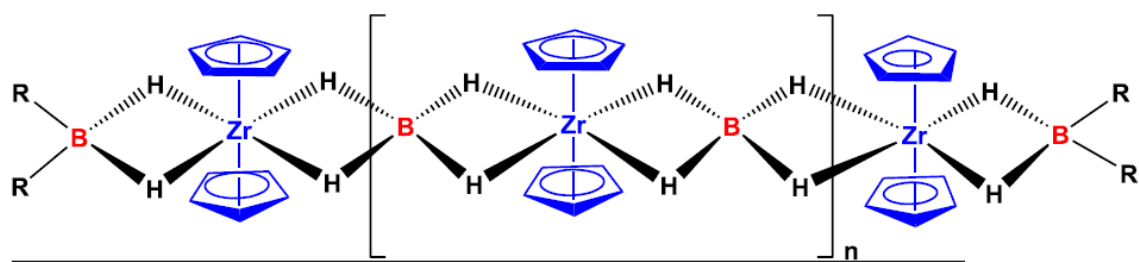


Fig. 8 The precursor used by Xie et al for a ZrB₂/ ZrC matrix: reprinted with permission from Elsevier, *Ceramics International*, 2015, 41[5], Eq. 1 in p. 6228 [194].

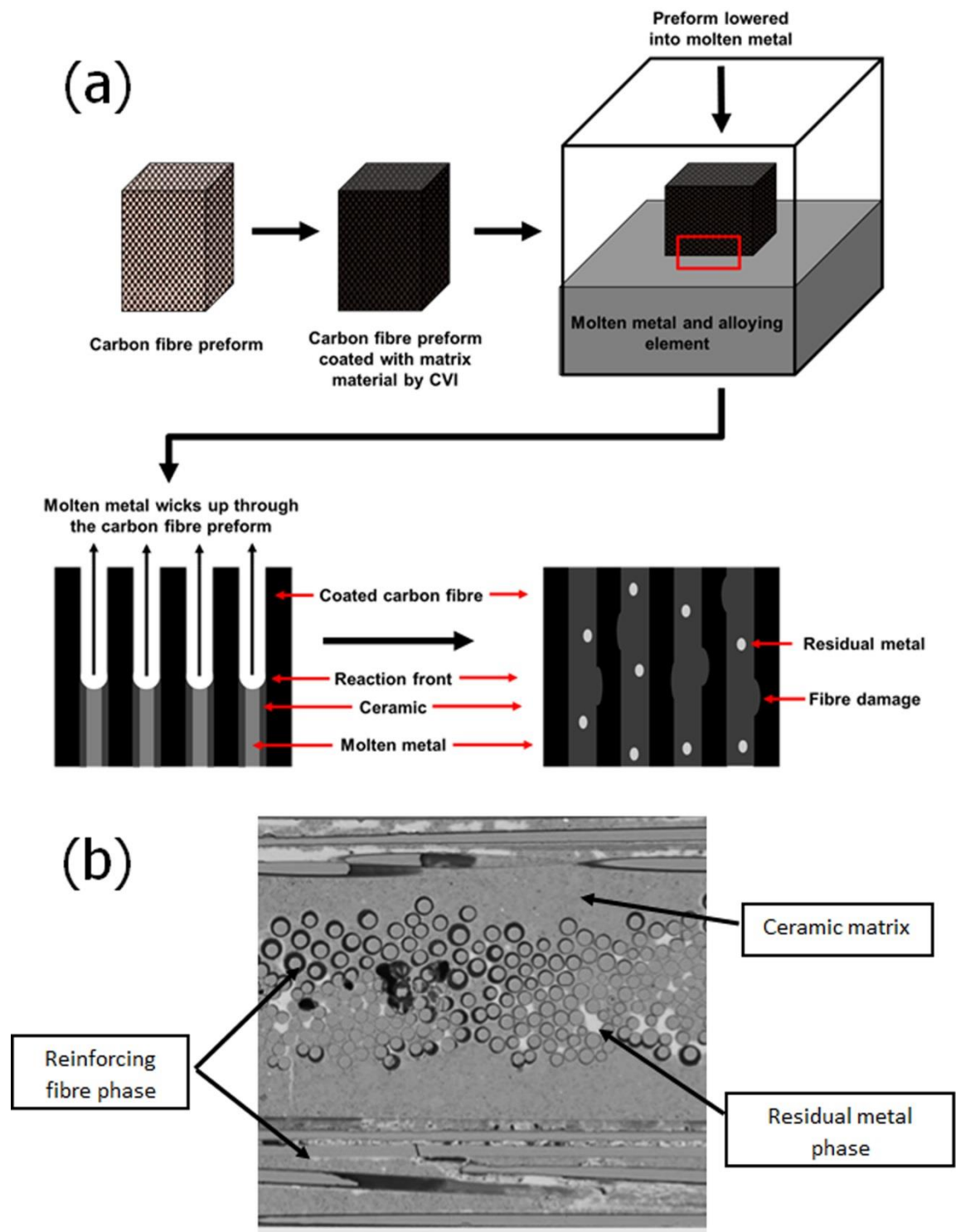


Fig. 9 (a) The reactive melt infiltration process and (b) residual free metal phase: reprinted with permission from Jeff Crompton, <https://uk.comsol.com/blogs/multiphysics-analysis-advanced-materials-ceramic-matrix-composites/> [216].

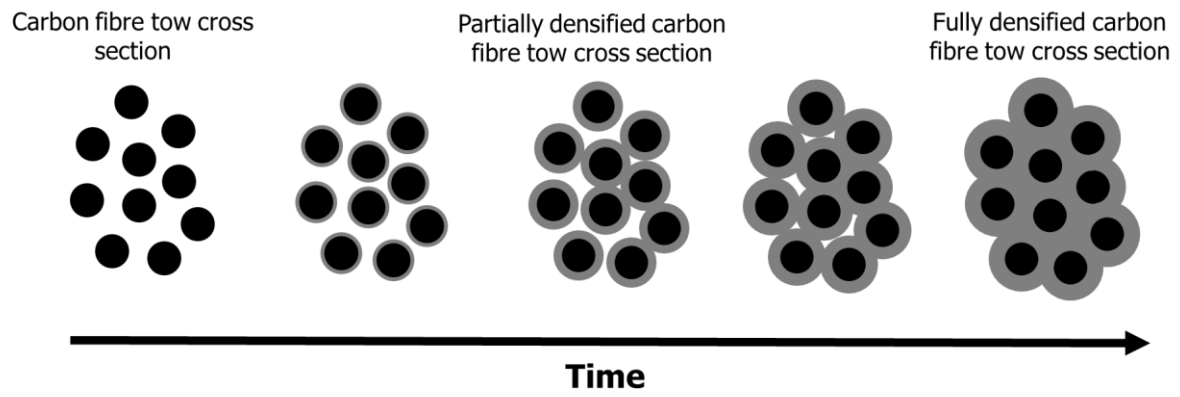


Fig. 10 Schematic showing the growth of ceramic deposit on the cross section of the fibres to the point of full densification by CVI method.

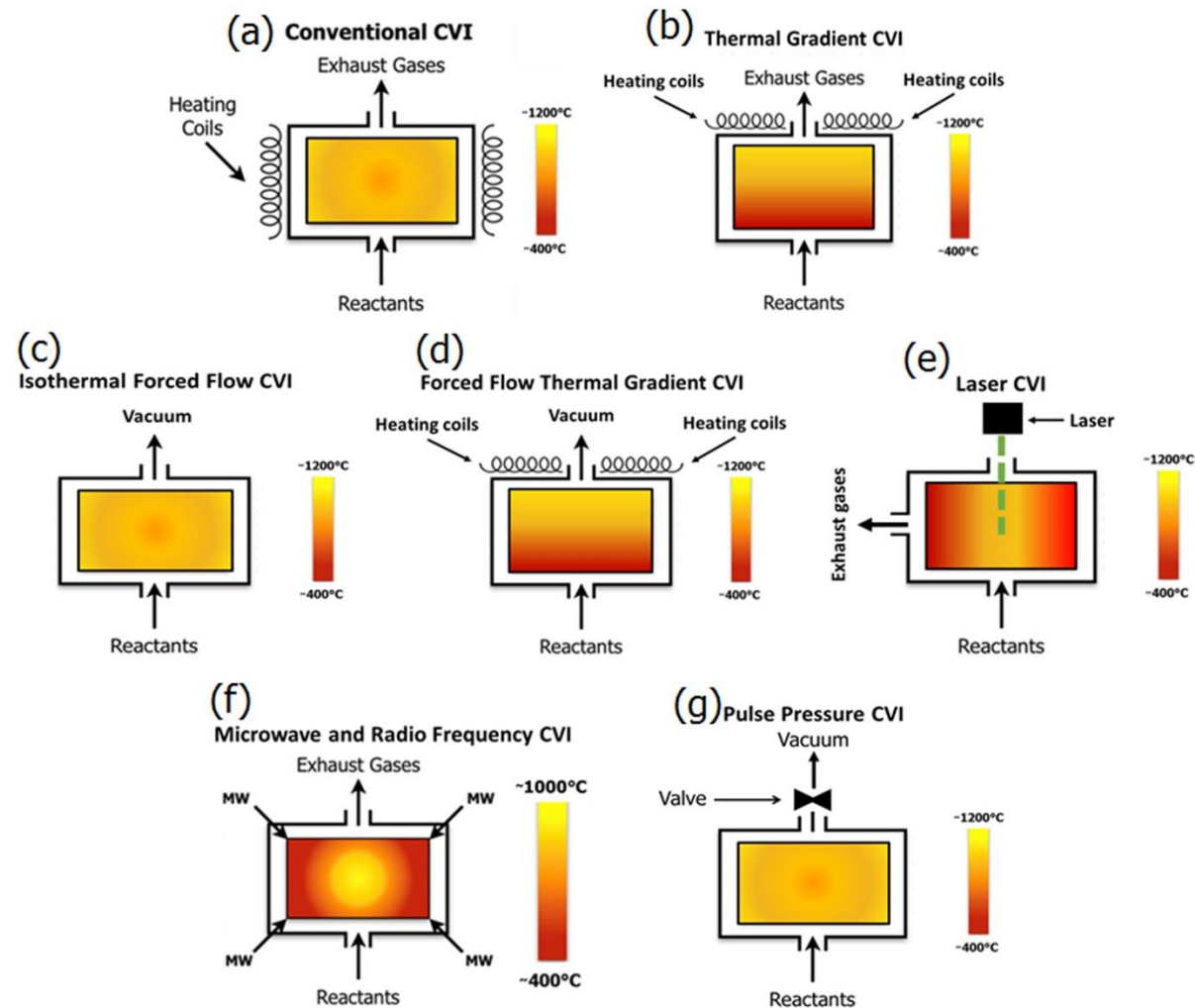


Fig. 11 a) Isothermal chemical vapour infiltration (ICVI), b) Thermal gradient (TGCVI), c) Isothermal forced flow CVI (FFCVI), d) Forced Flow Thermal Gradient CVI, e) Laser Chemical Vapour Infiltration (LCVI), f) Thermal gradient of Microwave and Radio Frequency CVI (MCVI and RFCVI) and g) pulse pressure CVI (PCVI).

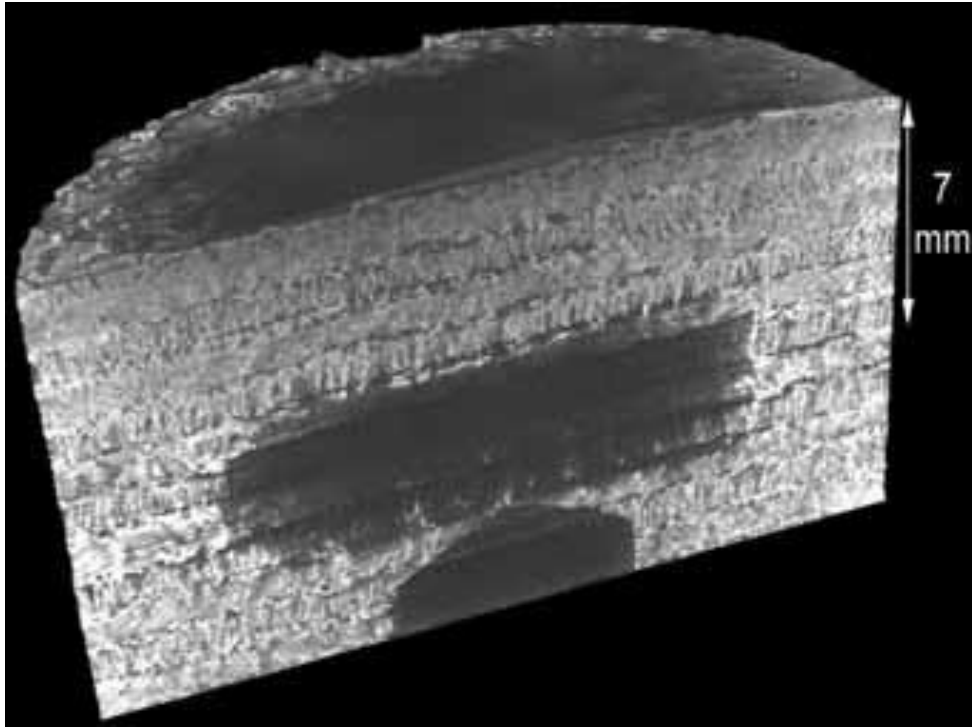


Fig. 12 3D micro-CT cross section of a UHTC composite prepared by squeeze impregnation showing powder penetration: reprinted with permission from Am. Ceram. Soc. Bull. 91, (2012), Fig.11 in p. 26 [17].

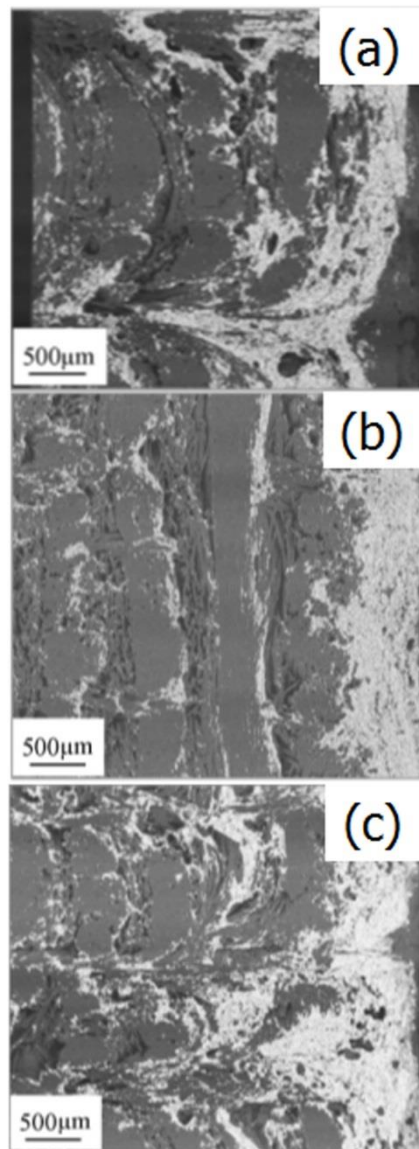


Fig. 13 Backscattered electron images of particles distribution in C / C-UHTC composites: (a) C / C - ZrB₂, (b) C / C - 4ZrB₂ - 1SiC, and (c) C / C - 1ZrB₂ - 2SiC - 2HfC: reprinted with permission from Elsevier, Mater. Sci. Eng. A 465, (2007) Fig.1 in p. 3 [10].

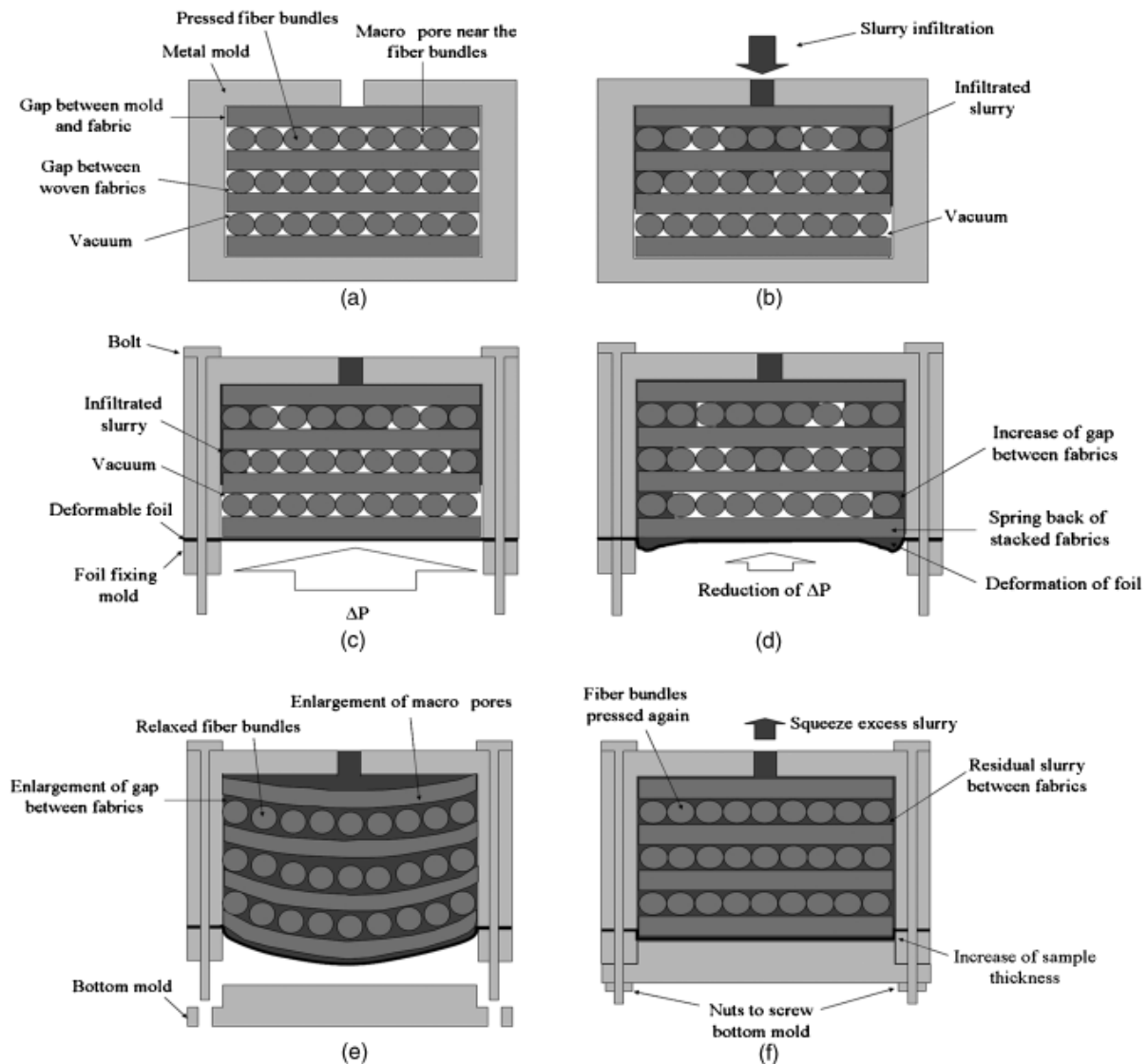


Fig. 14 Schematics of moulds for conventional vacuum-assisted pressure casting and a new deformation process. (a, b) Conventional fixture of a firm mould. Woven fabric suppress the infiltration of slurry. (c) Mould with a deformable foil during initial infiltration. The fabrics are pressed by the difference of pressure (ΔP) inside and outside of the mould. (d) Onset of outward deformation of the foil by the slurry. (e) Completion of the full deformation and infiltration of the slurry. (f) Removal of excess slurry by squeezing the mould: reprinted with permission from John Wiley and Sons, *J. Am. Ceram. Soc.* 90, (2007) Fig.1 in p. 2658 [258].

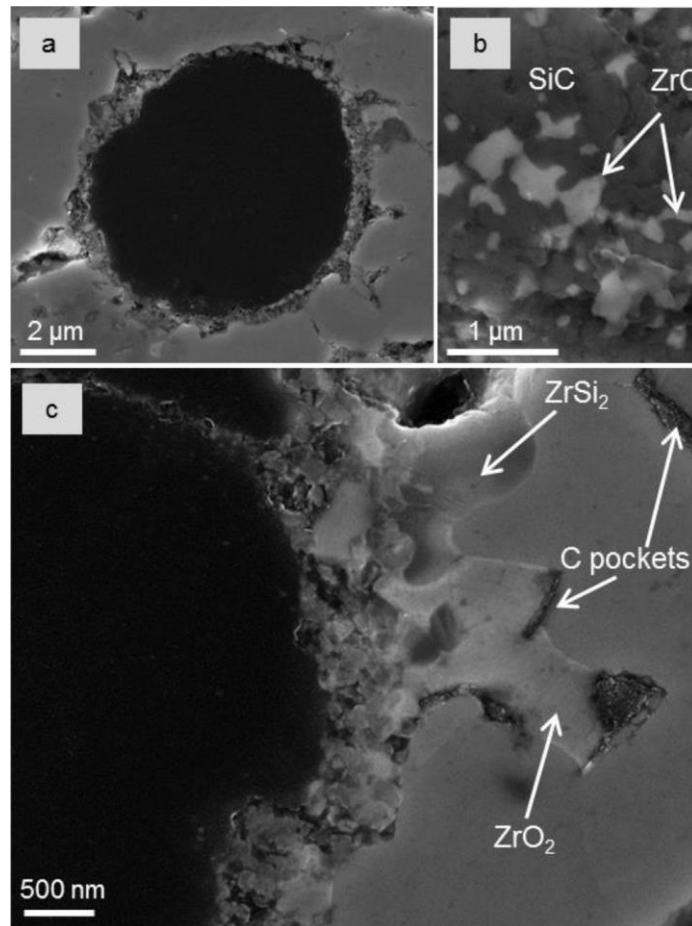


Fig. 15 a) Cross section of Cf-ZrB₂ composite using ZrSi₂ as sintering aid. b) and c) Details of the fibre / matrix interface show the formation of brittle phases of SiC and ZrC: reprinted with permission from Elsevier, Journal of the European Ceramic Society 36 (2016) Fig.3 in p. 19 [113].

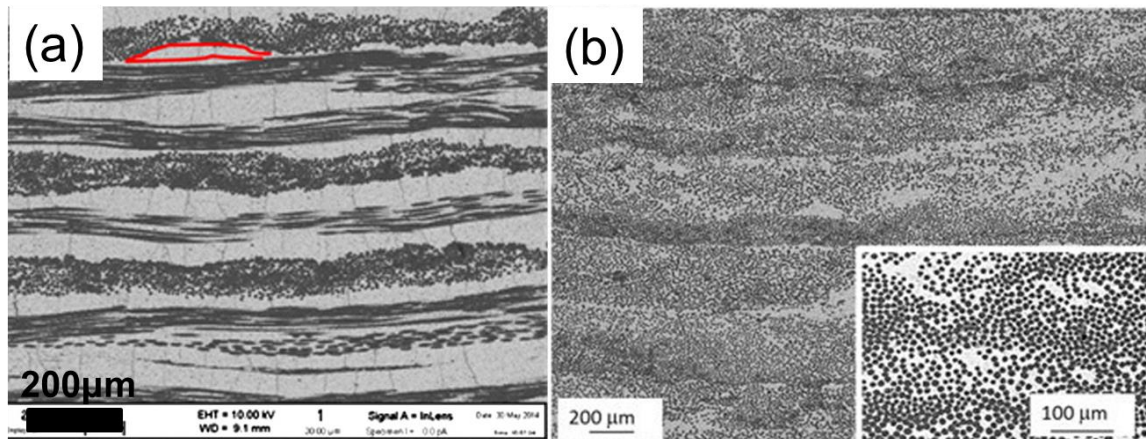


Fig.16 (a) Cross section of $C_f - ZrB_2$ composites produced by vacuum bagging followed by hot pressing at $1700^\circ C$ for 20 mins: reprinted with permission from Elsevier, Materials & Design 85 (2015) Fig.3d in p. 130 [279]. (b) Cross section of $C_f - ZrB_2$ composites, which was prepared by the infiltrate of ZrB_2 into unidirectional fabrics that were stacked in $0 - 0^\circ$ configuration. The sample was densified at $1800 - 1900^\circ C$ for 30 – 40 mins: reprinted with permission from ISTE, Scientific Reports 8[9148] (2018) Fig.2a in p. 3 [281].

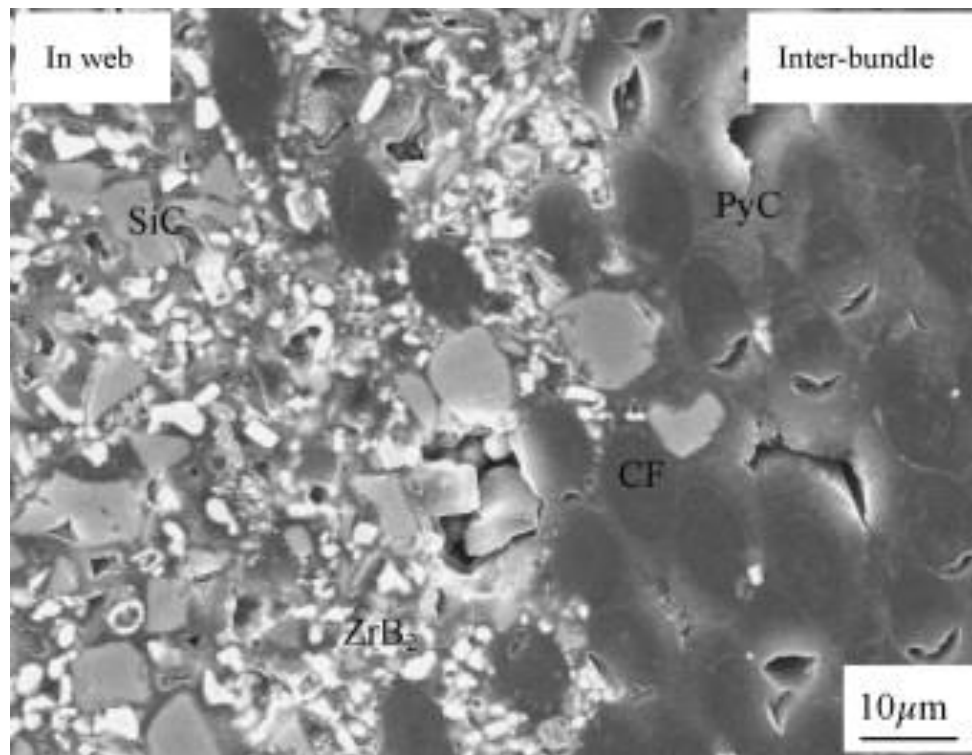


Fig. 17 The local microstructure of (Fig. 12a) after a carbon CVI at a higher magnification: reprinted with permission from Elsevier, Materials Science and Engineering: A 465 (2007) Fig.2 in p. 3 [281].

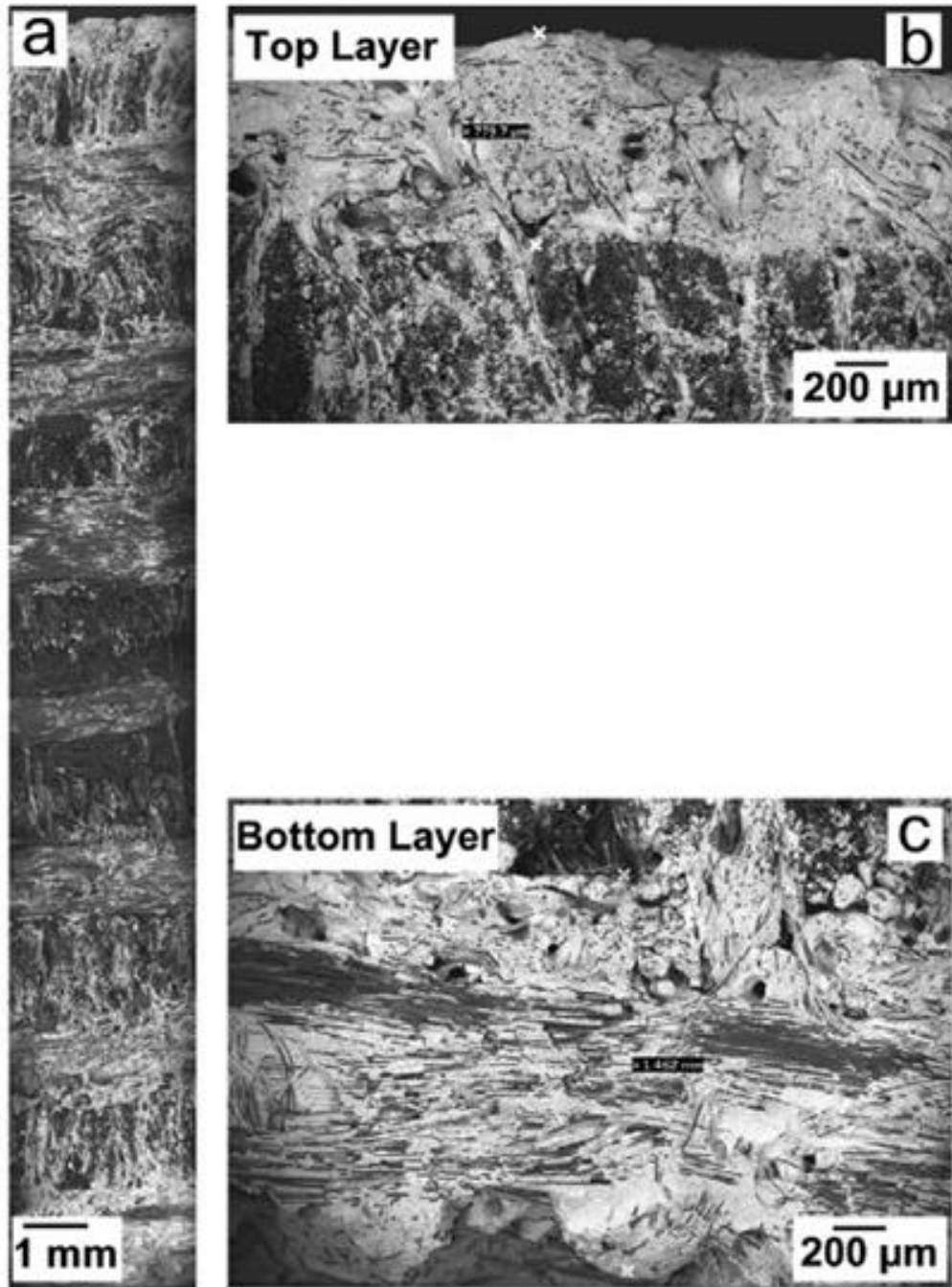


Fig. 18 Powder distribution of a UHTC composite produced by slurry infiltration (a) The detailed microstructure of the top (b) and bottom of the composite (c): reprinted with permission from Elsevier, J. Eur. Ceram. Soc., 33[2], Fig.2 in p. 425 [288].

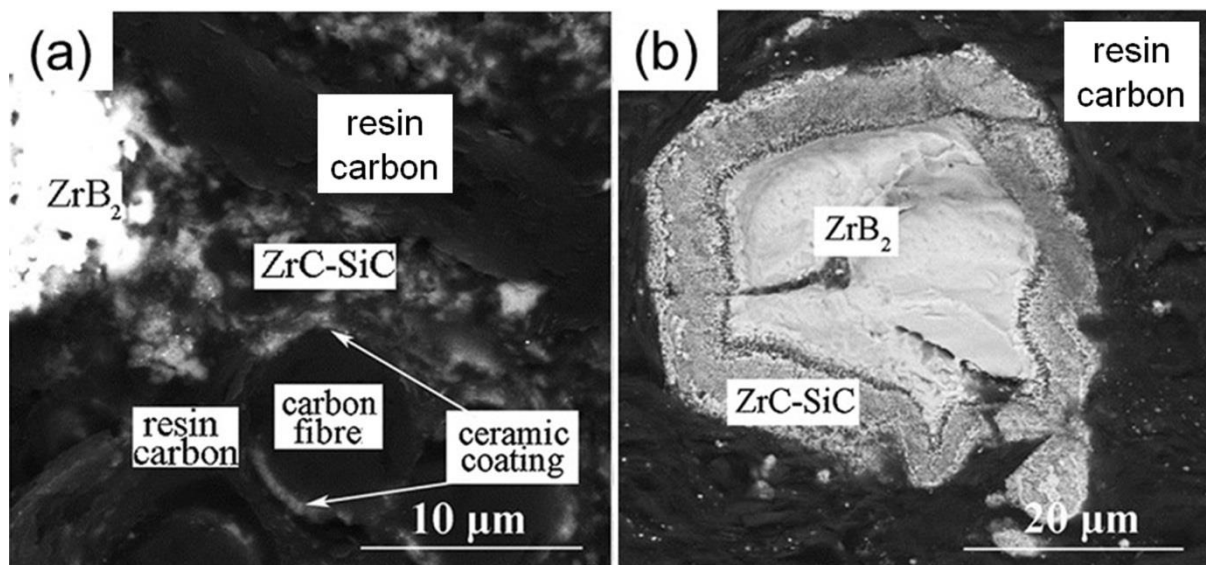


Fig. 19 BSE images (a) (b) on the cross section of the C/C-ZrB₂-ZrC-SiC composites prepared by PIP at different magnifications): reprinted with permission from Elsevier, Corros. Sci., 98 (2015), Fig. 4 in p. 554 [290].

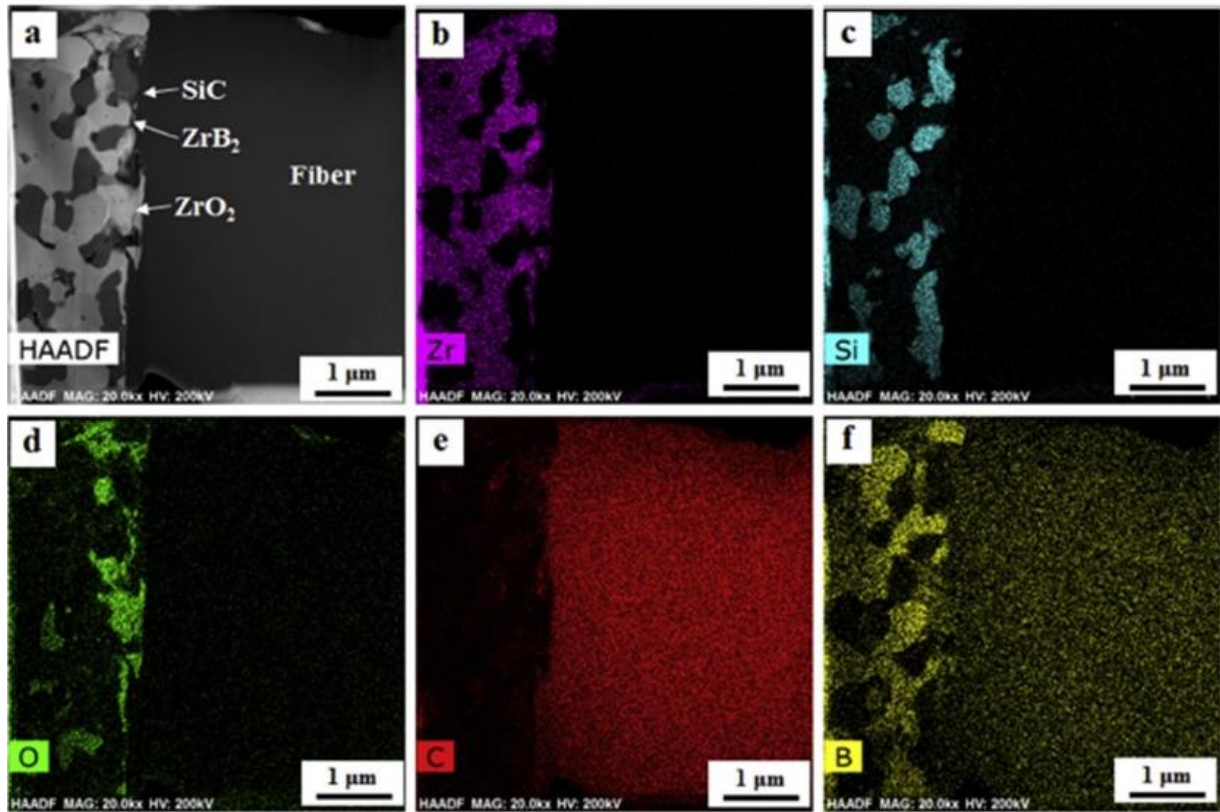


Fig. 20 A tight and clean interface on the C_f/ZrB_2-SiC composite prepared by SIP and hot pressing, and corresponding elemental distributions: reprinted with permission from Elsevier, *Journal of the European Ceramic Society*, 39 (2019), Fig. 6 in p. 802 [289].

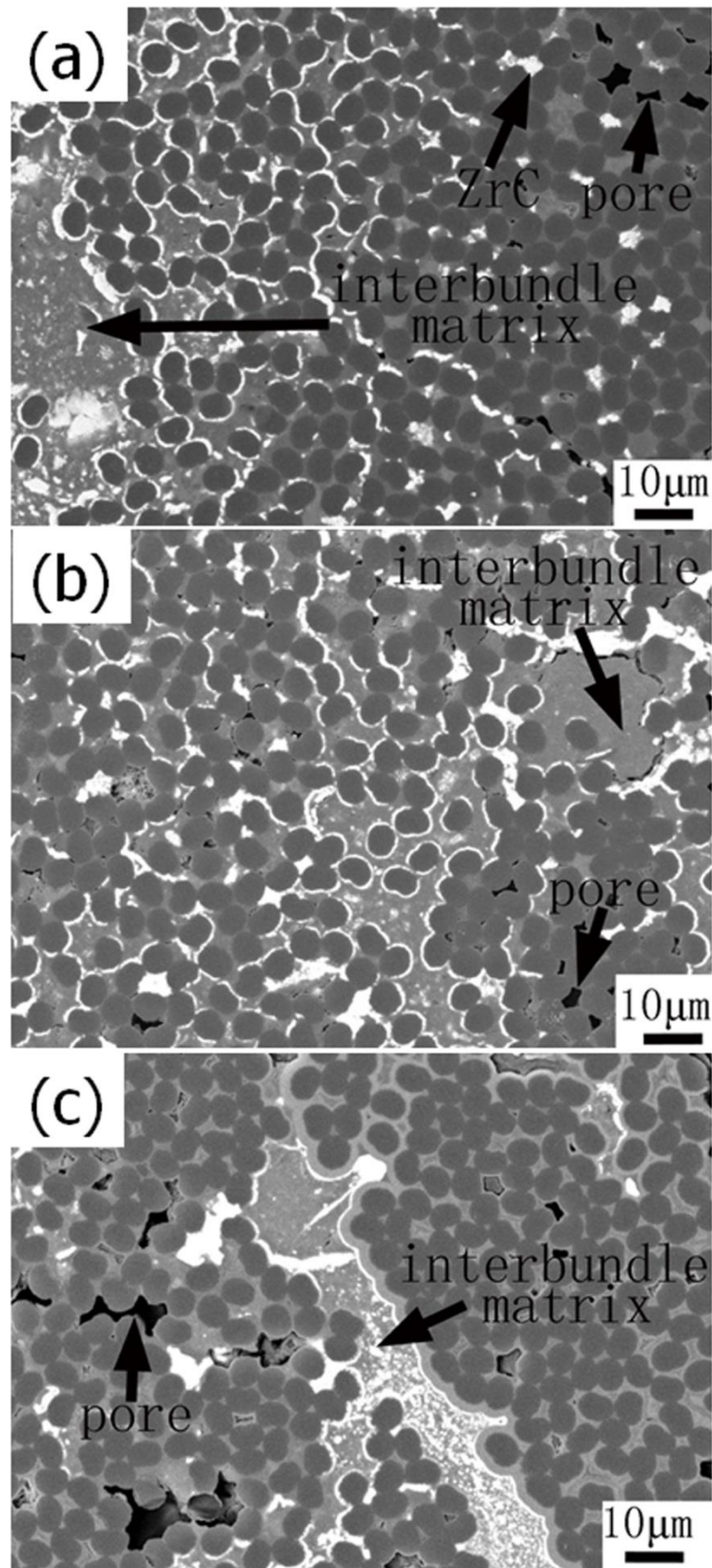


Fig. 21 The polished surface of C/ZrC-SiC produced by PIP+CVI with different interface (a) none; (b) PyC; (c) PyC+SiC: reprinted with permission from John Wiley and Sons, J. Am. Ceram. Soc., 91[10], Fig.1 in p. 3435 [294].

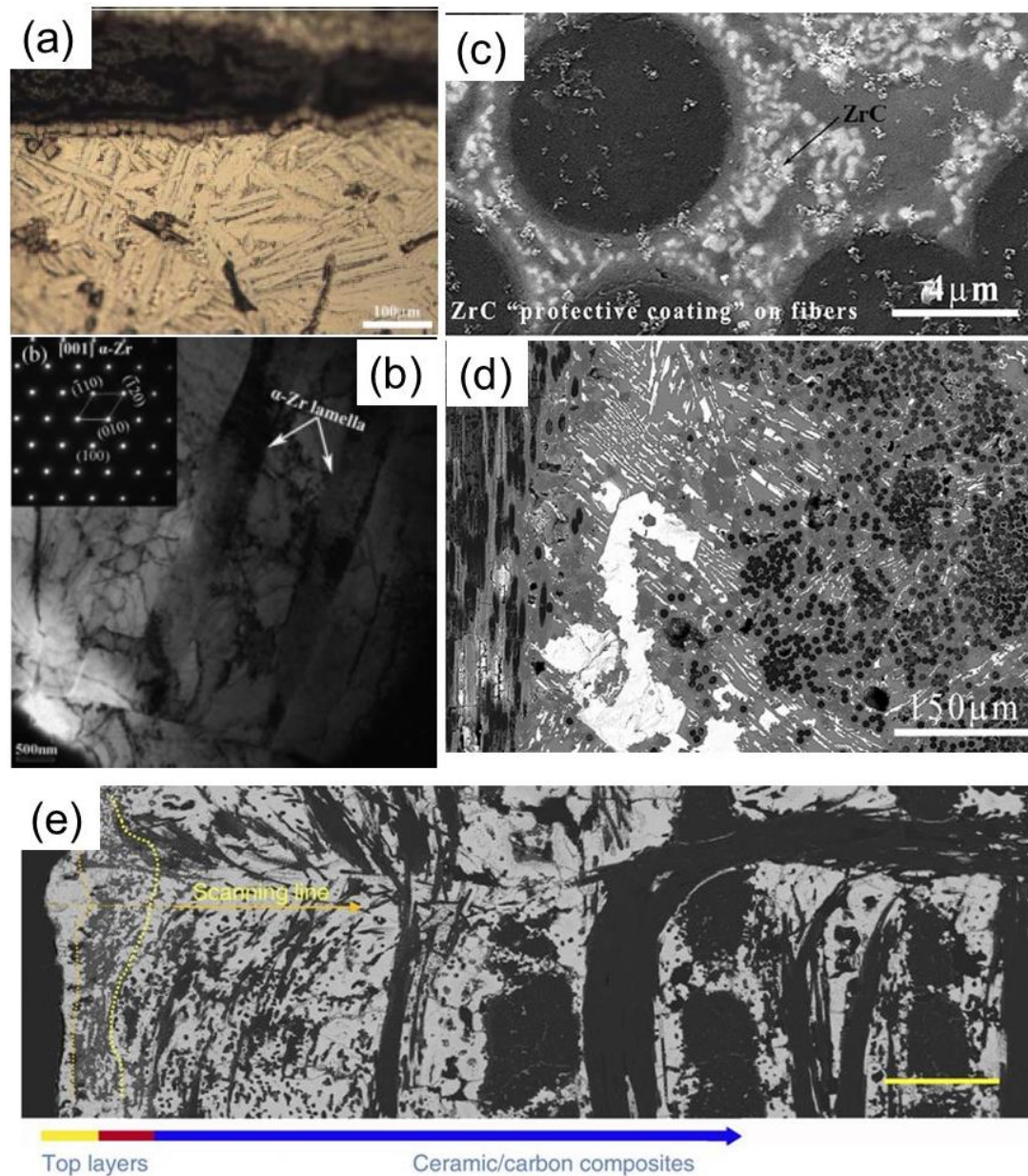


Fig. 22 The microstructure of C_f/ZrC (a,b): reprinted with permission from John Wiley and Sons, *Int. J. Appl. Ceram. Technol.*, 8[2], Fig.6a & Fig.7b in p. 324 & 335 [295]; $C_f/ZrC-SiC$ (c,d): reprinted with permission from John Wiley and Sons, *J. Am. Ceram. Soc.*, 101[8], Fig.1B and Fig.3A in p. 3255 & 3256 [296]; $C_f/Zr-Ti-B-C$ (e) composite densified by RMI: reprinted with permission from Author, *Nat. Commun.*, 8[15836], Fig.4a in p.4 [297].

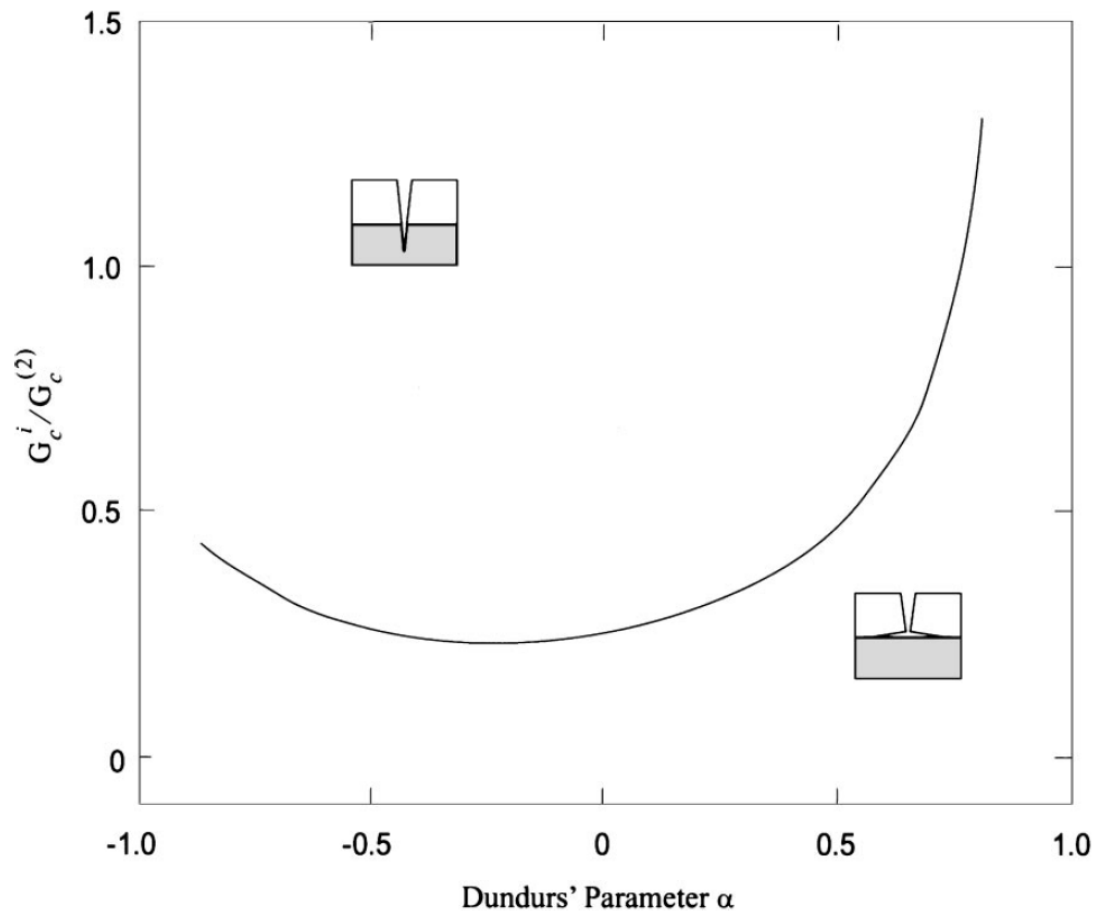


Fig. 23 Debonding map showing crack penetration and crack deflection regimes as a function of Dundurs's parameter [124].

Selection, Processing, Properties and Applications of Ultra-High Temperature Ceramic Matrix Composites, UHTCMCs - A Review

Total 13 tables

Table 1 UHTCMCs reinforced with Chopped fibre / whisker / CNT / graphene reinforcement.

Sr. No.	Matrix	Reinforcement phase	Processing method and conditions	Density / %TD	Hardness / GPa	Fracture toughness / MPa m ^{1/2}	Strength / MPa	Reference
1	ZrB ₂	Multi-walled carbon nanotubes, CNT (10 vol%)	Aqueous hetero-coagulation followed by SPS at 1700°C	97.0	-	-	-	[84]
2	ZrB ₂ -SiC (20 vol%)	Multi-walled CNTs (2 wt%)	Hot press 1900°C, 1h, 30 MPa	~96.0	15.5	4.6	616	[91], [116]
3	ZrB ₂ -SiC (20 vol%)	Multi-walled CNTs (10 vol%)	Hot press 1850°C, 1h, 20 MPa	93.9	8.6	5.1	-	[102]
4	ZrB ₂ -SiC	Multi-walled CNTs (2.5 wt%)	Hot press 2000°C, 1h, 30 MPa	>99.0	21.7	6.0	542	[91], [103]
5	ZrB ₂ -SiC (20 vol%)	Multi-walled CNTs (5 wt% & 15 vol%)	SPS 1600-1800°C, 5-10 min, 25-40 MPa	94.6-99.1	11.5-23.1	4.9-8.0	214-565	[91], [104]
6	ZrB ₂	Multi-walled CNTs (2-6 vol%)	SPS 1900°C, 15 min, 70 MPa	95.0-99.0	14.1-16.4	1.5-3.5	150-315	[91], [105]

7	ZrC-TiC	Multi-walled CNTs (0.25-1 wt%)	SPS 1750°C, 5 min, 40 MPa	98.5	20.0-21.0	4.2-5.0	-	[91], [107]
8	ZrC-SiC	Multi-walled CNTs (0.25-1 wt%)	SPS 1750°C , 5 min, 40 MPa	99.0	21.6-20.2	5.8-5.2	-	[91], [108]
9	HfB ₂	Multi-walled CNTs (10 vol%)	SPS, 1800°C, 8 min, 30 MPa	99.3	21.8	7.8	894	[87]
10	TaC	Multi-walled CNTs (4 wt%)	SPS, 1850°C, 10 min, 100-363 MPa	>94.0	10.6-22.9	1.1-1.6	-	[99]
11	ZrB ₂ - Si ₃ N ₄ (8 vol%)	Chopped pitch-derived C fibres (46 vol%)	Hot Press, 1800°C, 30 MPa	85.0	-	2.4	103	[109]
12	ZrB ₂ - Si ₃ N ₄ (8 vol%) - SiC (3 vol%)	Chopped high modulus pitch-derived C fibres (45 vol%)	SPS, 1900°C, 60 MPa	>96.7	-	-	200	[110]
13	ZrB ₂ & ZrB ₂ -ZrSi ₂ (20 vol%)	Short carbon fibres with/without heat treated (20 vol%)	Hot Press, 1600°C, 30 min, 30 MPa	98.9 & 97.9	-	7.6 & 6.9	481 & 437	[111], [112]
14	ZrB ₂ -Si ₃ N ₄ (5 vol)	Chopped C fibres (10-20 vol%)	Hot press 1700°C, 10 min, 40 MPa	95.1-98.3	-	3.6-4.0	270	[113]
15	ZrB ₂ -SiC (20 vol%)	Short C fibres (10-20 vol%)	Hot Press 1850°C & 2000°C, 30 & 60 min, 16 & 30 MPa	100 & 99.3	19.2	6.4-6.6	397-445	[95], [106], [114]

16	ZrB ₂ -SiC (2.5-15 wt%)	C fibres (2.5 – 10 wt%)	PS 2100°C-2150°C, 1h, Ar	87.0-95.0	11.0-15.0	3.0-5.9	-	[117]
17	HfB ₂ -SiC (20 vol%)-B ₄ C (2 wt%)- C (1 wt%)	Short Pitch-based carbon fibres (20-50 vol%)	Hot press 2100°C, 60 min, 20 MPa	98.1-99.5	-	5.6-6.1	160-250	[118]
18	ZrB ₂ -SiC (20 vol%)	Graphite nano-flakes (10 vol%)	Hot Press 1850°C, 60 min, 20 MPa	99.6	16.5	7.1	-	[89]
19	ZrB ₂ -SiC (20 vol%)	Graphite flakes (10 & 15 vol%)	Hot Press 1900°C, 60 min, 30 MPa	99.7 - 100	10.7-11.2	4.3-6.1	387-491	[85], [120], [121]
20	ZrB ₂	Graphene nano-platelets (2-6 vol%)	SPS, 1900°C, 15 min, 70 MPa	84.5-96.9	13.5-15.9	2.1-2.8	204-316	[86]
21	ZrB ₂ –SiC (20 vol%)	Graphene nano-platelets (10 vol%)	SPS, 1800°C, 6 min, 35 MPa	100	-	-	-	[57]
22	ZrB ₂ –SiC (20 vol%)	Graphene oxide (GO) (2 & 5 vol%)	Hot press 1950°C, 60 min, 30 MPa	98.9 & 99.2	22.9 & 22.8	6.1 & 7.3	698 & 1055	[88]
23	ZrC-SiC (25 vol%)	Graphene nano-platelets powder (5 wt%)	Hot press 1850°C, 60 min, 20 MPa	99.1	15.7	6.4	-	[89]
24	ZrC-SiC	Macro porous Graphene	Slurry infiltration followed by SPS	97.6	-	4.3	220	[90]
25	ZrB ₂ ZrB ₂ -Si ₃ N ₄ ZrB ₂ -ZrSi ₂	SiC chopped fibres (0-30 vol%)	Hot press & SPS, 1400°C-1900°C, 10 & 5 min, 50 MPa	93.0-100	-	3.7-6.2	370-457	[92], [93], [115]

	ZrB ₂ -MoSi ₂ ZrB ₂ -TaSi ₂ (5-10 vol%)							
26	ZrB ₂ -Si ₃ N ₄ (5 vol%)	Chopped Hi-Nicalon SiC fibres (15 vol%)	Hot press 1720°C, 10 min, 50 MPa	99.0	13.0	5.2	389	[94]
27	ZrB ₂ -Si ₃ N ₄ (5 vol%)	3rd generation SiC short fibres (3 vol%)	Hot press 1700°C, 15 min, 30 MPa	99.0	-	-	-	[93]
28	ZrB ₂ -ZrSi ₂ (10 vol%)	SiC chopped fibres (20 vol%)	Hot Press, 1650°C, 10 min, 50 MPa	100	-	6.2	385	[96]
29	HfB ₂ -Si ₃ N ₄ (8 vol%) HfB ₂ -ZrSi ₂ (10 vol%)	Chopped Hi-Nicalon SiC fibres (20 vol%)	SPS, 1550°C -1800°C, 5 min, 75 MPa	95.0-99.9	25.0-38.0	3.8-5.4	399-680	[97]
30	HfC + TaSi ₂ (10 vol%)	Short chopped SiC fibres (15 vol%)	Hot press 1750°C, 14 min, 40 MPa	94.8	15.1	3.82	375	[98]
31	ZrB ₂	SiC whiskers (10- 30 vol%)	Hot press 1750°C, 60 min, 28 MPa	94.0-98.0		5.9-7.6	360-380	[100]
32	ZrB ₂ -SiC (20 vol%)	ZrO ₂ fibres (15 vol%)	Hot press 1850°C, 60 min, 30 MPa	98.6	18.4	6.8	1085	[101]

Table 2 Mechanical properties of carbon fibres produced by PAN and Pitch precursor [128], [134]-[141]

Trade name	Manufacturer	Precursor	Tensile strength /MPa	Tensile modulus /GPa	Elongation %
Torayca T300	Toray	PAN	3530	230	1.5
Torayca T800	Toray	PAN	5340-5490	294	1.9-2.0
Torayca T1100	Toray	PAN	7000	324	2.0
Torayca M60	Toray	PAN	3820	588	0.7
Tenax	Toho (Teijin Group)	PAN	4100-5100	240-265	1.7-2.1
Tenax IMS	Toho (Teijin Group)	PAN	4500-6000	290	1.6-2.1
Tenax UMS	Toho (Teijin Group)	PAN	4000-4700	390-550	0.7-1.2
TR series	Mitsubishi	PAN	5520	255	2.1
MR series	Mitsubishi	PAN	7000	325	2.2
HS40	Mitsubishi	PAN	4610	455	1.0
34 series	Mitsubishi	PAN	4482-4826	234	1.9-2.0
37-800	Mitsubishi	PAN	5585	234	2.1
K13D2U	Mitsubishi	Pitch	3700	935	0.4
K13C2U	Mitsubishi	Pitch	3800	900	0.6
Hextow IM10	Hexcel	PAN	6964	310	2.0

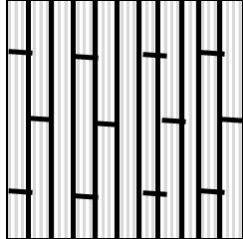
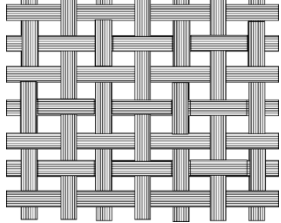
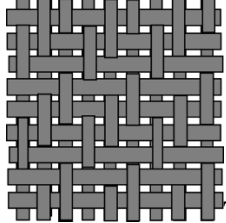
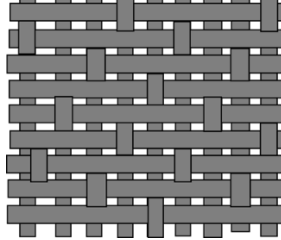
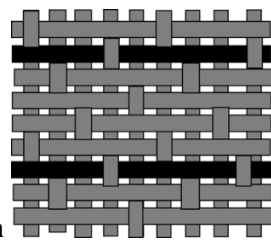

Hextow HM63	Hexcel	PAN	4688	441	1.0
Thornel T650	Solvay	PAN	4280	255	1.7
Thornel P55	Solvay	Pitch	1900	414	0.5
Thornel P100	Solvay	Pitch	2400	830	0.2
Tayrifil TC42S	Formosa plastic Corp.	PAN	5690	290	--
Tayrifil TC55	Formosa plastic Corp.	PAN	4400	380	--
Sigrafil	SGL Carbon	PAN	5000	270	1.9
GRANOC YS90A	Nippon Graphite Fiber Corporation	Pitch	3530	880	0.3
GRANOC YSH50A	Nippon Graphite Fiber Corporation	Pitch	3830	520	0.7

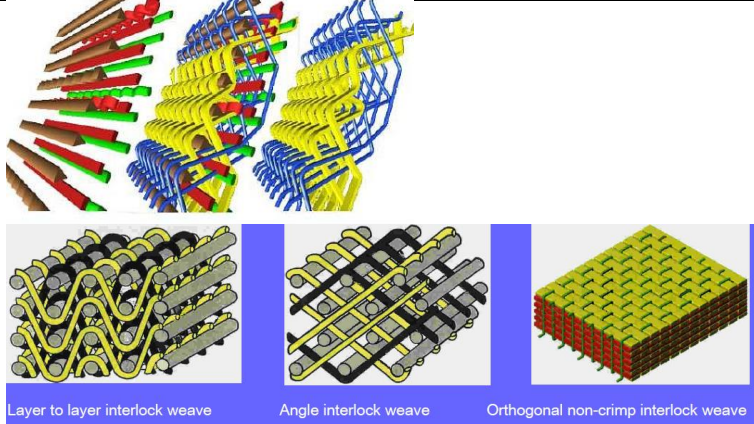
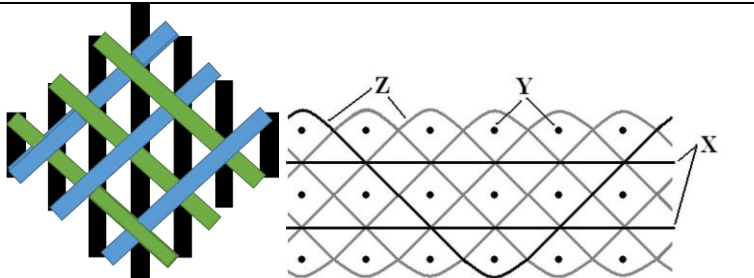
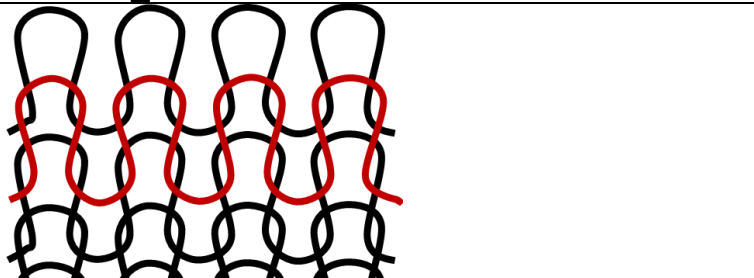
Table 3 Physical, mechanical and thermal properties of the commercially available SiC fibre [144] - [147].

Trade name (manufacturer)	Production method (curing atmosphere)	Temp. production	Composition /wt%	Structure	Fibre diameter /μm	Density /g cm ⁻³	Tensile strength /GPa	Tensile Modulus /GPa	Thermal conductivity /W m ⁻¹ K ⁻¹	Cost /EUR per kg
Nicalon (Nippon carbon)	Polymeric precursor (inert)	1200	56.6 Si+ 37.1 C + 11.7 O	2 nm crystallite in amorphous Si-C-O phase	14	2.55	3.0	220	3.0	1000
Tyranno LOX-M (Ube Industries)	Polymeric precursor (inert)	1200	55.4 Si + 32.4 C + 10.2 O + 2 Ti	1 nm crystallite in amorphous Si-C-O phase	11	2.35	3.3	186	1.4	1200
Hi-Nicalon (Nippon carbon)	Polymeric precursor (inert)	1300	62.4 Si + 37.1 C + 0.5 O	5 nm crystallite in amorphous Si-C-O phase	14	2.74	2.8	270	8.0	3250
Tyranno ZMI (Ube Industries)	Polymeric precursor (inert)	1300	56.1 Si + 34.2 C + 8.7 O + 1 Zr	5-10 nm crystallite in amorphous Si-C-O phase	11	2.48	3.4	193	2.5	1400
Hi-Nicalon Types S (Nippon carbon)	Polymeric precursor (inert)	1600	68.9 Si + 30.9 C + 0.2 O	100 nm crystallites near-stoichiometric	12	3.10	2.6	420	18	7000
Tyranno SA3 (Ube Industries)	Polymeric precursor (inert)	1600	67.8 Si + 31.3 C + 0.3 O + 2 Al	200 nm crystallites near-stoichiometric	7 to 10	3.10	2.8	380	64.5	6500

Sylramic	Polymeric precursor (inert)	>1700	67.0 Si + 29.0 C + 0.8 O + 2.3 B + 0.4 N 2.1 Ti	100 nm crystallites near-stoichiometric	10	2.95	2.8	310	40-45	8000
Sylramic iBN (ATK-COI)	Polymeric precursor (inert)	>1700	SiC/BN	>100 nm crystallites near-stoichiometric and BN coating	10	3.05	3.2	400	>46	10500
SCS 6 and Ultra (Specialty Materials)	Chemical vapour deposition	1300	70 Si + 30 C + C filament	100 nm columnar SiC on C filament, SiC/C coating	140	3.00	5.9	415	70	8300
Sigma (TISICS)	Chemical vapour deposition	not available	11 W + 86 SiC + 1.3 C + 1.7 TiB ₂	W filament, 80 µm SiC layer and duplex C/TiB ₂ layer	100	3.50	4.0	400	not available	7600

Table 4 Different preform types, manufacturing techniques, advantages and disadvantages.

Preform	Design	Advantages	Disadvantages
Low crimp, uniweave		High in-plane properties, good tailor ability, highly automated process	Low transverse and out of plane properties, poor fibre stability, labour intensive layup
2D Woven	 Plain  Twill  Satin  Matt	Low crimp, Good in-plane properties, good limited drapability, highly automated process, suited for large covering area and extensive database.	Plain- high crimp, poor mechanical properties, Satin – different fibre orientation so it's good for mechanical properties but the interlace positions are irregular.
2D Braid		Good balance in off-axis, automated process, suitable for complex curved shapes, good drapability	Size limitation, low out of place properties

3D Woven	 <p>The diagrams for 3D Woven show three types of interlock weaves: 'Layer to layer interlock weave' (a 3D perspective of multiple layers of threads interlocking), 'Angle interlock weave' (a 2D schematic of threads crossing at an angle), and 'Orthogonal non-crimp interlock weave' (a 3D perspective of threads crossing at right angles without crimp).</p>	Moderate in-plane and out of plane properties, automated process,	Poor drapability, limited shapes are possible, limited tailorability for off axis
3D Braid	 <p>The diagrams for 3D Braid show a 3D perspective of three colored threads (black, blue, green) braiding together, and a 2D schematic of a woven pattern with axes labeled X, Y, and Z.</p>	Good balance for in-plane and Out of plane properties, Suitable for complex shapes	Slow process, size limitation
Multi axial warp knitting	 <p>The diagram for Multi axial warp knitting shows a 2D schematic of a mesh structure formed by black and red loops.</p>	Good tailorability for balanced in plane properties, highly automated process, multilayer high though put, suitable for large covering area Complex shapes can be formed	Low out of plane properties

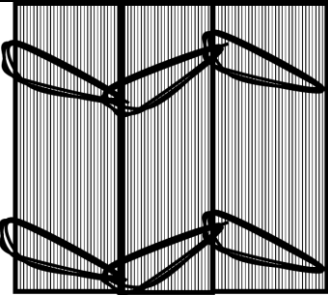
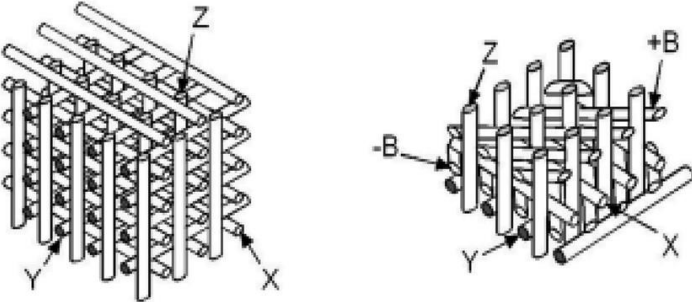
Stitched Fabrics		Good in plane properties, highly automated process, provides excellent damage tolerance and out of plane strength and excellent assembly aid	Small reduction in in plane properties, poor accessibility to complex curved shapes
Noobed	 <p>reprinted with permission from Journal of the Indian Institute of Science., 95[3] (2015) Fig. 2 in p. 223 [193]</p>	Multi directional delamination ballistic resistance, impact damage tolerance, Un crimped fibres	Yet to develop on large scale and for making complex shapes.

Table 5 Summary on the advantages and disadvantages of various densification / consolidation methods

Densification / Consolidation technique	Advantages	Disadvantages
Precursor infiltration and pyrolysis	<ul style="list-style-type: none"> ▪ The composition of the ceramic deposit is highly versatile due to chemistry of precursor. ▪ A large degree of control of the physical properties of the precursor is obtainable again by tailoring the chemistry of the precursor, allowing significant improvements made to the wettability, viscosity, or thermal properties (i.e. thermally curing) for a given procedure. ▪ Precursor can be introduced through vacuum – procedurally simple. ▪ As a liquid precursor, penetration into the fibre tow is facile due to the capillary pressure. This area is notoriously hard to penetrate through slurry based processes. 	<ul style="list-style-type: none"> ▪ Low yields of ceramic from precursor will require that many cycles of infiltration and pyrolysis are required for densification, increasing time and cost for a given component. ▪ The matrix will always be porous and can contain micro-cracks, due to the escape of gaseous by-products and volumetric shrinkage from precursor to ceramic. ▪ Reactive chemicals and repeated heat treatments can cause fibre degradation, leading to a loss of mechanical properties
Reactive Melt Infiltration	<ul style="list-style-type: none"> ▪ It produces a near fully dense matrix ▪ The processing time is shorter than for most ceramic matrix composite fabrication processes and is subsequently relatively cheap. ▪ The closed porosity at the surface can often eliminate the need for a final oxidation resistant coating. ▪ A reaction bonded UHTC matrix is effectively produced. 	<ul style="list-style-type: none"> ▪ For fibre composites the high temperatures required for reactive metal infiltration exposes the carbon fibres to very aggressive molten metals, often above 1400°C. ▪ The exothermic nature of the reaction between constituents can also further increase the temperature locally, causing more damage. ▪ The metal in this form is highly reactive and, if infiltration conditions are not strictly controlled, serious degradation of the carbon fibre preform, will occur leading to deleterious consequences on the properties. ▪ Residual metallic phases, which have relatively low oxidation resistance and a

		<p>lower melting point than the ceramic phases present. This metallic phase can lead to accelerated creep, crack propagation and further attack when the material is operating at high temperature.</p>
Chemical Vapour Infiltration	<ul style="list-style-type: none"> ▪ The deposited material can have a high purity. ▪ It is a low temperature process, thus fibre damage can be avoided. ▪ It is a versatile process. Many binary compounds can be deposited, as well as multi-coatings and functional graded materials, without stopping the process. ▪ Intricate shapes can be prepared without damaging the continuous fibres used for reinforcement. ▪ The morphology and microstructure of the coating can be tailored by changing temperature, pressure and precursor feed rate. ▪ High reproducibility ▪ High deposition rates are possible. ▪ The resulting composites can offer excellent mechanical and anti-ablation properties ▪ Deposit has high thermal conductivity and good creep resistance 	<ul style="list-style-type: none"> ▪ Processing times of industrial scale CVI is currently very long, on the order of 2-3 months, due to isothermal heating rates and premature surface porosity closure that requires the process to be stopped a number of times. ▪ Large energy input is required due to the extended process times. ▪ Corrosive by-products require special safety precautions, expensive equipment and maintenance costs are subsequently high, which further increase the cost of the manufacturing process. ▪ It is very difficult to obtain fully dense composites; densities of ~90% of theoretical are therefore typical. ▪ The cost of some precursors is high, in particular rhenium and hafnium chlorides. ▪ Low infiltration depth for large radicals such as Hf, Zr and Ta
Slurry impregnation process	<ul style="list-style-type: none"> ▪ Production of a slurry of ceramic particles is cheap, quick and easy ▪ Simple procedure to introduce a slurry to a fibrous substrate ▪ Properties of the slurry are easily tuneable based on the chemicals used 	<ul style="list-style-type: none"> ▪ Homogeneous penetration of large preforms is difficult ▪ Stable suspensions of dense ceramic particles (e.g. HfB_2) are hard to make; an issue is possible with respect to scalability ▪ Issues exist with clogging the surface of preforms with ceramic particles

	<ul style="list-style-type: none"> ▪ Impregnation cycles are easy (requiring only impregnation and drying) to bring the green composite to moderate levels of densification 	<ul style="list-style-type: none"> ▪ Low penetration into fibre tows due to large particle sizes relative to tow entrance size ▪ Produces a material with a discontinuous porous matrix
Hot pressing	<ul style="list-style-type: none"> ▪ High Fibre volume fraction ▪ High density achievable ▪ Short manufacturing time ▪ Apparatus is the same used for the sintering monolithic ceramics ▪ Chemicals involved have minor implications on H&S (if compared to PIP and CVI) 	<ul style="list-style-type: none"> ▪ Matrix-fibre interaction due to high temperature and pressure ▪ Fibre degradation due to high temperature ▪ near-net shape components are not achievable
Pressureless sintering	<ul style="list-style-type: none"> ▪ High Fibre volume fraction ▪ Low pressure, theoretically, reduced the matrix-fibre interaction risk and fibre degradation ▪ Short manufacturing time ▪ Near-net shapes are, in theory, possible ▪ Chemicals involved have minor implications on H&S (if compared to PIP and CVI) 	<ul style="list-style-type: none"> ▪ Lower density than HP and SPS ▪ Low pressures requires higher sintering temperatures and time than HP and SPS
Spark plasma sintering	<ul style="list-style-type: none"> ▪ High Fibre volume fraction ▪ High densities achievable ▪ Short manufacturing time ▪ Reduced sintering temperatures ▪ Reduced sintering times ▪ Chemicals involved have minor implications on H&S (if compared to PIP and CVI) 	<ul style="list-style-type: none"> ▪ Although lower sintering temperature and time, matrix-fibre interaction has been reported ▪ Equipment is more expensive than conventional HP and Pressureless furnaces ▪ Near-net shape components are not achievable
Hot isostatic pressing	<ul style="list-style-type: none"> ▪ High Fibre volume fraction ▪ Near-net shapes are, in theory, possible ▪ Chemicals involved have minor implications on H&S (if compared to PIP and CVI) 	<ul style="list-style-type: none"> ▪ Equipment is more expensive than conventional HP and Pressureless furnaces ▪ Usually works with high pressure

Table 6 Literature reported data on RMI of UHTCMCs.

Matrix	Constituents	Processing conditions	Properties	Reference
ZrC	3D C _f preforms Pyro. C interface Zr-Si alloy (91.2 at.% Zr & 8.8 at.% Si) Eutectic formed at 1570°C	C deposited by CVI RMI at 1800°C at 8.8×10^{-2} Pa in flowing Ar	Density increased from 1.33 g cm ⁻³ to 2.46 g cm ⁻³ 5% porosity Zr ₂ Si phase still present Pore size between 20-200 µm Flexural strength 239.5 MPa Linear ablation rate 0.0028 mm s ⁻¹	[227]
	2D C _f felts Pyro. C interface and other unspecified interface Zr : Si : C : ZrO ₂ powder in a ratio of 3 : 5 : 1 : 0.2	80 h of CVI using CH ₄ to deposit carbon at 1050 - 1150°C and 5 - 15 kPa Graphitised at 2500°C in flowing Ar RMI at 2000 - 2300°C, furnace dwell 2h	Mass ablation rates 1.33 µm s ⁻¹ and 0.24 mg s ⁻¹	[228]
	3D C _f preform Pyro. carbon interface Zr molten powder	C deposited using CVI Ar atmosphere at 1850°C	No residual Zr detected using XRD	[229]
	C _f An unspecified interface then a pyro. C interface Molten Zr	Carbon deposited using CVI	Residual α-Zr detected and mechanism for formation proposed	[230]
SiC-ZrB ₂ -ZrC	2D C _f preform SiC interface B ₄ C-phenol formaldehyde resin slurry ZrSi ₂ alloy powder	Interface produced using CVI of CH ₃ SiCl ₃ at 1000°C Preform impregnated with resin 4x and pyrolysed at 900°C RMI performed at 1800°C under vacuum Sealed using SiC CVI	ZrSi ₂ alloy residual found in microstructure Linear ablation rate 0.002 mm s ⁻¹	[231]
	3D C _f / B ₄ C - C preform Pyro. C and SiC interface B ₄ C - C sol ZrSi ₂ alloy	Interfaces produced using CVI Pyrolysis of the sol 900°C Carbothermal reduction 1500°C in Ar RMI performed at 1750 - 1900°C	Higher temperatures resulted in better densification	[232]

ZrC-ZrB ₂	2D C _f preforms Pyro C interface Eutectic Zr – B alloy (Zr : B = 86 : 14)	Interface produced using CVI of propylene 900°C Alloy was prepared by arc melting Zr and B powder RMI performed at 1800°C	Resulting density 3 g cm ⁻³ 4% open porosity No residual alloy detected Linear ablation rate 0.0001 mm s ⁻¹	[224]
	3D C _f preforms Impregnated with phenolic and resin and B ₄ C particles Zr powder	Impregnation process was repeated 4 times before being pyrolysed at 2200°C in Ar RMI performed at 2000°C	Density of 3.07 g cm ⁻³ Open porosity of 9.1% Flexural strength of 147 MPa Mass ablation rate was 0.0039 g s ⁻¹ Linear ablation rate was 0.01 mm s ⁻¹	[225]
ZrB ₂	2D C _f preform TiB ₂ interface Zr ₂ Cu alloy	Interface produced using CVI at 800°C, at 300 mbar for 4h, resulting in a 4 µm coating RMI performed at 1100 - 1500°C under vacuum	C _f showed no critical degradation due to TiB ₂ coating	[220]
	2D C _f preform B ₂ O ₃ phenolic based preforms TiB ₂ interface Zr ₂ Cu or Zr ₂ Cu - 1at.% B or Zr ₂ Ag - 1at.% B	Interface produced using CVI at 800°C, at 300 mbar for 2 h, resulting in a 2 µm coating RMI performed at 1500 - 1900°C under vacuum	Addition of B ₂ O ₃ decreases ceramic yield and causes fibre degradation 2 µm coating insufficient to stop fibre degradation	[226]
HfC	3D C _f preform Pyro. C and SiC interface Phenol formaldehyde resin HfSi ₂ alloy powder	Interfaces produced using CVI at 1000°C Resin pyrolysed three times at 1500°C RMI performed at 1600 - 1700°C under vacuum	Residual HfSi ₂ was detected	[207]

Table 7 Precursors and the conditions needed for the deposition of oxide / non-oxide ceramics [236], [237].

Matrix deposited	Reactant gases	Temperature / °C
C	CH ₄ -H ₂	1000-1200
HfC	HfCl ₄ -(CH ₄ or C ₃ H ₆ -H ₂ -Ar)	900-1600
ZrC	ZrCl ₄ -(CH ₄ or C ₃ H ₆ -H ₂ -Ar)	900-1600
TaC	TaCl ₅ -(CH ₄ or C ₃ H ₆ -H ₂ -Ar)	900-1500
SiC	CH ₃ SiCl ₃ -H ₂	900-1300
Si ₃ N ₄	SiCl-NH ₃ -H ₂	1000-1400
TiB ₂	TiCl ₄ -BCl ₃ -H ₂	800-1200
	TiCl ₄ -B ₂ H ₆ -H ₂	600-1100
ZrB ₂	ZrCl ₄ -BCl ₃ -H ₂ -Ar	900-1200
	ZrCl ₄ -B ₂ H ₆ -H ₂	600-1100
HfB ₂	HfCl ₄ -BCl ₃ -H ₂ -Ar	900-1200
	ZrCl ₄ -B ₂ H ₆ -H ₂	600-1100
	Hf(BH ₄) ₄	≤300°C
SiO ₂	SiH ₄ -O ₂ -H ₂	300-750
TiO ₂	TiCl ₃ -H ₂ O	800-1000
ZrO ₂	ZrCl ₄ -CO ₂ or O ₂ -H ₂	900-1100
Al ₂ O ₃	AlCl ₃ -CO ₂ or O ₂ -H ₂	900-1000
HfO ₂	HfCl ₄ -CO ₂ or O ₂ -H ₂	900-1100
Ta ₂ O ₅	ZrCl ₄ -CO ₂ or O ₂ -H ₂	900-1100
YSZ	Zr(C ₁₁ H ₁₉ O ₂) ₃ -Y(C ₁₁ H ₁₉ O ₂) ₃	735

Table 8 Chemical vapour infiltration variants w.r.t. temperature, pressure, heating [242].

	Temperature		Pressure				Heating	
CVI / CVD Process type	Uniform	Gradient	Uniform	Gradient	Atmospheric	Low	Radiative	Inductive
Plasma enhanced low pressure	X	X	X	X		X	X	
Thermal gradient, radiantly heated, isobaric		X	X		X	X	X	
Thermal gradient, inductively heated, isobaric		X	X		X	X		X
Liquid immersion, thermal gradient, inductively heated isobaric, atm. pressure		X	X		X	X		X
Isothermal, forced flow	X			X	X	X	X	X
Isothermal, pulsed pressure	X			X	X			
Thermal gradient, forced flow		X		X	X			
Microwave-heated, isobaric or forced-flow		X	X	X	X	X		
Catalyst-enhanced, isothermal, isobaric	X		X		X		X	
Particle-transport enhanced, isothermal, isobaric	X		X		X		X	

Table 9 Mechanical properties, density achieved and sintering conditions of UHTCMCs processed by hot pressing.

System	Sintering aids/ non-UHTC phase	Vf / %	T / °C	P / MPa	ρ_r / %	MOR / MPa	K_{IC} / MPa m^{1/2}	Ref
C _f - ZrB ₂	Si ₃ N ₄	70	1800	40	78	90	--	[279]
C _f -ZrB ₂	B ₄ C	40	1900	40	-	327	13.8	[275]
C _f -ZrB ₂	SiC, Si ₃ N ₄	20	1900	30	-	310	6.72	[276]
C _f - ZrB ₂	SiC	40	1800-	30-40	92	235 ± 40	6.4 ± 0.8	[283]
		55	1900		88	125 ± 35	7.3 ± 0.9	
		65			85	140 ± 40	7.5 ± 1.4	
C _f - ZrB ₂	SiC	55	1800- 1900	30-40	96	152 ± 12	10.6 ± 1.6	
C _f - ZrB ₂	SiC and Si ₃ N ₄	40-45	1800- 1900	30-40	92-95	355 ± 40 500 ± 51 (1200°C) 547 ± 80 (1500°C)	9.6 ± 0.7 8.7 ± 1.2 (1500°C)	[281]
SiC _f -ZrB ₂	ZrSi ₂	50	1600	40	95	145 ± 10	--	[278]

Abbreviation used:; ch=chopped, Vf = fibre volume fraction, T = temperature, P = pressure, ρ_r = relative density, MOR= Modulus of Rupture, K_{IC} = fracture toughness

Table 10 Properties of carbon fibre reinforced ultra-high temperature ceramic matrix composites prepared by different approaches.

Materials	General characteristic	Detailed Fabrication process	Density / g/cm³	Open porosity / %	Flexural strength / MPa	Elastic modulus / GPa	Reference
C _f / HfB ₂ -C	Non-sintered + 2D preform	Injection + infiltration of the HfB ₂ -C slurry into the preform + carbon CVI	3.2 ± 0.16	16	121.37 ± 18.30	28.3 ± 3.2	[179]
C _f / ZrC	Non-sintered PIP + 3D preform	Infiltration of ZrC precursors (ZrO ₂ / C sol) into the preform, reduction at 1200°C and further heat treatment at 1600°C.	1.98	12.4	107.6	28.8	[308]
C _f / ZrC-SiC	Partially sintered + 2D preform	C preform without any treatment; infiltration of ZrC-PCS slurry into the preform plus hot pressing; PIP with PCS + pyrolyzed at 1100°C + final heat treatment at 1800°C	2.47	6.6	178±77	106±13	[294]
C _f / ZrC-SiC	As above	Preform initially treated by CVI of PyC; others steps same as above	2.18	4.9	748±15	141±12	[294]
C _f / ZrC-SiC	As above	Preform initially treated by alternated CVI of PyC/SiC; others steps same as above	2.25	7.4	559±121	138±15	[294]
C _f / ZrC-SiC	RMI + 3D needled preform	(PyC-SiC) ₃ deposited in preform by CVI, further infiltrated by ZrC precursors to generate C _f /ZrC-C; RMI of Si within preform to form dense C _f /ZrC-SiC-ZrSi ₂	2.52	1.68	380	61	[296]
C _f / ZrB ₂ -ZrC-SiC	RMI + 3D needled preform	(PyC-SiC) deposited in preform by CVI, further infiltrated by B-containing sols to generate Cf/B ₄ C-C after heat treatment; RMI of Zr-Si alloy within preform to form dense C _f /ZrB ₂ -ZrC-SiC	2.42 ± 0.01	9.4 ± 0.1	184 ± 9	/	[306]

$C_f / ZrC-SiC$	RMI + 3D braided preform	Preform infiltrated by PCS and PR to form $C_f/SiC-C$ after heat treatment; RMI of Zr-Si alloy with the preform to form dense $C_f/ZrC-SiC$	2.94	5.3	101.5±8.16	35.18±9.58	[191]
$C_f / ZrC-Zr$	RMI + 2D preform	Carbon fibres coated with ZrO_2 / HfN by CVD and then woven into 2D preform. C/C skeleton formed by coating with preform by CVD; RMI of Zr into the preform to form $C_f/ZrC-Zr$	/	/	/	/	[295]
C_f / ZrC	RMI + 2D preform	C/C preform infiltrated by RMI of Zr_2Cu alloy at 1200°C to generate C_f/ZrC composites	/	/	172±12	/	[307]
$C_f / C-ZrC$	CVI + MRI + 3D preform	C/C preform infiltrated by RMI of Zr-Si alloy at 1800°C	2.46	5.0	240		[227]
C_f / ZrB_2	Vacuum bagging + hot pressing + 1D fabrics	1D fabrics coated with slurry containing ZrB_2 powders and additives; fabrics stacked and pressed by vacuum bagging, final densification at 1600-1800°C by hot-pressing	3.3	/	90	/	[279]
$C_f / ZrB_2-SiC-Si_3N_4$	Slurry infiltration + hot pressing + unidirectional fabrics	$ZrB_2 / SiC / Si_3N_4$ slurry infiltrated into C fabrics stacked in 0-0° configuration. Hot pressed at 1800-1900°C under 30-40MPa	/	Very small amount	355 ± 40 () 63 ± 7 (⊥)	239() 188(⊥)	[281]

Table 11 Thermal properties (melting point, CTE, thermal conductivity, diffusivity, Cp) of UHTCs and UHTCMCs.

Material	Coefficient of Thermal Expansion, CTE / $\times 10^{-6} \text{ K}^{-1}$	Thermal Conductivity / $\text{W m}^{-1}\text{K}^{-1}$	Thermal Diffusivity / $\text{mm}^2 \text{ s}^{-1}$	Specific Heat Capacity / $\text{J g}^{-1}\text{K}^{-1}$	Reference
C _{sf} -HfB ₂ -SiC		54.4 - 93.8			[118]
C _f -HfC	3.36 (1473 K)	4.18 \pm 0.14 (473 K – 2073 K)	4.2 - 7.5	0.42 - 0.68	[205]
C _f -HfC-SiC	2.95 (1473 K)	3.33 \pm 0.42 (473 K – 2073 K)	1.9 - 6.1	0.49 - 0.78	[205]
C _f /C-3.5wt% HfC	1.20 - 3.25	16.5 (\perp) - 19.8 (\parallel) (298 K); 24.5 (\perp) - 27.5 (\parallel) (673 K); 23.0 (\perp) - 26.5 (\parallel) (1073 K)	8.7 - 22.0	0.57 - 1.50 (298 K – 1073 K)	[340]
C _f /C-6.5wt% HfC	1.60 - 4.00	18.5 (\perp) - 24.8 (\parallel) (298 K); 25.5 (\perp) - 32.0 (\parallel) (673 K); 24.0 (\perp) - 30.5 (\parallel) (1073 K)	16.0 - 24.4	0.60 - 1.55 (298 K – 1073 K)	[340]
C _f /C-9.5wt% HfC	2.00 - 4.70	14.0 (\perp) - 17.0 (\parallel) (298 K); 18.5 (\perp) - 26.0 (\parallel) (673 K); 18.0 (\perp) - 25.0 (\parallel) (1073 K)	6.5 - 21.5	0.61 - 1.75 (298 K – 1073 K)	[340]
C _f /C-SiC/HfC coating	3.5 - 4.6				[341]
C _f /C-SiC/HfC coating-HfC nanowires	4.9 - 6.6				[341]
C _f /C-SiC		14.5 25 - 53			[342], [343]
C _f /C-SiC-ZrB ₂	3.05 - 3.45				[326]
C _f /C-SiC-ZrB ₂ -SiC nanowires	2.95 - 3.3				[326]
C _f /C-SiC-ZrB ₂ -SiC nanowires Pre-oxidation	2.75 - 3.15				[326]
C _f /C-SiC-ZrB ₂ -ZrC		37.4 - 45			[210]
C _f /SiC		9.4 6.2 - 8.4		0.85 - 1.35	[221], [327]
C _f /ZrB ₂ -ZrC		8.1 - 11.7		0.8 - 1.33 ¹	[327]
C _{sf} -ZrB ₂ -20vol% SiC		48.3 - 104.7			[328]
C _f /C-ZrB ₂ -SiC(compact) & C _f /C-ZrB ₂ -SiC(porous) & C _f /C-SiC(compact)		3.29			[329]

C _{pw} -ZrB ₂ -ZrC		8 - 12			[330]
C _{sf} -ZrB ₂ -ZrC		45 - 70			[330]
HfB ₂	6.3	72 - 105		0.25	[221]
HfC	6.8 7.7 (298 K – 885 K) 7.66 ± 0.11 (298 K – 2273 K)	21 - 27		0.182	[205], [221], [331], [332]
HfC _{0.98}	7.7 (1773 K)	21 - 28			[38]
HfC _{0.67}	7.7 (1773 K) ¹	14 - 24			[38]
HfC+15vol%MoSi ₂	7.26 (298 K – 1573 K)	22.0 - 36.3			[333]
HfC+15vol%TaSi ₂	9.99 (298 K – 1573 K)				[333]
HfC+15vol%TaSi ₂ -SiC fibres	7.01 (298 K – 1573 K)	20.7 - 26.5			[98]
HfN _{0.92}	7.7 (1773 K)	8 - 14			[38]
HfB ₂ -SiC-TaSi ₂	8.0 (298 K – 1523 K)	28 - 34			[342]
HfB ₂ -20vol%SiC	7.77 (293 K – 1273 K)				[349]
TaC	6.6 7.08 ± 0.33 (298 K – 2273 K)	22		0.19 ⁹	[221], [332]
TaC+15vol%MoSi ₂	6.51 (298 K – 1573 K)	24.1 - 47.3			[333]
TaC+15vol%TaSi ₂	7.63 (298 K – 1573 K)				[98]
TaC+15vol%TaSi ₂ -SiC fibres	6.66 (298 K – 1573 K)	27.8 - 37.2			[98]
MoSi ₂	Ave. 9.32 (298 K – 1573 K) 7.3 - 10.5 (298 K – 1273 K)				[335], [336]
TaSi ₂	Ave. 9.78 (298 K – 1573 K)				[335]
SiC	4.3			0.58	[221]
ZrB ₂	6.8 (300 K – 1300 K) & 8.4 (1300 K – 1675 K) 5.9	53 56.4		0.43	[221], [322], [337]
ZrC	7.3	18 - 44		0.37	[221], [338]
ZrB ₂ -(10-40)vol%MoSi ₂		76.60 - 87.95		~0.53	[339]
ZrB ₂ -20vol%MoSi ₂ -(5-30) vol%SiC		82.09 - 97.55		0.53 - 0.60	[339]

ZrB ₂ -40vol% MoSi ₂ -(5-30) vol% SiC		80.83 - 95.15		0.52 - 0.59	[339]
ZrB ₂ -(10-40)vol% ZrSi ₂		74.20 - 98.30			[339]
ZrB ₂ -20vol% SiC	7.85 (293 K – 1273 K)	76.2 - 103.8		0.514	[349], [337], [116]
ZrB ₂ -30vol% SiC	6.8 (300 K – 1300 K) & 7.8 (1300 K – 1675 K)	56 - 63.5			[322], [337]
ZrB ₂ -20vol% SiC-5vol% Si ₃ N ₄	7.59 (293 K – 1273 K)				[349]
ZrB ₂ -20vol% ZrC-20vol% SiC-5vol% Si ₃ N ₄	8.20 (293 K – 1273 K)				[349]
ZrB ₂ -SiC-TaSi ₂	7.4 (298 K – 1523 K)	33 - 41			[342]
ZrB ₂ -20vol% SiC-0.2wt% CNTs		90.9		0.511	[116]
ZrB ₂ -ZrC-SiC		65 - 85			[58]
ZrB ₂ -33.3mol% ZrC-33.3mol% SiC		72.6			[337]
ZrB ₂ -15mol% ZrC-15mol% SiC		85.6			[337]
ZrB ₂ -55mol% ZrC-30mol% SiC		51.8			[337]
ZrB ₂ -15mol% ZrC-30mol% SiC		89.0			[337]

Table 12 Electrical properties of UHTCMCs reported in the literature.

Materials	Electrical Conductivity $\times 10^4$ / $\Omega^{-1}\text{cm}^{-1}$	Electrical Resistivity $\times 10^{-5}$ / $\Omega\text{ cm}$	Reference
ZrB ₂ -(10-40)vol% MoSi ₂	8.11 - 7.22	1.23 - 1.34	[339]
ZrB ₂ -40vol% MoSi ₂ -(5-30)vol% SiC	7.35 - 4.07	1.36 - 2.46	[339]
ZrB ₂ -(0-40)vol% SiC	-	1.025 - 8.793	[349]
ZrB ₂ -(5-30)vol% SiC	1.989 - 1.199	-	[350]
ZrB ₂ -20vol% SiC	-	1.60 - 3.10 (298 K – 700 K)	[348]

ZrB ₂	-	0.80 - 1.60 (298 K – 650 K)	[348]
HfB ₂ -(5-30)vol% SiC	2.229 - 1.342	-	[350]
HfB ₂ -5vol% SiC	-	0.70 - 1.90 (298 K – 650 K)	[348]
HfB ₂	-	0.25 - 1.25 (298 K – 650 K)	[348]

Table 13 Thermal ablative methods and properties of various UHTCMCs.

Material	Fabrication method	Density / g cm ⁻³	Ablation method	Temperature / °C		Time / s	Heat flux / MW m ⁻²	Ablation rate	Ref
				Flame	Surface				
C _f /ZrB ₂ -ZrC-SiC	PIP	2.44	Plasma wind tunnel	-	2027	300	-	0.010 g s ⁻¹	[209]
C/SiC-HfC	RMI	2.60	Plasma wind tunnel		1650 - 2500	60 - 600	3.5 - 5	-	[357]
C _f /SiC-ZrC	CVI-PIP	-	Plasma wind tunnel	2227	-	60	-	-	[358]
C/C-ZrC-SiC	PIP	2.03-2.14	Plasma flame	-	2300	60	-	3.51 mg s ⁻¹ - 1.88 μm s ⁻¹ 1.57 mg s ⁻¹ - 0.37 μm s ⁻¹	[359]
C/C-ZrC-SiC	PIP	1.98	Plasma flame	-	2342	180	-	1.73x10 ⁻³ g s ⁻¹ 1.94x10 ⁻⁴ mm s ⁻¹	[360]

50 vol% C _f - 50 vol% ZrB ₂	HP	3.4	HVOF	2713	1277	30	3.7	Negligible	[109]
C/C-ZrC	CVI-RMI	2.46	Pulse laser	-	3000	20	1000	0.028 mm s ⁻¹	[227]
C/C-ZrC	CVI-RMI	-	Laser beam-CO ₂	-	3000	-	1000-2000 W	-	[229]
C/C-ZrC	CVI-RMI	-	OAT	-	3000	20	4.2	0.002 mm s ⁻¹	[229]
C/ZrB ₂ -SiC	CVI-SP	2.10	OAT	-	2800 - 3300	20	4.2	0.66 mm s ⁻¹	[181]
C _f /HfB ₂	VI-CVI	2.17-2.87	OAT	-	2600	60	17	4.1x10 ⁻³ g s ⁻¹ - 8.3x10 ⁻³ g s ⁻¹ 0 mm s ⁻¹	[187]
C/ZrC	PIP	-	OAT	>3000	2000 - 2300	300	4.2	0.006 g s ⁻¹ 0.004 mm ⁻¹	[361]
C/C-ZrC-SiC	PIP	2.22	OAT	3000	2400	120	-	3.75x10 ⁻⁴ g s ⁻¹ 2.48x10 ⁻³ mm s ⁻¹	[182]
C/C-SiC-ZrB ₂	RMI	-	OAT	3000	2050	60	2.4	0.013 g s ⁻¹ 0.0014 mm s ⁻¹	[362]
C/C-ZrC-SiC	PIP	2.1	OAT	-	1823-1612 2402-2013	60	2.4 4.2	1.33-0.27 mg s ⁻¹ ; 0.585 mg s ⁻¹ cm ⁻² 6.16-3.67 mg s ⁻¹ ; 18.092 mg s ⁻¹ cm ⁻²	[363]
C/C-SiC-ZrC-HfC	TCVI-PIP	2.3-2.6	OAT	3000	2400	120	2.4	0.151 mg s ⁻¹ cm ⁻² 0.225 μm s ⁻¹	[364]
C/C-ZrB ₂ -ZrC-SiC	TCVI-PIP	2.1	OAT	-	1800 2400	60	2.4 - 4.2	15.7 μm s ⁻¹ 22.8 g s ⁻¹ cm ⁻² - 36.5 μm s ⁻¹	[210]
C/SiC-HfC	CVI-RMI	2.61	OAT	3000	2500-3200	20	4.2	2.9x10 ⁻³ g s ⁻¹ - 2.2x10 ⁻² mm s ⁻¹	[207]
C/SiC-HfC	CVI-PIP	3.19	OAT	3000	2500-3200	20	4.2	1.5x10 ⁻³ g s ⁻¹ - (-0.4)x10 ⁻² mm s ⁻¹	[207]
C/C-SiC-ZrC	PIP	2.24	OAT	3000	2400	120	-	0.0019 g s ⁻¹ - 0.012 mm s ⁻¹	[365]
C/C-ZrC-SiC	PIP	2.22	OAT	3000	2550	120	4.2	(-0.30) mg s ⁻¹ - 1.5 μm s ⁻¹	[366]
C/C-ZrC-ZrB ₂ -SiC	LPCVI-PIP	2.1	OAT	-	2077	120	2.4	0.36x10 ⁻⁴ g s ⁻¹ cm ⁻² - 2.04x10 ⁻⁴ mm s ⁻¹	[197]
C/C-SiC-ZrB ₂	LPCVI-RMI	-	OAT	3000	-	60	2.4	0.0014 g s ⁻¹ - 0.013 mm s ⁻¹	[222]
C _f /HfC-SiC	PIP	2.48	OAT	3000	-	60	-	0.51 mg cm ⁻² s ⁻¹ - 0.006 mm s ⁻¹	[367]
C/SiC-ZrB ₂	CVI-PIP	2.56	OAT	-	-	20	4.2	(-0.04) g s ⁻¹ - (-0.074) mm s ⁻¹	[198]
C/ZrC-SiC	CVI-RMI	3.09	OAT	-	2000	30	-	0.0071 g s ⁻¹ - 0.0047 mm s ⁻¹	[368]
C/C-HfB ₂ -SiC	PIP-RMI	1.85	OAT	-	-	90	2.4	0.129 mg cm ⁻² s ⁻¹ - 2.06 μm s ⁻¹	[369]

C/SiC-ZrB ₂ -TaC	CVI-SP	2.35	OAT	-	3000	20	4.2	0.026 mm s ⁻¹	[370]
C/ZrB ₂ -SiC	CVI-SP	2.1	OAT	-	3000	20	4.3	0.066 mm s ⁻¹	[181]
C/C-SiC-ZrB ₂	ICVI-RMI	2.25	OAT	3000	-	60	2.4	$0.61 \cdot 10^{-3} \text{ g s}^{-1} - 6.72 \cdot 10^{-3} \text{ mm s}^{-1}$	[371]
C _f /ZrB ₂	VI-CVI	2.11	OAT	3000	2590	60	17	0.011 g s ⁻¹ - 0.08 mm s ⁻¹	[18]
C _f /ZrB ₂ -SiC	VI-CVI	2.01	OAT	3000	2550	60	17	0.010 g s ⁻¹ - 0.09 mm s ⁻¹	[18]
C _f /ZrB ₂ -SiC-LaB ₆	VI-CVI	1.91	OAT	3000	2525	60	17	0.012 g s ⁻¹ - 0.10 mm s ⁻¹	[18]
C _f /HfB ₂	VI-CVI	1.93	OAT	3000	2640	60	17	$9.5 \cdot 10^{-3} \text{ g s}^{-1} - 0.03 \text{ mm s}^{-1}$	[18]
C _f /HfC	VI-CVI	2.07	OAT	3000	2530	60	17	0.03 g s ⁻¹ (surface layer fell off)	[18]

